Numerical Simulation to Study Solar Wind Turbulence and Coronal Heating

A Thesis Submitted

To

Sikkim University

In Partial Fulfilment of the Requirement for the
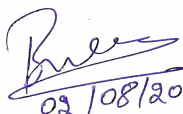**Degree of Doctor of Philosophy**

By

Bheem Singh Jatav

Department of Physics
School of Physical Sciences

August 2021

I would like to dedicate this thesis to my loving parents

DECLARATION

I declare that the thesis entitled "**Numerical Simulation to Study Solar Wind Turbulence and Coronal Heating**" submitted by me for the award of **Doctor of Philosophy in Physics** of Sikkim University is my original work. The content of this thesis is based on the numerical simulation which I have performed myself. This thesis has not been submitted for any other degree to any other University.
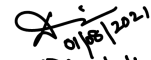
02/08/2021

(**Mr. Bheem Singh Jatav**)

Roll. No: 13PDPH01

Registration No: 13/PD/PY/05

CERTIFICATE

This is to certify that the Ph. D. thesis entitled "**Numerical Simulation to Study Solar Wind Turbulence and Coronal Heating**" submitted to **Sikkim University** in partial fulfilment of the requirements for the degree of **Doctor of Philosophy in Physics**, embodies the result of bona-fide research work carried out by **Mr. Bheem Singh Jatav** under my guidance and supervision. No part of thesis has been submitted for diploma, associateship, fellowship or any other degree.

All the assistance and help received during the course of the investigation have been duly acknowledged by him.

01/08/2021
(Digitally signed)

Dr. Hemam Dinesh Singh

Ph. D. supervisor

Department of Physics

Place: Gangtok

Date: 01/08/2021

6 माइल, सामदुर, तादोंग -737102
गंगटोक, सिक्किम, भारत
फोन-03592-251212, 251415, 251656
टेलीफैक्स -251067
वेबसाइट - www.cus.ac.in

6th Mile, Samdur, Tadong -737102
Gangtok, Sikkim, India
Ph. 03592-251212, 251415, 251656
Telefax: 251067
Website: www.cus.ac.in

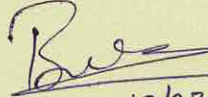## सिक्किम विश्वविद्यालय
SIKKIM UNIVERSITY

(भारत के संसद के अधिनियम द्वारा वर्ष 2007 में स्थापित और नैक (एनएएसी) द्वारा वर्ष 2015 में प्रत्यायित केंद्रीय विश्वविद्यालय)
(A central university established by an Act of Parliament of India in 2007 and accredited by NAAC in 2015)

PLAGIARISM CHECK CERTIFICATE

This is to certify that plagiarism check has been carried out for the following Ph. D. thesis with the help of URKUND software and the result is within the permissible limit of 4 % as per the norms of Sikkim University.
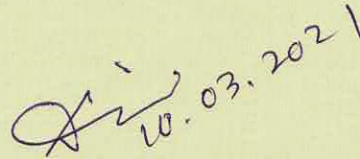
"Numerical Simulation to Study Solar Wind Turbulence and Coronal Heating"

Submitted by **Mr. Bheem Singh Jatav** under the supervision of **Dr. Hemam Dinesh Singh** of the Department of Physics, School of Physical Sciences, Sikkim University, Gangtok, Sikkim, India.
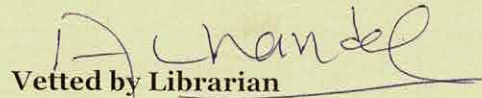
10/03/21

(Mr.Bheem Singh Jatav)

Signature of the Candidate

10.03.2021

(Dr. Hemam Dinesh Singh)

Contoursigned by Ph. D. Supervisor

Assistant Professor
Department of Physics
सिक्किम विश्वविद्यालय
Sikkim University

Vetted by Librarian

पुस्तकालयाध्यक्ष
Librarian
केन्द्रीय पुस्तकालय Central Library
सिक्किम विश्वविद्यालय
Sikkim University

Acknowledgements

It is a pleasure to express my gratitude to all those people who help this thesis possible. First of all, I would like to thank my supervisor, Dr. Hemam Dinesh Singh, for his support and assistance, for everything I have learned from him. Dr. Singh has been a great inspiration for me because of the high intellectual's computational plasma physics knowledge. I would also like to admire him for his pedagogical competence in space plasma physics, and his kindness, patience and kindness towards everyone students on this department.

I would like to acknowledge the financial support of the RGNF, UGC, India.

I wish to thank to the present Dean and Head of the department Dr. Subir Mukhopadhyay and former Head of the department Dr. Amitabha Bhattacharyya for providing me the best facility to work in such a great department. I also would like to thank former and present Vice Chancellor Prof. T. B. Subba and Prof. Avinash Khare, who have registered me for Ph. D. Programme and provide me a further extension to finish Ph. D. work. Finally, i would like to thanks other departmental research committee members Dr. Archana Tiwari, Prof. Anand Phatak, Dr. Ajay Triphati and Dr. Dhurba Rai, for encouragement of my research work.

I thank all colleagues at department of physics for creating a stimulating atmosphere in which it has been a true delight to work.

Finally, i thank to Mr. Nar Bahadur Subba and Mr. Bikram Thapa for their kind help and cooperation during the research work of my Ph.D in computer lab.

Abstract

The solar wind turbulence and coronal heating have been an open problem in solar physics in spite of having proposed many theoretical models to explain it. Dispersive Alfvén wave (DAW) is one of the main candidate which is responsible for inhomogeneous heating of solar wind and coronal plasmas. In this thesis, we explore some of the magnetohydrodynamic and kinetic properties of nonlinear Alfvén waves in the context of solar wind, solar corona and the magnetospheric turbulence as well as the heating of the plasma particles. It studies about the formation of coherent, filamentary Alfvénic structures, their decay processes, their role in particle heating and acceleration, and their relevance for creating the power-law spectra of turbulence observed in solar wind and corona. The dynamical equations satisfied by DAWs follow the form of modified nonlinear Schrödinger equation. The equations were numerically solved by pseudo-spectral method of simulation by taking Fast Fourier Transform and forward difference method with predictor corrector scheme. By assuming an energy inputs in the form of pump waves in the kinetic range or electron inertial range, the author studies numerically the evolution of these waves that lead to filamentary nonlinear structures, or to creation of spatio-temporal turbulence. The magnetic filaments of DAWs with high intensity are generated as the waves propagate along the direction of magnetic field. The transverse modulation of Alfvén waves resulting in coherent structures formation has a significant effect on the evolution of the turbulent magnetic spectra and density fluctuations. The perpendicular characteristic scale of the magnetic coherent structurs is of the order of ion Larmor radius for the kinetic Alfvén waves (KAWs) and it is of the order of electron skin depth for the inertial Alfvén waves (IAWs). The applications of the dynamical models and numerical simulations of KAWs at 1AU solar wind parameters and coronal loops, and IAWs at the coronal holes are also discussed. The dynamical motions are dependent on the type of plasma inhomogeneity represented by four different kinds of initial conditions in our numerical simulation. The perturbation present in the magnetic field gets the energy from the pump DAWs. As the waves propagate, magnetic coherent structures are generated when there is a balance between the wave diffraction and nonlinearity effects resulting from plasma inhomogeneity profile. The collapse of the DAW wave packets takes place when this balance is

no more, thereby leading to the transfer of energy from the waves to the particles in the plasma such as electrons and ions. This transfer of energy at perpendicular wavevector is more for uniform initial pump KAWs rather than those for non-uniform initial pump waves of Gaussian wavefronts. The transfer of energy at kinetic small scales when the wavenumber is less than ion gyroradius and comparable to electron inertial length causes solar wind turbulence and heating of the plasma. In our study, the power spectral index follows Kolmogorov scale of $-5/3$ in the inertial range followed by deeper index varying from -2.5 to -8 in the kinetic dissipation range. The scaling anisotropy of turbulent power spectra in the kinetic scales of plasma particles can importantly influence the plasma heating and turbulent energy transfer processes. For the heating of plasma particles via the wave-particle interactions, in general, the electric power spectra of the turbulent waves are more important than the magnetic power spectra. For the fluctuating electric/magnetic fields, the distribution function of the charged particles satisfies the Fokker-Plank equation. By solving this distribution function in steady state condition, we show that the extension of the distribution thermal tail depends on the wavenumber spectral indices of the electric/magnetic field power spectra. Therefore, charged particles at the end of the distribution function thermal tail have higher velocity and thereby energizing the solar coronal or auroral plasmas. Since the formation of magnetic filaments and it's collapse are considered as one of the faster way to transport energy, our present study may provide some clues to understand the phenomena of energy distribution via dissipation in the solar wind, solar corona and other relevant plasma environments.

List of Publications

Journal Articles

- Hemam Dinesh Singh and Bheem Singh Jatav: **Coherent Structures and Spectral Shapes of Kinetic Alfvén Wave Turbulence in Solar Wind at 1 AU**, *Research in Astronomy and Astrophysics*, January 2019, Vol. 19 No. 7, 93(14pp). doi: 10.1088/1674–4527/19/7/93

- Hemam Dinesh Singh and Bheem Singh Jatav: **Anisotropic Turbulence of Kinetic Alfvén Waves and Heating in Solar Corona**, *Research in Astronomy and Astrophysics*, July 2019, Vol. 19 No. 12, 185(16pp) doi: 10.1088/1674–4527/19/12/185

- Hemam Dinesh Singh and Bheem Singh Jatav: **Inertial Alfvén Waves and Particle Energization in Solar Coronal Holes and Aurora** *(to be submitted)*

Conference Papers and Workshops

- Bheem Singh Jatav: **Numerical Simulation of Kinetic Alfvén Waves for Intermediate-β Plasma to Study Localized Structure of Solar Wind**, *24th Raman Memorial Conference*, 23rd - 24th February, 2018, Savitribai Phule Pune University, Pune, India.

- Bheem Singh Jatav: **Numerical Simulation of IAW (Inertial Alfvén Wave) to Study Nonlinear Structures and Spectral Index for Aurora** *6th PSSI Plasma Scholars Colloquium 2018*, 24-26 August 2018, SMIT Majitar, Rangpo, East Sikkim-737136, INDIA

- Bheem Singh Jatav and Hemam Dinesh Singh: **Coherent Structures of Kinetic Alfvén Waves in Solar Corona** – *12th International Conference on Plasma Science and Applications*, 11-14 November 2019, University of Lucknow, India

- Bheem Singh Jatav: **Computational Astrophysics and Cosmology Workshop (COMAC2018) MHD Simulations in Astrophysics and Space Plasma**. – *Workshop*, 2-6 July 2018, National Astronomical Research Institute of Thailand, Chiang Mai, Thailand.

Acronyms

AW: Alfvén Wave

SAW: Shear Alfvén Wave

DAW: Dispersive Alfvén Wave

IAW: Inertial Alfvén Wave

KAW: Kinetic Alfvén Wave

*K*41: Kolmogorov 1941 Theory

IK: Iroshnikov-Kraichnan Theory

GS: Goldreich-Shridhar Theory

IMF: Interplanetary Magnetic Field

MHD: Magnetohydrodynamic

SOHO: Solar and Heliospheric Observatory

TRACE: Transition Region and Coronal Explorer

PSP: Parker Solar Probe

ACE: Advanced Composition Explorer

CME: Coronal Mass Ejections

AU: Astronomical Unit

IC: Initial Condition

SDO: Solar Dynamics Observatory

DC: Direct Current

NLSE: Nonlinear Schrödinger Equation

SXT: Soft X-ray Telescope

FFT: Fast Fourier Transform

UVCS: Ultraviolet Coronograph Spectrometer

ARTEMIS: Acceleration, Reconnection, Turbulence and Electrodynamics of the Moon's Interaction

with the Sun

MMS: Magnetospheric Multiscale Mission

$FAST$: Fast Auroral SnapshoT

List of Symbols

n_i: Ion Number Density

n_e: Electron Number Density

n_j: Number Density of Species j

n_0: Plasma Number Density

Z: Charge State

ρ_q: Charge Density

ρ_{qj}: Charge Density of Species j

ρ_m: Mass Density

n_j: Number Density of Species j

q_j: Electric Charge of Species j

e: Charge of Electron

ϵ_0: Vacuum Permeability

μ_0: Permittivity in Free Space

$\vec{J}$: Current Density

$\vec{E}$: Electric Field

$\vec{B}$: Magnetic Field

p: Pressure

$\vec{v}$: Velocity

m_i: Mass of Ion

m_e: Mass of Electron

$\vec{v}_i$: Velocity of Ion

$\vec{v}_e$: Velocity of Electron

γ: Ratio of Specific Heats of Plasma (c_p/c_v)

c_p: Amount of Heat Required to Raise the Temperature of a Substance of 1Kg Mass by One Degree

Celsius at Constant Pressure

c_v: Amount of Heat Required to Raise the Temperature of a Substance of 1Kg Mass by One Degree
Celsius at Constant Volume

p_j: Pressure of Species j

p_i: Ion Pressure

p_e: Electron Pressure

q_j: Charge of Species j

q_i: Charge of Ion

q_e: Charge of Electron

ρ_j: Mass Density of Species j

ρ_i: Mass Density of Ion

ρ_e: Mass Density of Electron

P_B: Isotropic Magnetic Pressure

B_0: Ambient Magnetic Field

T_B: Magnetic Tension

$\vec{v}_A$: Velocity of Alfvén Wave

ω: Plasma Frequency

ω_{ci}: Ion-Cyclotron Frequency

ω_{ce}: Electron-Cyclotron Frequency

c: Speed of Light

λ_L: Long Wavelength

$\vec{v}_{ti}$: Ion Thermal Velocity

$\vec{v}_{te}$: Electron Thermal Velocity

$\vec{k}$: Wavevector

$k_\perp$: Perpendicular Wavenumber

$k_\parallel$: Parallel Wavenumber

c_s: Ion Acoustic Speed

ω_i: Ion Gyrofrequency

β: Thermal to Magnetic Pressure Ratio

T: Temperature

$\mathbf{Z}$: Plasma Dispersion Function

ω_{pe}: Electron Plasma Frequency

ω_{pi}: Ion Plasma Frequency

λ_e: Collision-less Electron Skin Depth (Electron Inertial Length)

T_i: Ion Temperature

T_e: Electron Temperature

a_e: Average Electron Thermal Speed

Γ_0: Modified Bessel Function

Table of contents

List of figures

Chapter 1

Introduction

1.1 Background of the Thesis

One of the major issue in astrophysical plasma is the solar coronal heating problem, where photosphere near the Sun is having temperature of around $5780K$ only and the solar corona located far away from the Sun having temperature of around $2 \times 10^6 K$. Recently, the analysis of various spacecraft observations such as Solar and Heliospheric Observatory ($SOHO$), Transition Region and Coronal Explorer ($TRACE$), Hinode and Solar Dynamics Observatory (SDO) have showed that the solar atmosphere is inhomogeneous in magnetic field and plasma density. Therefore, the magnetic fine structures known as magnetic filaments which are the manifestation of field aligned plasma density or temperature gradients play a very significant role in the coronal heating.

Generally, the solar corona can be divided into two regions: coronal holes (open regions) and coronal loops (closed regions). The solar wind emanating from the Sun with streams of plasma particles, originates from the coronal holes which are cooler and less dense. The solar wind permeates throughout the space carrying the associated magnetic field lines and energetic charged particles. Alfvén, 1942 for the first time, presented the role of Alfvén waves (AWs) and solar magnetic field lines to understand solar coronal heating problem. Since then, many physical phenomena to understand the

coronal heating problem have been proposed. Among these, two prominent theories are: heating by waves (Narain and Ulmschneider, 1996; Hood et al. 1997; Goossens, 1994; Priest et al. 2000; Poedts and Goossens, 1989; Ruderman, 1999) and heating by flares or magnetic reconnections (Jain et al. 2005; Hood et al. 2009; Sturrock et al. 1999; Cassak and Shay, 2012). The importance of AWs in the heating of solar plasma, particularly in solar corona, were also reported from many spacecraft data analysis and theoretical studies (Parker, 1979; De Pontieu et al. 2007; Okamoto et al. 2007; Cirtain et al. 2007).

Pure AWs can not sufficiently dissipate to heat the plasma to reach up to the coronal temperature because of the large transverse scale length (Wu & Chen 2013). When the transverse wavelengths of the AWs are comparable to the main kinetic length scales of the plasma, λ_e or ρ_i or ρ_s (whichever is longer); where λ_e is the electron inertial length, ρ_i is the ion gyroradious and ρ_s is the ion acoustic gyroradius; the AWs become dispersive and are known as dispersive AWs (DAWs). The DAWs can be classified into two categories: the inertial Alfvén waves (IAWs) when $\lambda_e > \rho_i$ or ρ_s and the kinetic Alfvén waves (KAWs) when ρ_s or $\rho_i > \lambda_e$. Many studies supported that the dispersive properties of DAWs are mainly responsible for heating the inhomogeneous plasmas such as solar wind and corona (De Azvedo et al. 1994; Voitenko, 1995; Voitenko, 1996; Elfimov et al. 1996; Asgari-Targhi and Van Ballegooijen, 2012; Morton, 2015; Testa et al. 2014).

The objective of this thesis is to numerically study the propagation of DAWs in an inhomogenous solar plasma having field aligned plasma density fluctuations due to ponderomotive force and Joule heating. The dynamical equations satisfied by the magnetic field envelopes are coupled with the field aligned plasma density perturbations. These equations are of the form of nonlinear Schrödinger equation (NLSE). The nonlinearities in the field envelope equations will generate the localization of the wave packets as envelope solitons. As the waves propagate, the magnetic field coherent structures collapse and the dissipation of energies from large scales to small scales via low wavenumbers to higher wavenumbers takes place. In this thesis, the dynamical equations satisfied

by the DAWs were solved numerically using pseudo-spectral method of simulation. The plasma parameters required for the numerical simulations were taken from the spacecraft data relevent to solar corona and solar wind. The pictorial representations of the simulation results are presented as field intensity profiles, spectral contour plots of the magnetic field intensities, phase space plots and spectra of magnetic/electric field fluctuations. From these we can investigate the formation of the coherent magnetic field structures, the cascade of energies at different wavenumbers and the effect of initial plasma inhomogeneities. Transverse collapse of the field aligned magnetic coherent structures or magnetic filaments are considered as one of the efficient mechanism to cascade energies from large scales to small scales (Champeaux et al. 1998; Lavender et al., (2001)). Hence, the study of DAW dynamics leading to the formation of magnetic coherent structures (filaments) and their collapse will help to understand the turbulent power spectra and particle acceleration in many regions of solar and magnetospheric plasmas such as, solar winds, coronal holes, cusp region and the Earth's magnetosphere.

1.2   Models to Study Plasma

A plasma is a quasineutral gas of charged and neutral particles which exhibits collective behavior (Chen, 2006). The meaning of 'quasi-neutrality' in a plasma is that the overall charge densities of ions and electrons cancel each other in the equilibrium state. From the outside, it appears to be electrically neutral. If n_e and n_i are the electron and ion number densities, then the quasi-neutrality condition for a plasma consisting of only singly charged ions, is $n_i \approx n_e$. In the case of plasma consisting of multiple charged ions, this condition becomes

$$n_e \approx \sum_z z.n_z, \tag{1.1}$$

where z is the charge number of a positive ion and n_z is the density of z-times charged ions. In a plasma, electrons and ions can interact in two ways: the short range atomic forces (during collision) and the long-range electromagnetic forces due to currents and charge. The existence of long range electromagnetic forces implies that plasma can show collective behabior, such as oscillations, instabilities etc.

Plasma is formed wherever temperature is high enough or radiation is strong enough to ionize the atoms. Plasma can be divided into two categories: natural and laboratory plasmas. More than 99% of matters in the universe is in the plasma state. It includes the Sun, the stars and the interstellar medium. Plasma physics is responsible for the formation of the radiation belt at the Earth's magnetosphere, acceleration of the high speed solar wind that flows outward from the Sun and the stars, eruption of the sunspots and solar flares, generation of radio emission from the Sun and some astrophysical objects, coronal high temperature, heating and the acceleration of cosmic rays and hard/soft X-rays. Near the Earth's atmosphere, the ionosphere extending from around 50 km to 1000 km altitudes serves the vast protection from the harmful solar radiations to life on the Earth. Because of low temperature and high pressure, plasma cannot be formed naturally near the Earth except under some unusual conditions. The most common plasma phenomenon encountered near the Earth is lightning. The lighting takes place when the atmospheric gas is ionized and heated to a high temperature by the electrical currents present in the discharge. Since the electron and ion recombination rates are high in lightening plasma, it exists for very small fraction of a second. Another common example of natural plasma is the aurora formation occurred at high latitude regions of the Earth atmosphere, mostly within the Arctic and the Antarctic circles. When aurora is formed in the Arctic circle, they are known as aurora borealis (the northern lights) and in the Antarctic circle they are called aurora australis (the southern lights). It is

generated by energetic ions and electrons from solar winds enter the Earth's atmosphere and interact with gases at altitudes of around 80 to 400 km.

The laboratory plasmas for basic science and technological applications are found in high and low pressure electric discharges. Although the concept of plasma was introduced in 1928 by I. Langmuir and L. Tonks in connection with the partially ionised gas generated by the electrically connected low pressure inert gas, the early arc discharge plasmas between two carbon electrodes in air at atmospheric pressure were produced in 1803 by Petrov in Russia and Humphrey Davy in Britain (Conde, (2018)). The laboratory plasmas have wide range of applications, such as metal welding, thermal cutting, coating of materials, fluorescent lamps, plasma-screen televisions and material plasma processing. The design and operation of controlled thermonuclear fusion experiment to produce huge amounts of energy remains as a scientific and technological challenge till now.

The dynamics of plasma particles are governed by the interactions among the plasma particles and the internal fields produced by the particles themselves and the applied external fields. The internal electric fields will be generated as the particles move resulting the local concentration of positive and negative charges. It can also generate electric currents and thereby generating magnetic fields also. The laws of classical physics can be adequately applied to describe the dynamics of the charged particles. In general the momenta of the charged particles are high and the densities are low. Therefore, the de Broglie wavelengths of the charged particles are much smaller than the interparticle distances. So quantum mechanics does not play significant role in these conditions. Quantum mechanics starts becoming important only at very high densities and very low temperatures, for example degenarate electron gas available in dwarf and neutron stars. In order to understand the macroscopic properties of the plasma, the individual motions of each particles can be neglected as the plasma has a collective behaviour. The hierarchy of plasma phenomena is shown in figure (1.1). Theoretically, plasma can be studied by the following methods:
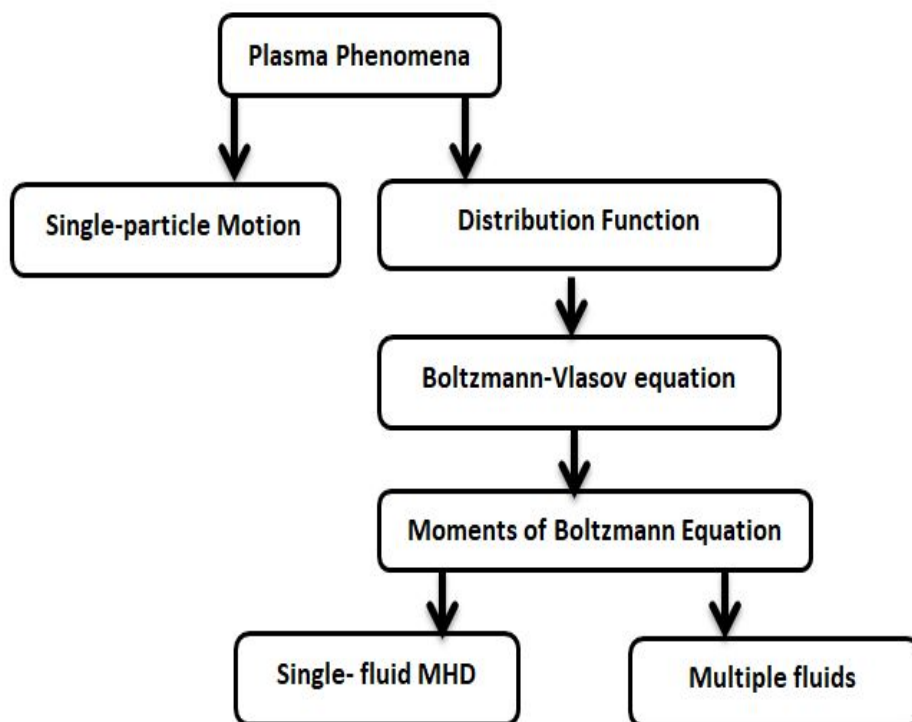
Fig. 1.1 Hierarchy of plasma phenomena

1.2.1　Single Particle Motion (Particle Orbit Theory):

In case of very low density plasma, the interactions among the charge particles are not significant. Therefore, to understand the plasma properties, we can study the dynamics of individual charge particles in the given field. In general, the equation of motion is governed by the Lorentz force as

$$m\frac{d\vec{v}}{dt} = q(\vec{E} + \vec{v} \times \vec{B}) \tag{1.2}$$

For non-uniform fields, it can be expanded by Taylor's series around the guiding centre and the series can be truncated after retaining the low order terms. This approximation is known as particle orbit theory. This approach can be applied at low density plasmas, such as Van Allen radiation belts, cosmic rays, solar corona, particle accelerators, cathode ray tubes and other low density laboratory plasmas. With the help of fast computers, we can follow the nonlinear motions of individual charged particles via simulation.

1.2.2　Kinetic Theory

Single particle approach does not consider the collective motions of the charged particles. Generally, non zero electric fields arise in a plasma self consistently. Therefore, in studying the plasma dynamics, one must consider the collective motions of many plasma particles. The kinetic theory is a statistical approach where the state of the plasma is described by a velocity distribution function $f_\alpha(r, v, t)$ which gives the phase space density of particles of the species at a point in phase space (r, v) at time t

$$f_\alpha(r, v, t) = \sum_\beta \delta(x - x_\beta(t))\delta(v - v_\beta(t)), \tag{1.3}$$

where the independent variables x and v are position and velocity, and $(x_\beta(t), v_\beta(t))$ describes the trajectory of the β-th particles in the phase space. The single particle moving along a trajectory $x(t)$ can be represented by the following delta function

$$\delta(x - x_\beta(t)) = \delta[x - x(t)]\delta[y - y(t)]\delta[z - z(t)]. \tag{1.4}$$

Similarly, we can write the velocity space distribution function for the particle moving along the trajectory $v(t)$ as

$$\delta(v - v_\beta(t)) = \delta[v - v_x(t)]\delta[v - v_y(t)]\delta[v - v_z(t)]. \tag{1.5}$$

The charge and current densities are given by moments of the distribution function as

$$\rho_q = \sum_\alpha \int q_\alpha f_\alpha(r, v, t) dv \tag{1.6}$$

and

$$j = \sum_\alpha \int q_\alpha v f_\alpha(r, v, t) dv. \tag{1.7}$$

The evolution of the distribution function is described by the kinetic equation known as collisional Boltzmann-Vlasov equation

$$\frac{\partial f}{\partial t} + \vec{v}.\frac{\partial f}{\partial \vec{r}} + \frac{q}{m}(\vec{E} + \vec{v} \times \vec{B}).\frac{\partial f}{\partial \vec{v}} = \left(\frac{\partial f}{\partial t}\right)_c, \tag{1.8}$$

where $\partial/\partial\vec{r}$ and $\partial/\partial\vec{v}$ are the gradients in configuration and velocity space respectively. The right hand side of equation (1.8) describes the evolution of the distribution function due to collision.

1.2.3 Fluid Theory

When the collisions between the plasma particles are very frequent, each species of the plasma particles follow a local equilibrium distribution function. Under this condition, each species can be treated as a fluid described by local density, velocity and temperature. The fluid approach describes the bulk properties of the plasma, so the unique trajectories

of all the particles as considered in single particle motion are not considered here. Instead of solving the Boltzmann-Vlasov equation for distribution function and integrating to get the quantities of interest, we can perform direct integration over Boltzmann-Vlasov equation and solve for the quantities of interest. This process is called taking the moments of the Boltzmann-Vlasov equation. The resulting equations are the basis of fluid theory. Zeroth moment of the Boltzmann-Vlasov equation gives the conservation of mass (continuity equation), first moment gives the conservation of momentum (force momentum balance equation) and second moment gives the conservation of energy (energy transport equation). The fluid model can be either single fluid model known as Magnetohydrodynamic (MHD) model or multi-fluid model.

1.2.3.1 Two Fluid Model

The fully ionized plasmas are treated more precisely by two-fluid model. Considering the plasma of two species (ions and electrons) in a fully ionized, isotropic and collisionless condition, the relevant equations are given as:

The continuity equation is

$$\frac{\partial n_j}{\partial t} + \nabla.(n_j \vec{v}_j) = 0, \tag{1.9}$$

where $j = i$ or e for ions and electrons respectively.

The momentum force balance equation is

$$m_j n_j \left[\frac{\partial \vec{v}_j}{\partial t} + (\vec{v}_j.\nabla)\vec{v}_j \right] = -\nabla p_j + q_j n_j (\vec{E} + \vec{v}_j \times \vec{B}). \tag{1.10}$$

The Maxwell's equations are:

$$\epsilon_0 \nabla.\vec{E} = \rho_q, \tag{1.11}$$

$$\nabla \times \vec{E} = -\frac{\partial \vec{B}}{\partial t},$$ (1.12)

$$\nabla . \vec{B} = 0,$$ (1.13)

and

$$\frac{1}{\mu_0} \nabla \times \vec{B} = \vec{J} + \epsilon_0 \frac{\partial \vec{E}}{\partial t}.$$ (1.14)

The equation of state is

$$p_j = C_j n_j^{\gamma_j},$$ (1.15)

where $\gamma = (c_p/c_v)$ is the ratio of specific heats.

The charge density ρ_q is given by

$$\rho_q = n_i q_i + n_e q_e.$$ (1.16)

The current density $\vec{J}$ is given by

$$\vec{J} = n_i q_i \vec{v_i} + n_e q_e \vec{v_e}.$$ (1.17)

1.2.3.2 One Fluid Model (MHD Model)

Under certain assumptions, plasma can be treated as a single fluid. The approach is called magnetohydrodynamics (MHD) where it does not differentiate between ions and electrons. This method is appropriate to apply in slowly varying conditions i.e. having relatively low frequencies ($\omega << \omega_p$ and $\omega << \omega_c$, where ω_p and ω_c are plasma and cyclotron frequencies respectively). This model can be applied in a highly ionised plasma with ions and electrons act in unison because of either strong external applied magnetic

field or frequent collisions among the particles. The MHD model can be applied to highly conducting plasma fluids, for example, interstellar medium, coronal loops, tokamaks etc. In this model, the multi-fluid equations are combined to give the set of equations for a single fluid. Firstly, we define the mass density and mass velocity as

$$\rho_m = n_i m_i + n_e m_e, \tag{1.18}$$

and

$$\vec{v} = \frac{1}{\rho_m}(n_i \vec{v}_i m_i + n_e \vec{v}_e m_e). \tag{1.19}$$

The simplified MHD equations for an isotropic plasma after neglecting the electron inertia (for a slowly varying plasma) and the Hall effect that arises because of current flow in a magnetic field can be written as

$$\frac{\partial \rho_m}{\partial t} + \rho_m \nabla.\vec{v} = 0, \tag{1.20}$$

$$\rho_m \frac{\partial \vec{v}}{\partial t} = -\nabla p + \vec{J} \times \vec{B}, \tag{1.21}$$

and

$$\vec{J} = \sigma(\vec{E} + \vec{v} \times \vec{B}) \tag{1.22}$$

These equations must be solved along with the reduced Maxwell's equations and equation of state as given below:

$$\nabla.\vec{E} = 0, \tag{1.23}$$

$$\nabla \times \vec{E} = -\frac{\partial \vec{B}}{\partial t}, \tag{1.24}$$

$$\nabla.\vec{B} = 0, \tag{1.25}$$

$$\nabla \times \vec{B} = \mu_0 \vec{J} \tag{1.26}$$

and

$$p\rho_m^{-\gamma} = constant. \tag{1.27}$$

Here, we have taken charge density $\rho_q = 0$ by assuming that there is no accumulation of space charge.

1.3   Alfvén Waves

In steady-state, the above MHD equations reduce to

$$\nabla p = \vec{J} \times \vec{B}, \tag{1.28}$$

$$\nabla \times \vec{B} = \mu_0 \vec{J} \tag{1.29}$$

and

$$\nabla.\vec{B} = 0. \tag{1.30}$$

Eliminating $\vec{J}$ we get

$$\nabla p = \frac{1}{\mu_0}(\nabla \times \vec{B}) \times \vec{B}. \tag{1.31}$$

The right hand side term of equation (1.31) can be written as
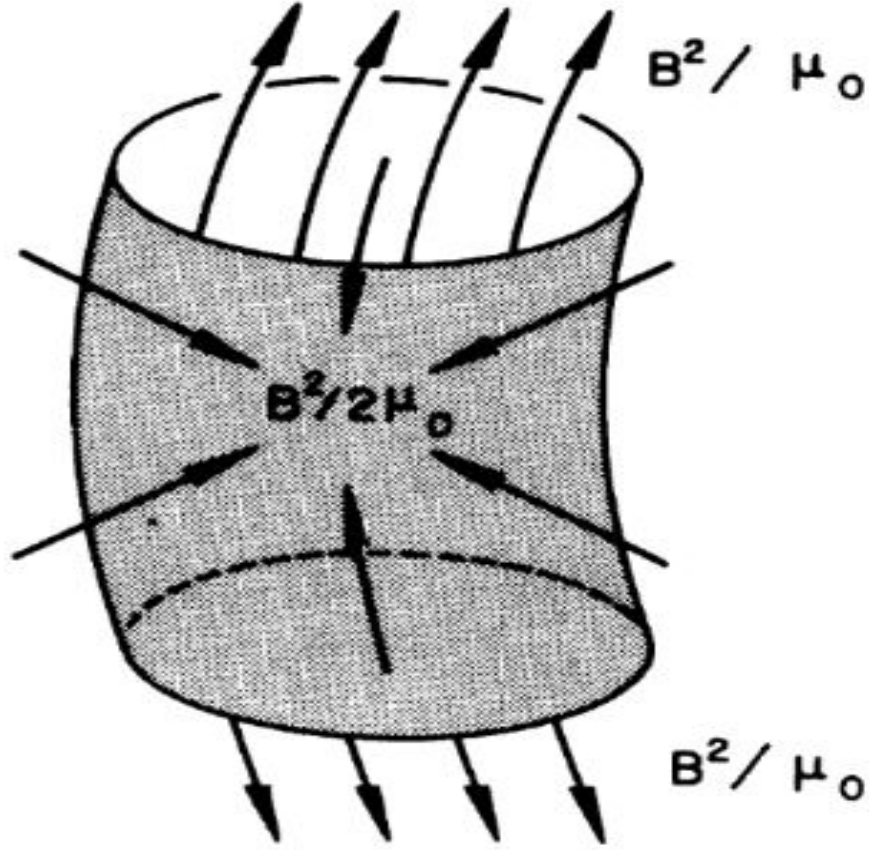
Fig. 1.2 The magnetic stress can be decomposed into two parts: (i) an isotropic magnetic pressure $B^2/2\mu_0$ and (ii) a magnetic tension B^2/μ_0 along the field lines (Bittencourt, (2004)).

$$(\nabla \times \vec{B}) \times \vec{B} = (\vec{B}.\nabla)\vec{B} - \frac{1}{2}\nabla(B^2) = \nabla.(\vec{B}\vec{B}) - \nabla.\left(\frac{1}{2}\mathbf{1}B^2\right), \qquad (1.32)$$

where $\mathbf{1}$ is a unit dyad. Now we define the magnetic stress dyad as

$$\tau^{(m)} = \frac{1}{\mu_0}(\vec{B}\vec{B} - \frac{1}{2}\mathbf{1}B^2). \qquad (1.33)$$

In matrix form, it can be written as

$$\tau^{(m)} = \frac{1}{\mu_0} \begin{pmatrix} (B_x^2 - B^2/2) & B_x B_y & B_x B_z \\ B_y B_x & (B_y^2 - B^2/2) & B_y B_z \\ B_z B_x & B_z B_y & (B_z^2 - B^2/2). \end{pmatrix} \tag{1.34}$$

.

Now equation (1.31) can be rewritten as

$$\nabla p = \nabla . \tau^{(m)} \tag{1.35}$$

or

$$\nabla . (\mathbf{1} p - \tau^{(m)}) = 0. \tag{1.36}$$

The stress tensor is positive if it is tensile, and negative if it is compressive. The negative stress tensor can be defined as the magnetic pressure dyad and it plays the same role as the fluid pressure dyad.

If we consider $\vec{B} = B\hat{\mathbf{z}}$, the off-diagonal elements of the magnetic stress dyad vanish.

$$\tau^{(m)} = \begin{pmatrix} -B^2/2\mu_0 & 0 & 0 \\ 0 & -B^2/2\mu_0 & 0 \\ 0 & 0 & B^2/2\mu_0 \end{pmatrix} \tag{1.37}$$

Thus, the principal stresses act like a tension B^2/μ_0 along the direction of the magnetic field, and a pressure $B^2/2\mu_0$ perpendicular to the direction of the magnetic field. We can also write the stress dyad as

$$\tau^{(m)} = \begin{pmatrix} 0 & 0 & 0 \\ 0 & 0 & 0 \\ 0 & 0 & B^2/\mu_0 \end{pmatrix} + \begin{pmatrix} -B^2/2\mu_0 & 0 & 0 \\ 0 & -B^2/2\mu_0 & 0 \\ 0 & 0 & -B^2/2\mu_0 \end{pmatrix}. \tag{1.38}$$

In this representation, the magnetic stress can be decomposed into two parts: (i) an isotropic magnetic pressure $P_B = B^2/2\mu_0$ and (ii) a magnetic tension $T_B = B^2/\mu_0$ along the magnetic field lines. The magnetic pressure $B^2/2\mu_0$ can always be combined with the kinetic fluid pressure. The magnetic tension B^2/μ_0 can be thought of as elastic cords acting in the fluid. Therefore, in a perfectly conducting fluid the plasma particles behave as if they are tied to the magnetic field lines. The theory of stretched string suggested that this tension may lead to a transverse wave propagating along the field lines, with speed $v_A = \sqrt{T_B/\rho_m} = B_0/\sqrt{\mu_0\rho_m}$, where ρ_m is the mass density of the conducting fluid. This wave is known as Alfvén wave which is a low frequency wave that exists in a conducting magnetized plasma.

Let us consider a system of uniform magnetic fields permeating to a perfectly conducting fluid, which are uniformly flowing initially to the magnetic field lines (figure 1.3(a)-1.3(e)). The fluid flow will distort the magnetic field lines, so magnetic field lines become curved as shown in figure 1.3(b). The curved magnetic field lines produce a Lorentz force on the conducting fluid that opposes the next curvature as explained by Lenz's Law. According to the Newton's second law, the Lorentz force changes the momentum of conducting fluid, which pushes it to minimize the magnetic field line distortion and restore the system in its equilibrium state.

Theoretically, Alfvén wave was first predicted by Hannes Alfvén (Alfvén, (1942)) in a perfectly conducting fluid. This prediction is of great importance because it gives a new option to understand the energy transportation in a conducting medium. Alfvén waves (AWs) were first experimentally demonstrated over seven years later in liquid mercury by Lundquist, (1949) and in sodium by Lehnert, (1954). Herlofson, (1950) investigated AWs and found it to be dispersive in nature. Wilcox et al., (1960) verified the speed of AWs and reflection of the wave from conducting and insulating end-plates in laboratory plasma experiment. Before the discovery of AWs only sound or acoustic waves were there due to the compressibility of the fluid. AWs are prominent due to their ubiquity in space
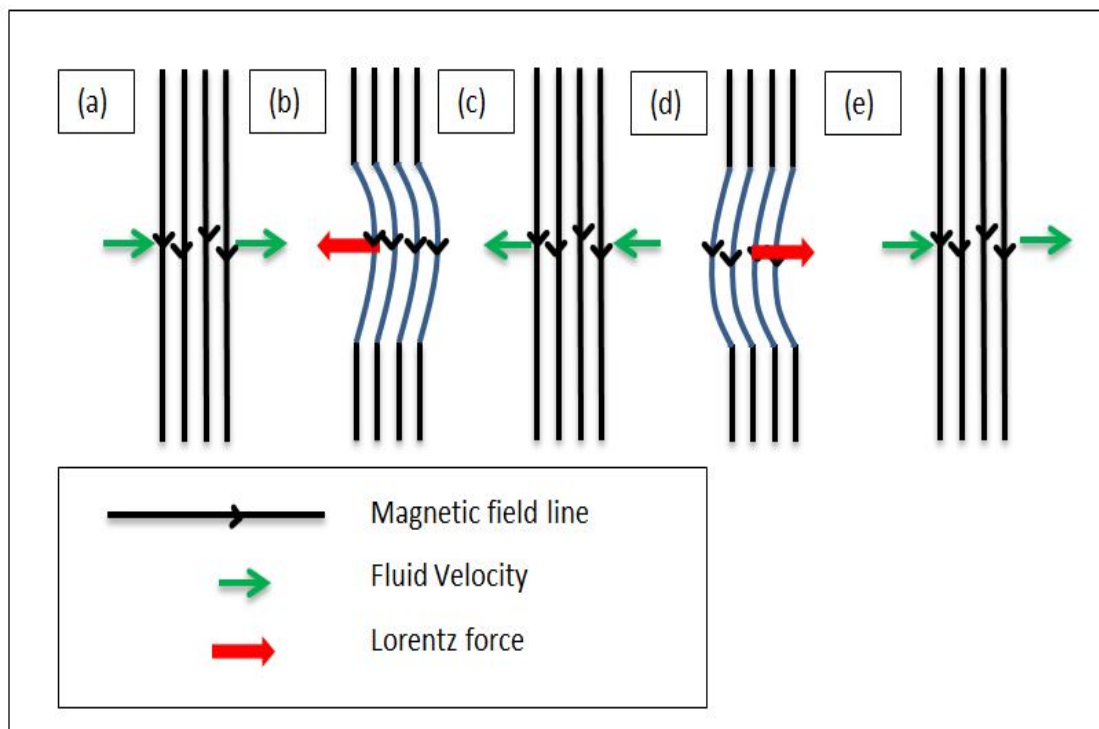
Fig. 1.3 Mechanism for forming Alfvén wave: (a) fluid velocity perpendicular to the uniform magnetic field (b) distorted magnetic lines giving rise to a Lorentz force that retards and eventually reverses the fluid velocity (c) field lines return to undisturbed position (d) reversed distortion and (e) repeats the cycle

and they can be easily excited via a variety of plasma instabilities (Hoshino & Goldstein, (1989)). AWs were observed at the solar wind (Belcher & Davis, (1971)), the Earth's magnetosphere (Voigt, (2002)), the solar photosphere (Nakariakov et al., (1999)) and the interplanetary plasma (Tsurutani & Ho, (1999)).

There are two distinct types of Alfvén waves, known as torsional and compressional Alfvén waves. The torsional wave is also known as the shear Alfvén wave (SAW). The torsional waves do not propagate at frequencies above the ion cyclotron frequency, so these waves are not appropriate in cold plasma. When the wave frequency reaches near the ion cyclotron frequency, it is usually called the ion cyclotron wave. The compressional waves (produced by the combined effects of plasma thermal and magnetic pressures) are also known as magnetoacoustic or magnetosonic waves. Above the ion cyclotron frequency the compressional waves are known as whistler waves, while at frequencies near the electron cyclotron frequencies, they are known as the electron cyclotron waves. In this thesis, we consider only torsional/ shear Alfvén waves.

The shear Alfvén wave characteristics depend on the length of the ion gyroradius (ρ_s) or the electron skin depth (λ_e) of the plasma. When the transverse wavelengths of AWs are comparable to the main kinetic length scales of the plasma, such as λ_e or ρ_i or ρ_s (whichever is longer) where λ_e is the electron inertial length, ρ_i is the ion gyroradious and ρ_s is the ion acoustic gyroradius, the AWs become dispersive and known as dispersive AWs (DAWs) (Kletzing, (1994)). The DAWs can be classified into two categories: the inertial Alfvén waves (IAWs) when $\lambda_e > \rho_i$ or ρ_s and the kinetic Alfvén waves (KAWs) when ρ_s or $\rho_i > \lambda_e$. The dispersive properties of AWs are determined by a dimensionless plasma parameter defined as $\beta = 8\pi n_0 T_e / B_0^2 = (m_e/m_i)(2v_{Te}^2/v_A^2)$, where $v_{Te}^2 = T_e/m_e$ is the square of electron thermal speed. For low-β plasma ($\beta << m_e/m_i$), which is the case of IAWs, the wave speed is greater than the electron thermal speed $v_A >> v_{Te}$. For intermediate-β plasma ($m_e/m_i << \beta << 1$), which is the case of KAWs, the wave speed is less than the electron thermal speed $v_A << v_{Te}$. The IAWs are applicable in

cold plasmas (e.g., the Earth's auroral region) whereas the KAWs are applicable in hot plasmas (e.g., solar corona and solar wind) (Vincena et al., (2004)). In the kinetic limit, the electrons have enough speed to respond adiabatically to the changes in the wave field. Many studies have supported that the dispersive properties of DAWs can explain the plasma particle heating in solar wind and corona (De Azvedo et al. 1994; Voitenko, 1995; Voitenko, 1996; Elfimov et al. 1996; Asgari-Targhi and Van Ballegooijen, 2012; Morton, 2015; Testa et al. 2014).

The dispersion relation for the DAWs can be defined by the determinant of the 2×2 matrix as derived by Lysak & Lotko, (1996):

$$\det \begin{pmatrix} \frac{c^2}{v_A^2} \frac{1-\Gamma_0(\mu_i)}{\mu_i} - n_\parallel^2 & n_\parallel n_\perp \\ n_\parallel n_\perp & \frac{\Gamma_0(\mu_e)}{k_\parallel^2 \lambda_e^2}(1 + \chi \mathbf{Z}(\chi)) - n_\perp^2 \end{pmatrix} = 0. \tag{1.39}$$

By assumung $c^2/v_A^2 >> 1$ and $k_\parallel^2 \lambda_e^2 << 1$, we can drop the unit terms in the diagonal elements. The other notations are $n_\parallel = k_\parallel c/\omega$, $n_\perp = k_\perp c/\omega$, $\mu_i = k_\perp^2 \rho_i^2$, $\mu_e = k_\perp^2 \rho_e^2$, $\chi = \omega/k_\parallel a_e$, $a_e = (2T_e/m_e)^{1/2}$ (average electron thermal speed) and Γ_0 is the modified Bessel function $\Gamma_0(\mu) = \exp^{-\mu} I_0(\mu)$ and $\mathbf{Z}$ is the usual plasma dispersion function.

The solution of equation (1.39) can be written as (Lysak & Lotko, (1996))

$$\left(\frac{\omega}{k_\parallel v_A}\right)^2 = \frac{\mu_i}{1 - \Gamma_0(\mu_i)} + \frac{k_\perp^2 \rho_s^2}{\Gamma_0(\mu_e)[1 + \chi \mathbf{Z}(\chi)]}, \tag{1.40}$$

where $\rho_s^2 (= c_s^2/\Omega_i^2 = T_e/m_i\Omega_i^2)$ is the ion acoustic gyroradius, Ω_i is the ion gyrofrequency and c_s is the ion acoustic speed.

For small ion gyroradius, $\Gamma_0(\mu_i) \approx 1 - \mu_i + (3/4)\mu_i^2$, then we have

$$\frac{\mu_i}{1 - \Gamma_0(\mu_i)} \approx 1 + \frac{3}{4}\mu_i. \tag{1.41}$$

By using $\chi << 1$ for hot electrons and $\Gamma_0(\mu_e) \approx 1$ for small electron gyroradius, as valid in the case of KAWs, equation (1.40) can be written as

$$\left(\frac{\omega}{k_\parallel v_A}\right)^2 \approx 1 + k_\perp^2\left(\rho_s^2 + \frac{3}{4}\rho_i^2\right). \tag{1.42}$$

This can be recasted as

$$\left(\frac{\omega}{k_\parallel v_A}\right)^2 \approx 1 + k_\perp^2\rho_s\left(\frac{3}{4} + \frac{T_e}{T_i}\right). \tag{1.43}$$

Here, the term containing 3/4 is from the expansion of Bessel functions and the term containing T_e/T_i is because of electron pressure effect.

For cold plasma where $\beta << m_e/m_i$, electron inertia rather than the finite ion gyroradius or electron pressure is the dominant effect. Therefore, for IAWs, neglecting the electron gyroradious, we get

$$1 + \chi Z(\chi) \approx -\frac{1}{2\chi^2} = -\frac{k_\parallel v_e}{\omega}^2, \tag{1.44}$$

where $v_e = T_e/m_e = a_e^2/2$. Thus, equation (1.40) can written as

$$\left(\frac{\omega}{k_\parallel v_A}\right)^2 = \frac{\mu_i}{1 - \Gamma_0(\mu_i)} - \left(\frac{\omega}{k_\parallel v_e}\right)^2\frac{k_\perp^2 c^2}{\omega_e^2}, \tag{1.45}$$

i.e.

$$\left(\frac{\omega}{k_\parallel v_A}\right)^2 = \frac{\mu_i}{1 - \Gamma_0(\mu_i)}\frac{1}{1 + k_\perp^2\left(\frac{c^2}{\omega_{pe}^2}\right)}. \tag{1.46}$$

By reducing the ion gyroradious to zero, as valid for IAWs, the first factor in equation (1.46) becomes unity.

$$\left(\frac{\omega}{k_\parallel v_A}\right)^2 = \frac{1}{1 + k_\perp^2\left(\frac{c}{\omega_{pe}}\right)^2}. \tag{1.47}$$

$$\frac{\omega^2}{k_\parallel^2 v_A^2} = \frac{1}{1 + k_\perp^2\lambda_e^2}\qquad\qquad . \tag{1.48}$$

For $k_\perp^2 \lambda_e^2 << 1$, the IAW dispersion relation reduces to MHD Alfvén wave dispersion relation ($v_A^2 = \omega^2/k_\parallel^2 = B_0^2/4\pi\rho_m$). At $k_\perp^2 \lambda_e^2 >> 1$ limit, the IAW loses its electromagnetic characteristic (Okuda & Dawson, (1973)).

Comparing equations (1.46) and (1.48), we find that the parallel phase velocity of the wave increases because of the effect of electron pressure and ion gyro radius while it decreases because of the effect of electron inertia.

1.4 Sun and Solar Wind: Plasmas in the Heliosphere

Plasma in the interplanetary space originates from the Sun and due to its high pressure, it escapes out as solar wind interacting with the magnetic fields of many planets. The solar wind extends far beyond the orbit of the outermost planet, Pluto, inflatting a cavity in the surrounding interstellar medium called the heliosphere. The solar wind is laced with the solar magnetic field caused by the currents flowing near the surface of the Sun. So the solar magnetic field is frozen-in into the solar wind. Heliospheric research can give us about the behabior of the solar wind near the Earth, interaction of the heliosphere with the interstellar medium, origin and evolution of solar wind and the interstellar cosmic rays.

1.4.1 The Sun

For an astrophysicist, the Sun is a typical $G2$ main-sequence star of luminosity V and brightness of absolute magnitude 4.8. It has surface temperature of about 5,780 K, radius of about $696,000 km$ (about 109 times that of the Earth) and mass of about $2 \times 10^{30} kg$. The mean distance from the Sun to the Earth is approximately $149.6 \times 10^6 km$ (known as 1 Astronomical Unit ($1AU$)). A large and violent eruptions take place on the Sun due to surface and coronal activities like sunspots, coronal mass ejections (CMEs), solar X-ray flares, faculae, prominences and coronal holes.
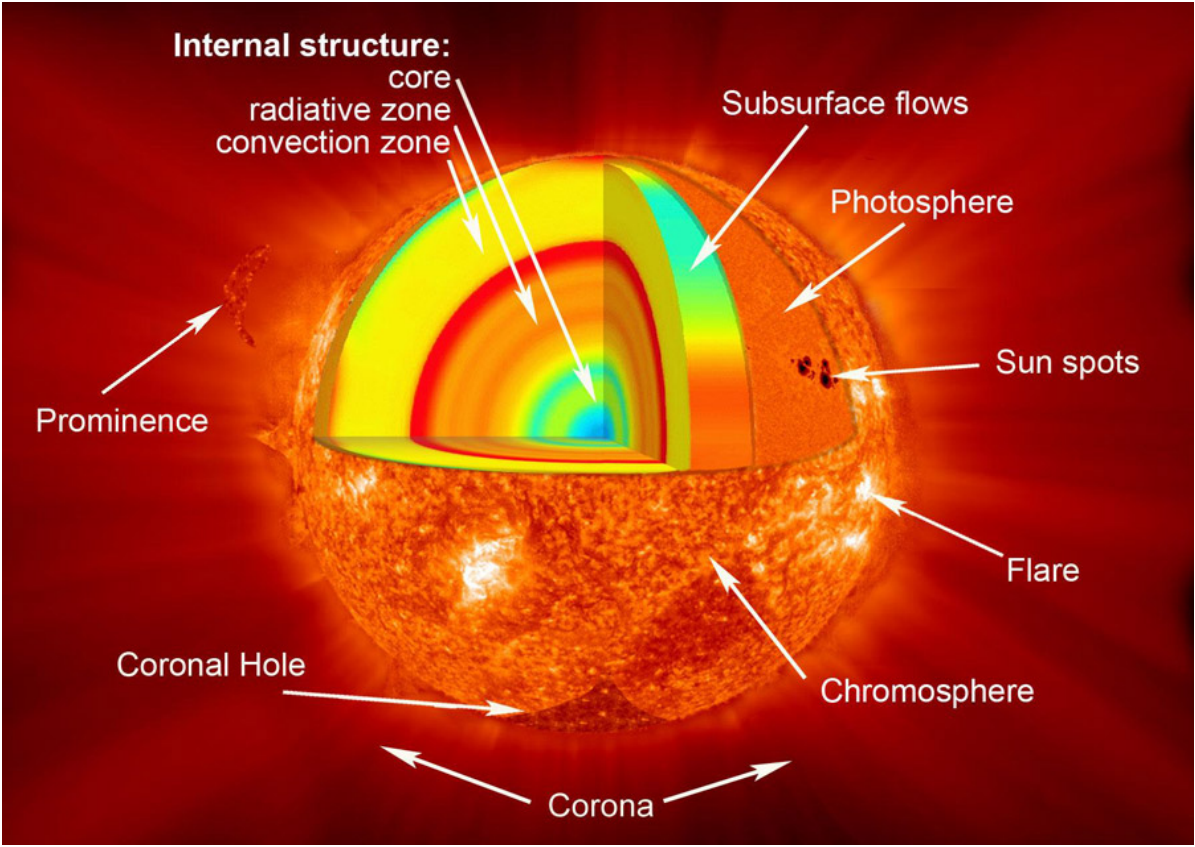
Fig. 1.4 Shows the internal structures of the sun as clipped from SOHO (Solar and Heliospheric Observatory) by ESA and NASA.

The Sun is oblate spheroid in shape and consists mostly hot hydrogens in plasma state. The hot hydrogen plasma is tenuous and gaseous near the Sun's surface, which gets denser down toward the Sun's core. Equatorial zones of the Sun rotate more rapidly than high latitude regions, causing differential rotation. Near the equator, the Sun rotates once in about every 25 days and it is about 36 days near the poles. Since the Sun is the nearest star to us, we can study not only its electromagnetic radiations but also solar emissions of different kinds of plasmas and energetic particles. The Sun is a magnetic variable star that fluctuates on time scales ranging from a fraction of a second to billions of years. Many forms of solar activities driven by the solar magnetic fields, such as solar flares, coronal mass ejections, high speed solar winds and solar energetic particles take place on the Sun.

The internal structure of the Sun is divided into three different regions: core, radiative and convective zones. Nuclear fusion which is the source of the Sun's thermal energy, takes place in the core region located at a radious of 0.3 times the radius of the Sun. The temperature of the core is about $15MK$ and the pressure is estimated at 265 billion bar. At the center of the core the density of the Sun is about $150gm/cm^3$ (approximately 10 times the density of gold and 150 times of water). The fusion energy is transported outward from the core to the radiative and convection zones by the process of radiation and convection respectively. The top layer of the convection zone is the photosphere where light (photon) is emitted. This visible photosphere has temperature of around $5780K$ and density of about $10^{-9}gm/cm^3$.

1.4.2   Solar Corona

Above the photosphere, the solar atmosphere is divided into three regions: (1) the choromosphere (2) the transition region and (3) the corona. The corona can not be seen usually by naked eyes because it is hidden by the bright light of the Sun's surface. However, it can be seen in visible light during a total solar eclipse as a structured,

irregular ring of rays around the solar disk. The solar corona extends many thousands of kilometers from the chromosphere with temperature of around $1.6MK$ and it emits X-rays (soft and hard) and ultra-violet radiations. Information about the source of the radiation is carried by each wavelength of the light emitted. Therefore, soft x-ray detectors provide a new tool to understand the physics of the solar atmosphere. At the solar photosphere, the temperature is about $5780K$. Instead of decreasing the temperature as one moves farther away from the heat source, the temperature of the solar corona is found approximately $1.6MK$. This extreme hot temperature of the corona needs an efficient heating mechanism. Several mechanisms have been proposed to account for this, but there has not been a fully agreed consensus theory till now (Schmelz, (2003)). The solar magnetic field plays a very important role in heating of the solar corona. Although, majority of the solar coronal plasma is confined by the solar magnetic field in the form of closed loops and twisted arcade-like structures, some coronal plasma expands into the interplanetary space as a supersonic outflow known as the solar wind.

1.4.3 Solar Wind

The solar wind results from the expansion of the outermost solar atmosphere from the solar corona, forming a supersonic flow of ionized plasma and magnetic field that permeates into the interplanetary medium. In the solar corona, plasma is continually heated to reach the condition that it can not be hold by the Sun's gravity. For the first time, the existence of solar wind was predicted by Parker in 1958 and later confirmed and measured by spacecraft observations (Brandt, (1970); Hundhausen, (1972)); Gringauz et al., (1960); Neugebauer & Snyder, (1962)). The constituents of the solar wind are mostly protons, alpha particles (He^{2+}), heavier minor ions (Bame et al., (1977)) and some negligible presence of neutral atoms (Petelski et al., (1980)). The solar wind expands upto a heliocentric distance of about $90AU$ in the solar system (Stone et al., (2005); Burlaga et al., (2008)). The solar wind flow can transport the energy over a

wide range of spectra of magnetic field fluctuations via the nonlinear wave-wave and wave-particle interactions (Goldstein et al., (1995); Bruno & Carbone, (2005)). The connection between solar activity and the Earth's magnetic field disturbance had been observed since the nineteenth century (Sabine, (1851); Stewart, (1861)). Near the Earth the average density of solar wind is about $10cm^{-3}$.

Mostly solar wind has been categorized into three types (Srivastava & Schwenn, (2000)) based on the varying boundary conditions (magnetiic field configurations) in the corona. They are (a) fast wind originating from large coronal holes (open magnetic fields) with velocities between $500km/s$ to $800km/s$, (b) slow wind originating from closed field regions such as small coronal holes and active regions, and the boundary layers of coronal streamers with velocity between $300km/s$ and $500km/s$ and (c) the variable transient solar wind such as coronal mass ejections driven through magnetic flux emergence and reconnection. The Ulysses spacecraft demonstrated such types of winds originating from the solar corona (Phillips et al., (1995); McComas et al., (1998); McComas et al., (2000); McComas et al., (2003); Ebert et al., (2009)). Although the study of solar coronal heating problem has been many decades, the physics of the heating mechanism has not been resolved till now.

1.4.4 The Magnetosphere

The interaction of the supersonic solar wind plasma with the Earth's dipole magnetic field forms a cavity, called the Earth's magnetosphere. The solar wind distorts the dipole magnetic field of the Earth, compressing the dayside and stretching the nightside out into a magnetotail. The magnetosphere consists of many interacting subsystems of both local (scale size of ~ 1 km) and global (scale size of 3×10^5 km). It can show turbulent and chaotic behaviors. Figure (1.5) shows the different geographical regions of the magnetosphere. Since the Earth's magnetosphere acts as an obstacle to the supersonic flow of the solar wind, the flow speed becomes subsonic forming a shock wave

at bow shock region. In this region, the solar wind plasma is heated, compressed and deflected around the magnetospheric obstacle. The boundary that separates the Earth's magnetosphere from the solar wind plasma is called the magnetopause region. In this region, the pressure of the Earth's magnetic field balances the dynamical pressure of the solar wind plasma. The region between the bow shock and the magnetopause is called the magnetosheath region. The dipolar region or inner magnetosphere consists of radiation belts and plasmasphere which can trap the plasma energetic charged particles due to the Earth's magnetic field. The plasmasphere is of doughnut-shape and it is the innermost region of the Earth's magnetosphere. It traps the cold plasma i.e. low energy charged particles centred around the Earth's equator and corotats with the Earth. The plasmasphere extends just above the upper ionosphere upto the altitude of $4.5 - 8.5$ Earth radii depending upon the geomagnetic conditions. The radiation belts which can trap highly energetic charged particles, are partly overlap with the plasmasphere. The inner Van Allen belt extends typically in between $1 - 2$ Earth radii and the outer Van Allen belt is located at the altitudes of around $4 - 7$ Earth radii. The dayside magnetosphere is compressed, while the night side is stretched, leading to form the magnetotail region of cylindrical volume of length $100's$ of Earth radii. The hot plasmas in the magnetotail region resides inside the plasma sheet region. The magnetotail acts as a magnetic energy reservoir that pumps several magnetospheric processes such as substorms. The direction of global energy convection in the magnetosphere is from nightside to dayside as opposite to the solar wind flow direction. Near the two poles of the Earth's magnetic field, the solar wind plasma can penetrate deep inside the magnetosphere along the Earth's field lines. These two regions are called cusp regions. When some of the solar wind plasmas enter inside the Earth's atmosphere, the ions of the solar wind collide with oxygen and nitrogen atoms from ionospheric atmosphere, releasing energy to produce visible airglow. It forms a visible ring called auroral zone around the polar regions of the Earth.

In the solar wind-magnetosphere coupling, when the solar wind changes in such a way as to invert the orientation of the IMF lines, the tail of the magnetosphere gets compressed and it can form magnetic reconnection. Two flows of plasma with anti-parallel magnetic fields are brought together at an x-type neutral line. The magnetic field lines are frozen in the plasma at far from the neutral line, however, it is unfrozen near the neutral line. Therefore, near the neutral line, the magntic field diffuses through the plasma, giving a new configuration of magnetic field lines. The x-type neutral line has a separatrix region that divides the inflowing plsama from the outflows of highly energetic particles. Inside the Earth's magnetosphere, there are two major regions of reconnection: (1) on the dayside magnetopause and (2) in the magnetotail. The reconnection helps the plasma energization process by converting the magnetic energy to particle-wave energy. Magnetic reconnection occurring on the dayside magnetopause can make the plasma particles infiltrate the ionosphere to form aurorae glow and can disturb the Earth's communication networks.
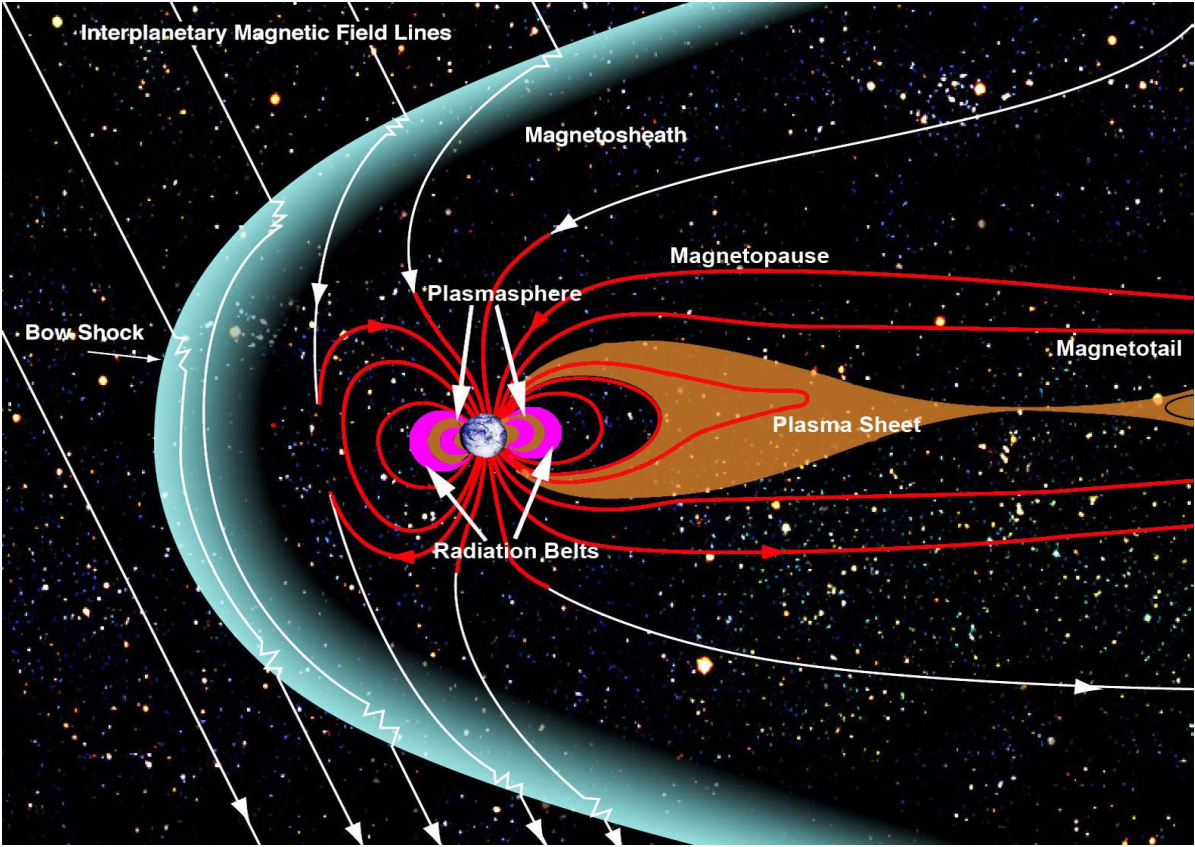
Fig. 1.5 Shows the solar wind magnetosphere system of Earth's environment as clipped from NASA/Goddard/Aaron Kaase

1.5   Importance of Alfvén Waves.

Alfvén waves play an important role in the dynamics of space and laboratory plasmas such as auroral ionosphere (Stasiewicz et al., (2000)), solar coronal plasma heating (Shukla et al., (2006) (Wu & Yang, (2007)), tokamak plasma heating (Vlad et al., (1999)) and large plasma devices (Carter & Dorfman, (2014)). They are mostly observed in the solar wind (Tu & Marsch, (1995); Coleman, (1966); Unti & Neugebauer, (1968); Belcher & Davis, (1971)), magnetosheath (Sahraoui et al., (2003)), auroral region (Stasiewicz et al., (2000)), solar flares (Melrose, (1992)), solar corona (Tomczyk et al., (2007)), the Earth's core (Bloxham et al., (2002)), and the other magnetized planets (Vinas et al., (1984)).

In magnetosphere, where the magnetosphereic plasma is hot and electron thermal speed exceeds the Alfvén speed, the kinetic Alfvén wave (KAW) is more appropriate while in cold plasma at low altitudes up to $3 - 4Re$ (geocentric distance), where the electron thermal speed becomes much smaller that the Alfvén speed, then the inertial Alfvén wave (IAW) is more appropriate.

The Alfvén wave behaves as an energy carrier in space plasma. Hasegawa, (1976) proposed that AWs are also responsible for particle acceleration in the auroral plasma. The heating of the solar corona by resonant absorption of AWs can provide the heat input wave pressure (ponderomotive force) mandatory to heat and accelerate the high speed solar wind (Hollweg, (1985); Parker, (1991)). The idea of large amplitude Alfvén waves propagating from corona to solar wind has stimulated that these waves play a prominent role to energize the solar wind (Belcher & Davis, (1971)).

The solar coronal heating problem has been raised from many decades since the corona was first demonstrated to consist of plasma with a temperature of around 1 MK. This temperature is much higher than the Sun's surface (photosphere) temperature of approximately 6000 K (Klimchuk, 2006). In various astrophysical phenomana, the plasma heating and particle energization processes take place. In recent decades there

are several theories to address the heating mechanisms and the results are compared with the data available from the space missions. Some prominent theories are wave-wave interaction(Yukhimuk et al. 2000), wave-particle interaction (Cairns et al. 2005), magnetic reconnection (Birn and Priest, 2007; Birn et al. 2012; Parnell and De Moortel, (2012)), turbulence in solar wind (Velli et al. 2015; Van Ballegooijen et al. 2011; Retino et al. (2008)) and shock wave formation (Reale, (2014); Feldman et al. (1983); Longcope and Tarr, (2015); Bareford and Hood, (2015))

The DAWs have parallel electric field (w.r.t. the ambient magnetic field) perturbations that can accelerate and heat plasma particles. The parallel electric field of DAW leads to Landau damping and coronal heating in space plasma (Stefant, (1970); Lysak & Lotko, (1996)). So, the KAW/IAWs are responsible for the transportation of energy from larger spatial scales to smaller spatial scales (Tsiklauri et al., (2005)). One such type of energy transportation is due to the transverse collapse of the magnetic coherent structures leading to the formation of magnetic filaments parallel to the ambient magnetic field (Champeaux et al., (1997); Champeaux et al. (1998); Lavender et al., (2001); Lavender et al., (2002)). These filamentary structures are in various regions of the solar and magnetospheric plasmas (Van Ballegooijen, (2004)), such as the solar corona, near the Earth's bow shock (Alexandrova & Mangeney, (2004)) and the auroral regions (Luhr et al., (1994)).

Many studies suggested that the interaction of AWs with different plasma regimes can form magnetic filamentary structures (Shukla & Stenflo, (1989); Champeaux et al., (1997); Shukla & Sharma, (2001); Shukla et al., (2004)). Several authors have also studied the filamentation of AWs via nonlinear Schrödinger equation (Champeaux et al., (1997); Lavender et al., (2002); Passot & Sulem, (2003)). However, there is still no consensus on the mechanism that is responsible for coronal heating and it remains as an unsolved problem (Klimchuk, (2006); Schmelz and Winebarger, (2015)).

1.6 Turbulence in Space Plasma

The turbulence is a ubiquitous phenomenon in a magnetized plasma fluid. Together with wavelike phenomena, turbulence exhibits characteristics of self-organization in the form of coherent structures such as magnetic filaments and electric current sheets in magnetized plasmas or vortices in rotating fluids. Therefore, the complexity of turbulent flows can also be studied through their deterministic coherent structures. The turbulent fluctuations are not fully random, but must necessarily consist of random phase and coherent phase. For example, the Dirac delta function can be decomposed into a set of plane waves by Fourier transform. All the constituent waves have the same phase and amplitude, which is helpful to check the phase coherence in the spatial domain. If the generated coherent structures are Gaussian bell, then the Fourier transform of the wave field is again a Gaussian. So, the bell-shaped coherent structures have the wavenumber range in phase coherence. If the coherent structures move without changing its form, then the group velocity of the waves should be same. This type of coherent structures no longer follows the dispersion relation in the linear mode (Nariyuki & Hada, (2006)).

The turbulent astrophysical plasmas and magnetic fields can be found in many parts of the solar system such as solar atmosphere, interplanetary space, the atmosphere of stars, and planetary magnetospheres. The study of turbulence in an electromagnetically conducting fluid is important to solve space plasma physics problems like coronal heating, acceleration and transport of galactic cosmic rays, and the magnetic reconnection process in the magnetosphere.

The power density spectrum of turbulence in the solar system environment shows a power-law in frequency and wavenumber, which represents the energy cascade and multi-scale interactions (wave-wave interaction or wave-particle interaction). The energy can be transferred in turbulence by two ways, either direct cascade or inverse cascade mechanisms. In direct cascade mechanism, the energy is transferred from large scales to small scales, while in inverse cascade mechanism the energy is transferred from small
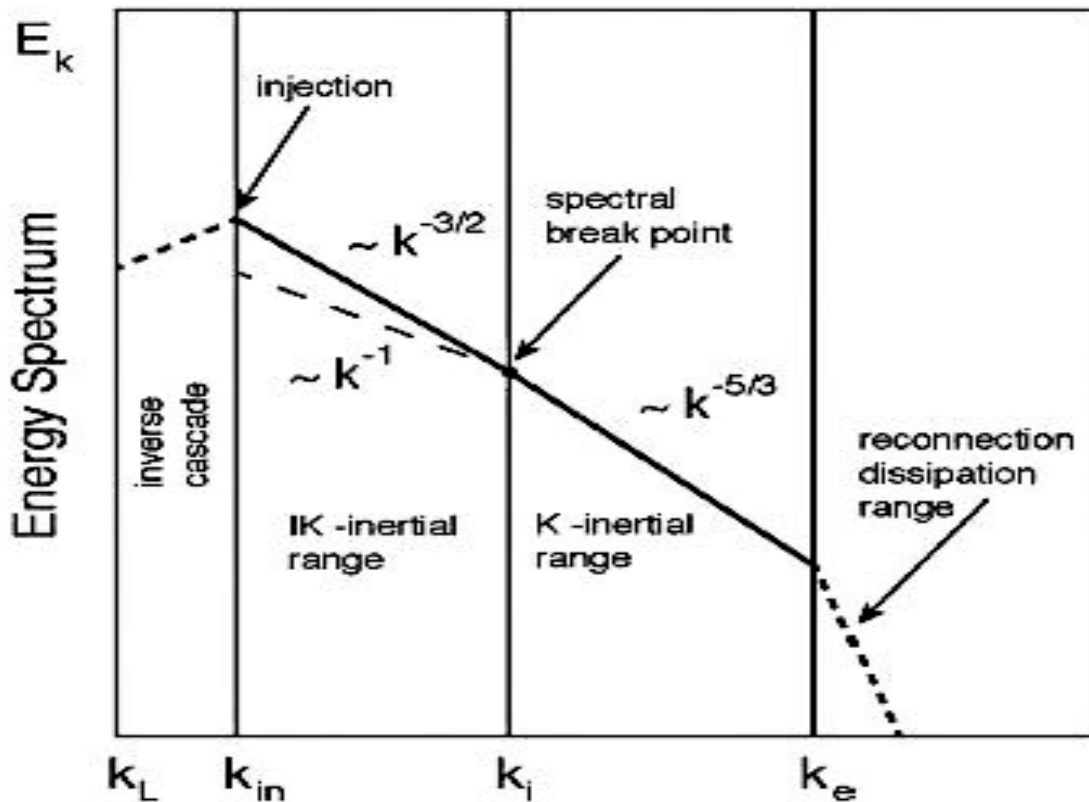
Fig. 1.6 Power spectra of solar wind in collision-less magnetohydrodynamic turbulence (Treumann et al., (2015))

scales to large scales. In most of the theories of turbulence, the energy injected into larger spatial scales is converted into the smaller spatial scales (or eddies) until it reaches the scales at which the turbulence energy interaction with plasma particles produces plasma heating.

To understand the intermittency of solar wind turbulence, Treumann et al., (2015) proposed structure of inertial range spectrum (Figure (1.6) in collision-less MHD Alfvénic turbulence evolving into a system of scale L, when the energy is injected into large- scale eddies of wave number $k_{in} = 2\pi/l_{in} >> k_L = 2\pi/L$. These structures indicate that the spectra of fluctuations can be divided into three ranges. At the largest scale, it is "energy containing scale" that provides the reservoir tapped by the turbulent cascade system. The inertial range or intermediate range is characterized by power law spectra, where

the nonlinear, inertial term in the equation of motion dominates over the dissipation. The inertial range categorized into two regions: Iroshnikov-Kraichnan (IK) inertial range and Kolmogorov (K)inertial range (Goldstein et al., (1995); Iroshnikov, (1964); Kraichnan, (1965a)). In IK-inertial range, the energy cascades from large-scale eddies to small-scale eddies in Alfvénic range, which is determined by the Alfvénic interaction time ($\tau_A = l_A/v_A$) leading to $k^{-3/2}$ spectral shape (Kraichnan, (1965b)). While in K - inertial range, the small-scale eddies reach to ion inertial scales ($k_i = 2\pi/\lambda_i$) and these eddies enter to the three-dimensional Kolmogorov range with spectral shape of $k^{-5/3}$ (Kolmogorov, (1991)). Further, when the width of the current eddies reach to the electron scale ($k_e = 2\pi/\lambda_e$), it is known as dissipation range. At this small scale dissipation range the fluctuations are converted to thermal energy, which can lead to heating of the solar plasma. The proposed spectral shape (figure 1.6) also demonstrates that the two different slopes merge at the spectral break point as confirmed by analyzing the spacecraft data from Mariner 10, CLUSTER, MESSENGER and Ulysses observations closer to the Sun (Alexandrova et al. (2009); Perri et al. (2010); Perri et al., (2011)).

Mostly three types of MHD turbulence theories were proposed to understand the energy transfer process in a magnetized plasma. These are Kolmogorov 1941 theory (K41) Kolmogorov, (1991), Iroshnikov-Kraichnan Theory (IK) and Goldreich-Sridhar Theory (GS). From the previous priori MHD turbulence assumptions, the energy spectrum is function of k, due to isotropic condition. The energy per wavenumber of MHD turbulence is $E(k) = \in^{\alpha'} k^{\beta'}$, where α' and β' are introduced to correct the physical dimension for kinetic energy spectrum. The $E(k)$ and $\in$ (dissipation rate) has the dimension $[L]^3[T]^{-2}$ and $[L]^2[T]^{-3}$. The obtained solution of energy per wavenumber is $\alpha' = 2/3$ and $\beta' = -5/3$. From Kolmogorov 1941 theory, the energy spectrum as a function of wavenumber in the inertial range of isotropic stationary turbulence is written as

$$E(k) = C_k \in^{2/3} k^{-5/3} \tag{1.49}$$

where C_k is the Kolmogorov constant having the value of 1.7 ± 0.2 (Bohr et al., (1998)). The similar dimensional analysis was done by (Iroshnikov, (1963); Kraichnan, (1965a) and it is known as Iroshnikov-Kraichnan (IK) theory. The time scale of wave interaction can be written as $\tau \sim [zk]^{-1}$ where $z(= \sqrt{b_0^2 + v_0^2})$ is the unit of velocity, v_0 and b_0 are the root mean square of velocity and magnetic field fluctuations respectively. The dimensions of different parameters are: the energy dissipation rate $\in = [L]^2[T]^{-3}$, the propagation velocity $b_0 = [L][T]^{-1}$, the wavenumber $k = [L]^{-1}$ and the energy per wavenumber $E(k) = [L]^3[T]^{-2}$. Then using the relation $\in = b_0^{\alpha'} k^{\beta'} E(k)^{\gamma'}$, the solution of one-dimensional isotropic cascade of energy spectra can be written as

$$E(k) = C_{IK}(\in b_0)^{1/2} k^{-3/2} \tag{1.50}$$

where C_{IK} is a constant that can be determined from experiments. IK-theory reasoned that the magnetic and kinetic energies of AWs are expected to be equal. Thus, if removing the background magnetic field and forcing turbulent system with kinetic energy at a scale larger than the inertial range, then the turbulent system returns to K-41 cascade. This has been verified via simulation by Muller et al., (2005)). Therefore, the background magnetic field reduces the strength of the nonlinear cascade from larger scale to dissipation scale.

Goldreich & Sridhar, (1995) presented the first anisotropic theory for the inertial range of strong incompressible MHD turbulence, which is known as GS theory. In this theory the linear time-scale is proportional to the magnetic field strength and nonlinear time-scale is proportional to the intensity of nonlinear interaction of magnetic fields. The assumption of this theory is to consider the nonlinear and linear time-scale as equal, which is called as "critical balance". This theory also assumes that the nonlinear cascade is purely two-dimensional in the perpendicular plane and has a three-dimensional MHD turbulence characteristic. Thus, the energy spectra in the perpendicular plane is proportional to $E(k_\perp) \propto k_\perp^{-5/3}$ and parallel wave vector is proportional to $k_\parallel \propto k_\perp^{2/3}$.

Then Goldreich & Sridhar, (1995) formulated the three-dimensional energy spectrum in MHD turbulence as

$$E(k_\perp, k_\parallel) = C_{GS} \frac{v_A^2}{k_\perp^{10/3} L^{1/3}} g' \left(\frac{k_\parallel L^{1/3}}{k_\perp^{2/3}} \right) \tag{1.51}$$

where C_{GS} is a dimensionless constantand, L is the dimensionless constant and energy containing at length-scale, g' is a dimensionless quantity. When we integrate the three-dimensional energy spectrum, it reduces to one-dimensional energy spectrum for perpendicular and parallel wave vectors (Tessein et al., (2009)) with $E(k_\perp) \propto k_\perp^{-5/3}$, $E(k_\parallel) \propto k_\parallel^{-2}$. Thus, the GS theory and IK theory are contradicting to each other.

The IK and GS MHD turbulence theories are the mostly accepted theories for the isotropic and anisotropic plasma fluids respectively. There are also many other MHD turbulence theories related to solar plasmas. These models can be classified as weak and strong turbulence, and balanced and imbalanced turbulence. The weak turbulence arises on account of the resonant condition that limit the volume of the interacting wave vectors. In strong turbulence there is no such limit (Kadomstev, (1965); Galtier et al., (2000); Gogoberidze et al., (2009)). If there is equal amount of energy transferred in the cascade for both Elsasser variables ($z^\pm$), then it is balanced turbulence, otherwise it it is imbalaced turbulence (Lithwick et al., (2007); Perez & Boldyrev, (2009)). Boldyrev (2005) proposed strong balanced turbulence having small scale eddies of three-dimensional anisotropy with energy spectrum $E(k_\perp) \sim k_\perp^{-(5+\alpha')/(3+\alpha')}$ where $\alpha' = 0$ for Kolmogrove theory (K41) and $\alpha' = 1$ for IK theory. There are few distinct theories proposed by researchers for imbalance turbulence on cascade and dissipation (Chandran, (2008); Beresnyak & Lazarian, (2009); Perez & Boldyrev, (2009); Podesta & Bhattacharjee, (2010)).

It is well known that the inertial range hydrodynamic turbulence is isotropic; whereas with the presence of the background magnetic field, the MHD turbulence becomes anisotropic (Shebalin et al, (1983); Oughton & Matthaeus, (2005)). However, energy

transferred along the magnetic field is weak compared to the energy transfered in the perpendicular direction. The energy of turbulent fluctuation in the solar wind is not distributed isotropically over the wavenumber space. Matthaeus et al., (1999) demonstrated that the distributed energy is isotropic with respect to the direction of the magnetic field at $k_\perp \rho_i \sim 10^{-3}$ wavenumber space, which creates "Maltese cross" pattern on contour plot of magnetic field. These observed results have prompted attempts to quantify the amount of energy splitted between parallel modes and perpendicular modes (Bieber et al., (1996)). Mostly 90% power resides in nearly perpendicular mode. Ruderman et al., (1999) proposed that phase mixing may be responsible for the perpendicular mode generation. Dasso et al., (2005) decomposed the "Maltese cross" into two: the dominantly perpendicular mode for slow solar wind and the dominantly parallel mode for fast solar wind. The slow solar wind originates from active regions of closed magnetic field (Woo & Habbal, (2005)), whereas fast solar wind originates from open field lines in coronal holes (Tu et al., (2005)).

1.7 Spacecraft Observations

Various space missions like SOHO (Solar and Heliospheric Observatory) (Domingo et al., (1995)), Ulysses, Voyager, Helios, Yohkoh, TRACE (Transition Region and Coronal Explorer), PSP (Parker Solar Probe) (Fox et al., (2016)) have been used to measure the solar wind and solar coronal parameters. To study the Earth's magnetosphere including the auroral region many spacecrafts like FREJA, POLAR, FAST (Fast Auroral SnapshoT), WIND (Ogilvie et al., (1995)), ACE (Stone et al., (1998)), DSCOVER (Burt & Smith, (2012)) and CLUSTER have been launched. Ulysses spacecraft was the first mission to probe the space environment that was launched out of the ecliptic orbit which goes over the Sun's poles at every 6.2 years (McComas et al., (1998)). This mission provided the evidence of the Alfvénic spectra in the polar regions of the Sun (Horbury et al., (1996)) and in the solar wind (Forsyth et al., (1996)). For the inner heliosphere

observation the two spacecrafts, Helios-1 in 1974 and Helios-2 in 1976 were launched. These missions observed primarily $in-situ$ measurements of solar wind properties, cosmic rays (Gurnett et al., (1975); Rosenbauer et al., (1977)) and coronal mass ejections (CMEs) (Jackson, (1985)). The Helios and Ulysses observations suggested that the Alfvénic fluctuation emanating from the solar corona have flat power spectra ($\sim f^{-1}$) (Goldstein et al., (1999)). However, it is difficult to observe the spectral anisotropies in the solar wind plasma by a single spacecraft data (Sari & Valley, (1976); Matthaeus et al., (1990)). Helios and Voyager spacecraft data suggested that the solar wind is an actively evolving magneto-fluid (Roberts et al., (1992)). The data of Helios-2 satellite analyzed by Hollweg et al., (1982) found that Alfvén waves are responsible for high speed streams. The Freja spacecraft data demonstrated that there are several regions of intense field-aligned currents having several scale sizes from larger scales to the smaller scales leading to the Alfvén wave filamentation (Lanchester et al., (2001)). Further CLUSTER spacecraft observations of current tubes verified this in the magnetosheath regions close to the bow shock (Alexandrova & Mangeney, (2004)). Some observed data of FREJA and FAST suggested that the physical nature of strong electric spikes with associated magnetic fields and density fluctuations in the auroral ionosphere and magnetosphere can be explained in terms of dispersive Alfvén waves (Louarn et al., (1994); Stasiewicz et al., (1997)). The POLAR spacecraft observations have verified the existence of large scale Alfvén waves in the auroral region of 4-6 Earth's radii leading to accelerate electrons and heat the plasma (Wygant et al., (2000)).

1.8   Outline of the Thesis

The objective of the present thesis is to study the DAW dynamics propagating in an inhomogeous plasma arising from the field aligned density fluctuations because of ponderomotive force and Joule heating. The dynamical field equations satisfy a modified nonlinear Schrödinger equation (NLSE). The magnetic wave equations couple with

the field aligned density perturbations, thereby the nonlinearity in the field equation leads to the localization of KAW wave packets as an envelope solitons. As the wave propagates, the transverse collapse of the coherent structures happens and the energy is dissipated from large scale to small scale via small wavenumber to high wavenumber space. The numerical simulation in pseudo-spectral method was carried out with the possible parameters of coronal loop and solar wind plasmas to study the formation of the coherent magnetic field structures, cascade of energy at different wave number scales and the effect of initial plasma inhomogeneities. Transverse collapse of the field aligned magnetic coherent structures is one of the efficient mechanism to transfer energy from large scale to small scale, as asymptotically predicted by the NLSE for the wave envelope (Champeaux et al. 1998; Lavender et al., (2001)). Therefore, the magnetic coherent structures (filaments) generated by DAWs play an important role in explaining the dissipation range of the turbulent spectra of solar wind and coronal regions. In the present thesis, non-linear dynamical equations of DAWs have been derived, when the non-linearity due to ponderomotive force and Joule heating are taken into account. On account of non-linear effects, the background number density of the plasma gets modified. This may be accounted by adiabatic and non-adiabatic response of the ion-acoustic wave propagating along the field lines. In the present thesis, the response has been taken to be adiabatic of the modified density, which leads to the non-linear evolution of the DAWs. The consequence of this is that the DAWs may be filamented or modulationally unstable. The dynamical equations have been solved numerically to get the intensity of the magnetic filaments evaluated along the filed lines. Magnetic and electric spectra have been evaluated and particle heating has been calculated by using Fokker-Plank equation.

A chapter wise summary of the thesis is as follows:

Chapter 1: Introduction

In this chapter, we introduce the relevant topics of thesis.

Chapter 2: Governing Equation

In this chapter we derive the dynamical equations satisfied by dispersive Alfvén waves by applying the two fluid model of the plasma.

Chapter 3:

This chapter explains about the pseudo-spectral method of simulation used in this thesis. The well known cubic NLSE was solved numerically and its results were compared with the analytical results.

Chapter 4: Generation of kinetic Alfvén Wave Turbulence in Solar Wind at 1 AU.

This chapter presents the generation of KAW coherent structures of magnetic filaments applicable to solar wind at 1AU. The inhomogeneity in the magnetic field which is represented as perturbation in the transverse direction of the magnetic field, takes the energy from the main pump KAWs and produces the filamentary structures. When the intensity is high enough, the filaments are broken down and the energy initially confined to low wavenumbers is redistributed to higher wave numbers, leading to cascade of energy at small scales less than ion acoustic gyroradius or comparable to electron gyroradius. The magnetic field spectral profiles are presented from the numerical simulation results. The dependence of the power spectra on different directions of the wavevector and initial conditions of the simulation representing the transverse magnetic field inhomogeneity are studied. The relevance of these results with other spacecraft observations and measurements are also pointed out.

Chapter 5: Transient Dynamics of Kinetic Alfvén Waves and Turbulence in Solar Coronal Loops

This chapter investigates the transient dynamics of KAWs with modified background density due to ponderomotive force and Joule heating. A numerical simulation based on pseudo-spectral method is used to study the evolution of KAW magnetic coherent

structures and generation of magnetic turbulence. Using different initial conditions of simulations, the dependance of KAW dynamics to the nature of the inhomogeneous solar plasma is thoroughly investigated. The saturated magnetic power spectra follows kolmogorov scaling of $k^{-5/3}$ in the inertial range, then followed by steep anisotropic scaling in the dissipation range. The KAW has anisotropy of $k_{\parallel} \propto k_{\perp}^{0.53}$, $k_{\parallel} \propto k_{\perp}^{0.50}$, $k_{\parallel} \propto k_{\perp}^{0.83}$ and $k_{\parallel} \propto k_{\perp}^{0.30}$ depending on the kind of initial conditions of inhomogeneity. The power spectra of magnetic field fluctuations showing the spectral anisotropy in wave number space indicate that the nonlinear interactions may be redistributing the energy anisotropically among higher modes of the wavenumbers. Therefore, anisotropic turbulence can be considered as one of the candidates responsible for the particle energization and heating of the solar plasmas.

Chapter 6: Inertial Alfvén Wave Turbulence and Particle Heating in Space Plasma

In this chapter, we investigate the transient dynamics of IAWs applicable in low- β plasmas. A numerical simulation based on pseudo-spectral method is used to study the evolution of IAW magnetic coherent structures and generation of magnetic turbulence. To understand the particle heating and it's dependance on turbulence, Fokker-Plank equation is studied. The distribution function is sensitive to spectral index and hence it may enhance the thermal tail of energetic particles in the space plasma.

Chapter 7: Conclusion

This chapter summerizes the overall work of the thesis.

Chapter 2

Governing Equations

In this chapter we derive the dynamical equation for dispersive Alfvén waves while they propagate in an inhomogenous plasma. Let us consider a low frequency DAW propagating in x-z plane ($\vec{k}_0 = k_{0x}\hat{x} + k_{0z}\hat{z}$) and an ambient background magnetic field $\vec{B}_0 = B_0\hat{z}$. By using two fluid model of the plasma, we can write the momentum-force balance equation and the consitutive field equations. We also apply the procedure of linearization in the equations. For that purpose the density, velocity and the electromagnetic fields are divided into an equilibrium part denoted by the subscript 0 and the perturbation part denoted by the subscript 1.

$$n = n_0 + n_1, \vec{v} = \vec{v}_0 + \vec{v}_1, \vec{E} = \vec{E}_0 + \vec{E}_1, \vec{B} = \vec{B}_0 + \vec{B}_1 \qquad (2.1)$$

In the equilibrium plasma, the undisturbed density, velocity and fields are constant and uniform, i.e.

$$\vec{\nabla}n_0 = \vec{v}_0 = \vec{E}_0 = 0 \qquad (2.2)$$

and

$$\frac{\partial n_0}{\partial t} = \frac{\partial \vec{v}_0}{\partial t} = \frac{\vec{E}_0}{\partial t} = 0. \tag{2.3}$$

Adopting the procedure of linearization i.e. neglecting the terms containing the higher powers of the perturbating amplitude factors we can write the equations as:

Equation of motion:

$$\frac{\partial \vec{v}_{j1}}{\partial t} \approx \frac{q_j}{m_j}\vec{E}_1 + \frac{q_j}{cm_j}(\vec{v}_{j1} \times \vec{B}_0) - \frac{\gamma_j k_B T_j}{n_{j0}m_j}\vec{\nabla}n_{j1}. \tag{2.4}$$

Continuity equation:

$$\frac{\partial n_{j1}}{\partial t} + n_{j0}\vec{\nabla}.\vec{v}_{j1} \approx 0. \tag{2.5}$$

Faraday's law:

$$\vec{\nabla} \times \vec{E}_1 = -\frac{1}{c}\frac{\partial \vec{B}_1}{\partial t}. \tag{2.6}$$

where $j = i, e$ represents either ions or electrons, $\vec{v}$ is the velocity, q is the charge, m is the mass, c is the speed of light in vacuum, γ (c_p/c_v) is the ratio of the specific heats and k_B is the Boltzmann constant. Furthur n represents the plasma number density. We assume the quasineutrality condition i.e. $n_{e0} \simeq n_{i0} \simeq n_0$ and $n_{e1} \simeq n_{i1} \simeq n_1$ and the isothermal condition i.e. $\gamma_e = \gamma_i = 1$.

From equation (2.4), we get the perpendicular components of the electron and ion velocities with using low frequency approximation ($\omega << \omega_{ci}, \omega_{ce}$ where $\omega_{ci} = eB_0/m_i c$ and $\omega_{ce} = eB_0/m_e c$ are the ion and electron cyclotron frequencies respectively) as follows:

$$(\vec{v}_{e1})_\perp \approx \frac{c}{B_0}\vec{E}_{1\perp} \times \hat{z} - \frac{k_B T_e}{m_e \omega_{ce} n_0}\hat{z} \times \vec{\nabla}_\perp n_1 \tag{2.7}$$

and

$$(\vec{v}_{i1})_\perp \approx \frac{e}{\omega_{ci}m_i}\left[\vec{E}_{1\perp} - \frac{k_B T_i}{en_0}\vec{\nabla}_\perp n_1\right] \times \hat{z} - \frac{i\omega}{\omega_{ci}^2}\frac{e}{m_i}\left[\vec{E}_{1\perp} - \frac{k_B T_i}{en_0}\vec{\nabla}_\perp n_1\right]. \qquad (2.8)$$

The parallel component of electron velocity is

$$\frac{\partial(\vec{v}_{e1})_z}{\partial t} = \frac{-eE_{1z}}{m_e} - \frac{k_B T_e}{m_e n_0}\frac{\partial n_1}{\partial z}. \qquad (2.9)$$

The current density is given by

$$\vec{J} \approx en_0(\vec{v}_{i1} - \vec{v}_{e1}). \qquad (2.10)$$

Now we will drop the subscript "1" while representing the perturbating parts of $\vec{v}, \vec{E}$ and $\vec{B}$ except while representing the varying part of n.

The y-component of Faraday's law is

$$\frac{1}{c}\frac{\partial B_y}{\partial t} = \frac{\partial E_z}{\partial x} - \frac{\partial E_x}{\partial z}. \qquad (2.11)$$

Using the conservation of current density equation, $\vec{\nabla}.\vec{J} = 0$, and writing the parallel and perpendicular components of current density as $\vec{J}_z \approx -en_0\vec{v}_{ez}$ and $\vec{J}_\perp \approx en_0(\vec{v}_{i\perp} - \vec{v}_{e\perp})$, we get

$$\frac{\partial^2 E_x}{\partial x \partial t} = \frac{B_0 \omega_{ci}}{c}\left(\frac{\partial v_{ez}}{\partial z}\right). \qquad (2.12)$$

By taking the z-component of Ampere's law and eliminating the parallel component of current density and substituting it in equation (2.12), we get,

$$\frac{\partial E_x}{\partial t} = -\frac{v_A^2}{c}\left(1 - \frac{n_1}{n_0}\right)\frac{\partial B_y}{\partial z}, \qquad (2.13)$$

where $v_A(= \sqrt{B_0^2/4\pi n_0 m_i})$ is the Alfvén speed.

Now we can calculate the time derivative of parallel electric field from the parallel component of Ampere's law. In that relation we substitute the parallel component of electron velocity from equation (2.9) and the continuity equation (2.5) to get

$$\frac{\partial E_z}{\partial t} = -\frac{v_{te}^2 \lambda_e^2}{c} \frac{\partial}{\partial x} \frac{\partial^2 B_y}{\partial z^2},$$
(2.14)

where $\lambda_e (= c/\omega_{pe})$ denotes the electron inertial length (collisionless skin depth), $\omega_{pe} (= \sqrt{4\pi n_0 e^2/m_e})$ denotes the electron plasma oscillation frequency and $v_{te} \left(= \sqrt{\frac{k_B T_e}{m_e}} \right)$ denotes the electron thermal speed.

We differentiate equation (2.11) *w.r.t.* time and inserting the *z*-derivative of equation (2.13) and the *x*-derivative of equation (2.14), we get the governing equation of DAWs propagating in an inhomogenous plasma medium as (Bellan & Stasiewicz 1998; Shukla et al. 1999; Shukla & Stenflo, 2000a, Sharma & Kumar, 2011)

$$\frac{\partial^2 B_y}{\partial t^2} = \lambda_e^2 \frac{\partial^4 B_y}{\partial x^2 \partial t^2} - v_A^2 \rho_s^2 \frac{\partial^4 B_y}{\partial x^2 \partial z^2} + v_A^2 (1 - \frac{\delta n_s}{n_0}) \frac{\partial^2 B_y}{\partial z^2},$$
(2.15)

where ρ_s ($= \lambda_e v_{te}/v_A = c_s/\omega_{ci}$) denotes the ion acoustic gyroradius at electron temperature and c_s ($= \sqrt{k_B T_e/m_i}$) denotes the ion sound speed. In the governing equation, only one component of magnetic field can be solved. The other components of the magnetic field can be found from the Faraday's law.

We take the Fourier transform of equation (2.15) and get the dispersion relation of DAWs as

$$\frac{\omega^2}{k_{0z}^2 v_A^2} = \frac{1 + k_{0x}^2 \rho_s^2}{1 + k_{0x}^2 \lambda_e^2}.$$
(2.16)

The governing equation (2.15) is valid for any arbitrary β plasmas. In low-β plasma ($\beta << m_e/m_i$) regime, the DAW is known as inertial AW. In this β regime, the above governing equation reduces to

$$\frac{\partial^2 B_y}{\partial t^2} = \lambda_e^2 \frac{\partial^4 B_y}{\partial x^2 \partial t^2} + v_A^2 (1 - \frac{\delta n_s}{n_0}) \frac{\partial^2 B_y}{\partial z^2}. \tag{2.17}$$

By taking Fourier transform, the dispersion relation of IAWs comes out to be

$$\frac{\omega^2}{k_{0z}^2 v_A^2} = \frac{1}{1 + k_{0x}^2 \lambda_e^2}. \tag{2.18}$$

In intermediate-β plasma ($m_e/m_i << \beta << 1$) regime, the DAW is known as kinetic AW. The governing equation for the KAWs in this β regime reduces to

$$\frac{\partial^2 B_y}{\partial t^2} = -v_A^2 \rho_s^2 \frac{\partial^4 B_y}{\partial x^2 \partial z^2} + v_A^2 (1 - \frac{\delta n_s}{n_0}) \frac{\partial^2 B_y}{\partial z^2}, \tag{2.19}$$

The dispersion relation of KAWs (Shukla & Stenflo, 2005) can be recovered by taking Fourier transform to equation (2.19) as

$$\frac{\omega^2}{k_{0z}^2 v_A^2} = 1 + k_{0x}^2 \rho_s^2. \tag{2.20}$$

The governing equations given above are satisfied by the perturbed magnetic fields of the KAW/IAW. It is also equally valid for a plane wave field superimposed by a nonuniform perturbation. One of the possible solution is a plane wave (linear polarisation) modulated by a slowly varying envelope $B_y'(x, z)$ which can be expressed as

$$B_y = B_y'(x, z, t) e^{i(k_{0x}x + k_{0z}z - \omega t)} \tag{2.21}$$

where $B_y'(x, z, t)$ is amplitude of the y component of the magnetic field. We assume that it is spatially slowly varying in comparison to the exponential part. Now we substitute it in equation (2.19) satisfied by KAWs to get

$$i\frac{2\omega}{v_A^2 k_{0z}^2} \frac{\partial B_y'}{\partial t} + i\frac{2}{k_{0z}} \frac{\partial B_y'}{\partial z} + \rho_s^2 \frac{k_{0x}^2}{k_{0z}^2} \frac{\partial^2 B_y'}{\partial z^2} + \rho_s^2 \frac{\partial^2 B_y'}{\partial x^2} + 2ik_{0x}\rho_s^2 \frac{\partial B_y'}{\partial x} + \frac{n_1}{n_0} B_y' = 0. \tag{2.22}$$

Again we substitute the slowly varying envelope solution given by equation (2.21) into the dynamical equation satisfied by IAWs (equation 2.17) to get

$$2i\frac{\omega}{v_A^2 k_{0z}^2}(1+k_{0x}^2\lambda_e^2)\frac{\partial B_y'}{\partial t} + \frac{2i}{k_{0z}}\frac{\partial B_y'}{\partial z} + \frac{1}{k_{0z}^2}\frac{\partial^2 B_y'}{\partial z^2} - \frac{2ik_{0x}\lambda_e^2\omega^2}{k_{0z}^2 v_A^2}\frac{\partial B_y'}{\partial x} - \frac{\lambda_e^2\omega^2}{k_{0z}^2 v_A^2}\frac{\partial^2 B_y'}{\partial x^2} + \frac{n_1}{n_0}B_y' = 0.$$
(2.23)

In an inhomogeneous plasma, a magnetic gradient force known as ponderomotive force acts upon the plasma. The effect of this force and electron Joule heating leads to density perturbation (Shukla & Stenflo 1999). Magnetic field aligned density perturbations in the form of density humps and cavities were found in laboratory and space plasmas (Gekelman et al. 1999). Considering slow changes in time with respect to density changes (adiabatic limit), the particle number density perturbation to the background plasma density becomes a function of magnetic field i.e. $n_1 = f(B_y')$. Then the above two equations (2.22) and (2.23) are of the form of NLSEs.

In the next chapters, the above two equations (2.22) and (2.23) are numerically solved with appropriate techniques and relevant plasma parameters applicable to the low and intermediate β plasma regimes. The numerical simulation results are represented graphically and interpreted to understand the DAW dynamics and other physical and observable processes happening in space plasmas. Furthur, the numerical results are compared with the results obtained from the spacecraft data.

Chapter 3

Numerical Methods

3.1 Introduction

Our model equations satisfied by the DAWs are of the form of nonlinear Schrödinger equations (NLSEs). In many physical nonlinear systems, the NLSE is the envelope wave equation. For example, in optical fibers the propogation of solitary waves is modeled by one dimensional NLSE (Agrawal, (2013)). The two spatial dimensional NLSE is used to model in many areas of plasma dynamics such as collapse of plasma waves (Zakharov, (1975)) and self-focusing of laser beams (Sun et al., (2008)). The NLSE in three spatial dimension can be used to model Bose-Einstein condensation (Antoine, (2013), Bao, (2003), Pitaevskii, (2003)). Recently, three dimensional NLSE has been used to study the propagation of spatial solitons in multi - mode fiber (Dai, (2010)) and nonlinear interactions of space plasma waves (Sharma and Gaur, (2014)). The NLSEs are exactly solvable because they are Hamiltonian integrable (Hilfer, (1999)). But this intergrability could be destroyed if the physical system is disturbed by some perturbations (Hu et al., (2011), Hoz and Vadillo, (2008) Hoz and Vadillo, (2016)). Non-integrable system may lead to chaos. Since we have considered the inhomogenious plasma environment of DAWs, many kinds of perturbations in magnetic fields and density can be present. So our model equation in the form of NLSE is not exactly integrable, therefore, we seek a suitable

numerical method to solve it. The numerical methods that can solve the nonlinear partial differential equations can be divided into two: finite difference methods and spectral methods. Among the finite difference methods, the Cranck-Nicholson implicit (Chang et al. (1999)) and Hopscotch (Gourlay, (1971)) methods are commonly used. The spectral methods are more computationally efficient than most of the finite difference methods (Agrawal, (2013)). The spectral methods have the advantage of computing the nonlinear terms efficiently using the Fast Fourier Transform. The model equation that we have derived in the last section will be numerically solved by using the pseudo-spectral method of simulation. It is known as pseudo-spectral method because the Fast Fourier Transform is taken only on speciefied discrete points in contrast to continous Fourier transform. In the spectral method, the differential equation is represented in the terms of a basis of some vector space and the differential equation is redused to an ordinary differential equation systems for the coefficients. Applying this idea, the continuous Fourier transform and finite element methods can be considered as spectral methods. But these methods have the disadvantage that the multiplication in the spatial variables becomes convolution, producing a big matrix-vector multiplication. In the pseudo-spectral method, the solution is represented in terms of the basis but the equation is imposed only at discrete points. Therefore, it can be said that the pseudo-spectral method is a spectral method in discrete space. Using the pseudo-spectral method, one can solve the non-linear partial differential equations very fast. For example, if we use spectral method to compute the nonlinear term $f(x)u_x(x,t)$, where x is continuous, we have an infinite convolution. However, in pseudo-spectral method, the discrete Fourier transform (DFT) can be performed by using the Fast Fourier transform (FFT) and again using the inverse FFT, the function can be converted to real space (x-space). In this way, the nonlinear terms are calculated in real space first for every step and it saves a lot of time.

3.2 Pseudo-Spectral Method

For a vector of discrete numbers $\{f[m,n]\}$ of size $M \times N$ with equally spaced in the directions of m and n respectively, the discrete Fourier transform (DFT) is given as,

$$F[k,l] = \frac{1}{\sqrt{MN}} \sum_{n=o}^{N-1} \sum_{m=o}^{M-1} f[m,n] \exp^{-2\pi i} \left(\frac{mk}{M} + \frac{nl}{N} \right), \tag{3.1}$$

for $0 \leq k < M-1$ and $0 \leq l < N-1$.

By applying inverse DFT, we can get back the vector $f[m,n]$ as

$$f[m,n] = \frac{1}{\sqrt{MN}} \sum_{l=o}^{N-1} \sum_{k=o}^{M-1} F[k,l] \exp^{2\pi i} \left(\frac{mk}{M} + \frac{nl}{N} \right), \tag{3.2}$$

for $0 \leq m < M-1$ and $0 \leq n < N-1$.

The computation of DFT of N points from the defination requires $O(N^2)$ operations. However, the algoritham of fast fourier transform (FFT) requires only $O(Nlog_2N)$ operations (Press et al., (1996)). If the number of data is large, this difference in the number of operations will result huge difference in computational speed and time. Therefore, the numerical technique of FFT is widely used in solving many scientific and engineering problems.

The main idea of 2D-FFT is to transform each row and each column by its corresponding 1D-FFT. Hence, a 2D-FFT of size M $\times$ N requires (M+N) 1-D FFT. The FFT subroutine we used in our present numerical code was taken out from the book, Numerical Recipes in FORTRAN authored by Press et al., (1996).

Let us consider the exactly solvable cubic 2D-NLSE as

$$i\frac{\partial u}{\partial t} + \frac{\partial^2 u}{\partial x^2} + \frac{\partial^2 u}{\partial y^2} + |u|^2 u = 0, \tag{3.3}$$

where u is complex-valued function.

To solve the problem by pseudo-spectral method, a bounded domain is required. For an unbounded domain, as in our case, we consider the periodic domain i. e. functions with fixed periodicity.

Let us assume that $u(x, y, t)$ satisfies the periodic boundary conditions with period $[-\pi, \pi]$.
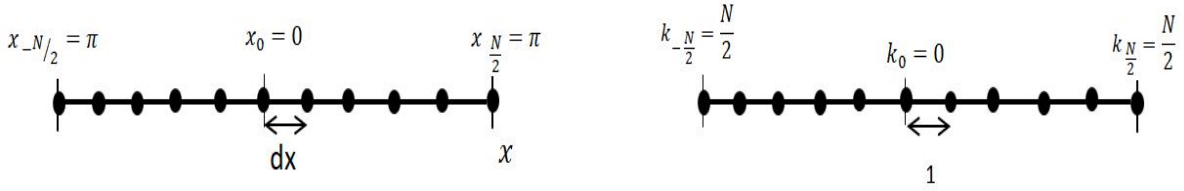
Fig. 3.1 Space and wave-number domains for the DFT

Let N be a positive integer, then we divide the interval $[-\pi, \pi]$ in the x-direction into N equally spaced grid-points with $dx = 2\pi/N_x$ and $x_j = j(dx)$, for any j $(j = 0, 1, ...N)$. The grid points in the x-direction are

$$x_{-N/2} = -\pi, x_{-N/2+1} = -\pi + dx, ..., x_0 = 0, ...; ., x_{N/2-1} = \pi - dx, x_{N/2} = \pi.$$

In the same way for y-direction also with spacing distance $dy = 2\pi/N_y$ and grid point $y_k = k(dy)$, for any $k(k = 0, 1...N)$. Given $u(x, y, t)$, our next step is to find the value of $u(x, y, t + \Delta t)$.

For the 2D FFT, we have

$$\hat{u}_{mn} = F_{m,n}(u_{jk}) = \frac{1}{N_x N_y} \sum_{j=o}^{N_x-1} \sum_{k=o}^{N_y-1} u_{jk} e^{-i(mx_j + ny_k)}, \tag{3.4}$$

for $-\frac{N_x}{2} \leq m \leq \frac{N_x}{2} - 1$ and $-\frac{N_y}{2} \leq n \leq \frac{N_y}{2} - 1$

and

$$u_{jk} = F_{jk}^{-1}(\hat{u}_{mn}) = \sum_{m=-\frac{N_x}{2}}^{\frac{N_x}{2}-1} \sum_{n=-\frac{N_y}{2}}^{\frac{N_y}{2}-1} \hat{u}_{mn} e^{i(mx_j+ny_k)}, \tag{3.5}$$

for $j = 0, 1, 2....N_x - 1$ and $k = 0, 1, 2, ...N_y - 1$.

Now taking the full and partial derivatives, we get

$$\frac{du}{dt} = \frac{du_{jk}}{dt} = \sum_{m=-\frac{N_x}{2}}^{\frac{N_x}{2}-1} \sum_{n=-\frac{N_y}{2}}^{\frac{N_y}{2}-1} \frac{d\hat{u}_{mn}}{dt} e^{i(mx_j+ny_k)} \tag{3.6}$$

$$\frac{\partial^2 u}{\partial x^2} = \frac{\partial^2 u_{jk}}{\partial x^2} = \sum_{m=-\frac{N_x}{2}}^{\frac{N_x}{2}-1} \sum_{n=-\frac{N_y}{2}}^{\frac{N_y}{2}-1} \hat{u}_{mn}(-m)^2 e^{i(mx_j+ny_k)} \tag{3.7}$$

$$\frac{\partial^2 u}{\partial y^2} = \frac{\partial^2 u_{jk}}{\partial y^2} = \sum_{m=-\frac{N_x}{2}}^{\frac{N_x}{2}-1} \sum_{n=-\frac{N_y}{2}}^{\frac{N_y}{2}-1} \hat{u}_{mn}(-n)^2 e^{i(mx_j+ny_k)} \tag{3.8}$$

Now we can evaluate $u_{xx} + u_{yy}$ as

$$F^{-1}[(m^2 + n^2)F\{u(x, y, t)\}] = F^{-1}[(m^2 + n^2)\hat{u}_{mn}] \tag{3.9}$$

Applying the leap-frog time step, the 2D NLSE appeared in equation (3.3) can be expressed as

$$\hat{u}_{mn}(t + \Delta t) = \hat{u}_{mn}(t - \Delta t) - 2i\Delta t(m^2 + n^2)\hat{u}_{mn}(t) - 2i\Delta t\{\widehat{|u_{jk}(t)|^2 u_{jk}(t)}\}_{mn} \tag{3.10}$$

Here it should be mentioned that the time steps are calculated in Fourier space. For the linear terms, the FFT is directly applied while for the nonlinear term, first the local product in real space is taken, then it is transformed to Fourier space. It is followed for every time steps using inverse FFT and direct FFT. This part is the essence of quasi-spectral method.

Following the ideas of Fornberg and Withham, (1978), the linear term can be modified to get

$$\hat{u}_{mn}(t + \Delta t) = \hat{u}_{mn}(t - \Delta t) - 2i \sin\{-\Delta t(m^2 + n^2))\}\hat{u}_{mn}(t) - 2i\Delta t\{|u_{jk}\widehat{(t)|^2 u}_{jk}(t)\}_{mn}$$
(3.11)

The reason for this modification is explained as follows. When the wavenumbers are low enough, all consistent difference approximations to a differential equations are accurate. As the wavenumber increases, this accuracy reduces rapidly. This losing accuracy with increasing wavenumber is particularly applied to the leap-frog time difference in equation (3.10). Considering the high wavenumber condition in equation (3.10), the linear term $\frac{\partial^2 u}{\partial x^2} + \frac{\partial^2 u}{\partial y^2}$ dominates the nonlinear term $|u|^2 u$. Therefore, the equation reduces to

$$\hat{u}_{mn}(t + \Delta t) = \hat{u}_{mn}(t - \Delta t) - 2i\Delta t(m^2 + n^2)\hat{u}_{mn}(t),$$
(3.12)

which is the approximation of the following equation in Fourier space

$$\frac{\partial u}{\partial t} + \frac{\partial^2 u}{\partial x^2} + \frac{\partial^2 u}{\partial y^2} = 0.$$
(3.13)

Similarly equation (3.11) reduces as

$$\hat{u}_{mn}(t + \Delta t) = \hat{u}_{mn}(t - \Delta t) - 2i \sin\{\Delta t(m^2 + n^2)\}\hat{u}_{mn}(t)$$
(3.14)

The equation (3.12) is still having the differencing error but it is not in equation (3.14) because it is exactly satisfied for any solution of equation (3.13), i.e. for any m, n and Δt, no matter how large the values are. It can be shown from the solution of equation (3.13) as

$$u(x, y, t) = e^{i(k_x x + k_y y - \omega t)} = e^{i(k_x x + k_y y - (k_x^2 + k_y^2)t)}.$$
(3.15)

Now, from this we have

$$u(x, y, t + \Delta t) = e^{-i(k_x^2 + k_y^2)\Delta t} u(x, y, t) \tag{3.16}$$

$$u(x, y, t - \Delta t) = e^{i(k_x^2 + k_y^2)\Delta t} u(x, y, t) \tag{3.17}$$

Therefore,

$$u(x, y, t + \Delta t) - u(x, y, t - \Delta t) = -2i \sin\{\Delta t(k_x^2 + k_y^2)\} u(x, y, t) \tag{3.18}$$

Now, substituting all these, our main equation to solve the given 2D cubic NLSE becomes

$$\hat{u}_{mn}(t + \Delta t) = \hat{u}_{mn}(t - \Delta t) - [e^{i(m^2 + n^2)\Delta t} - e^{-i(m^2 + n^2)}]\hat{u}_{mn}(t) - 2i\Delta t\{\widehat{|u_{jk}(t)|^2 u_{jk}}(t)\}_{mn} \tag{3.19}$$

The algorithm to implement equation (3.10) and (3.19) is described as follows:

First we define the Fourier transform of the initial condition as

$$\hat{u}_1 = \hat{u}_{mn}(t = 0) \tag{3.20}$$

Next we define $\hat{u}_2$ to represent $\hat{u}_{mn}$ at $t = \Delta t$. Here, for the sake of convenience, we drop the subscript mn to be appeared in u to denote Fourier space.

Lastly for $t = 2\Delta t$ to ($numsteps \times \Delta t$), we do the following by defining the intermediray value $\hat{u}'$

(1) $\hat{u}' = \Delta t(m^2 + n^2)\hat{u}$ for equation (3.10).

(or $\hat{u}' = \sin\{\Delta t(m^2 + n^2)\}\hat{u}$) for equation (3.11)

(2) $\hat{u}_2 = \hat{u}$

(3) $\hat{u}_3 = \hat{u}_1 - 2i\hat{u}' - 2i\Delta t\{\widehat{|u_2|^2 u_2}\}$

(4) $\hat{u}_1 = \hat{u}_2$

$\hat{u}_2 = \hat{u}_3$

For time integration, We apply Newton's forward method of iteration. To get better accuracy, we apply predictor- corrector method that defines the values of $\hat{u}_{mn}(t)$ at a particular time t as the average of $\hat{u}_{mn}(t - dt)$ and $\hat{u}_{mn}(t + dt)$. Finally, we get $u(x, y, t) = F^{-1}(\hat{u}_{mn}(t))$.

The difference between equations (3.10) and (3.11) is the approximation of the linear part of equation (3.3). The linear part of equation (3.11) has to be satisfied by any solution of equation (3.13). Equation (3.10) is linearly stable for $\frac{\Delta t}{(\Delta x)^2} < \frac{1}{\pi^2}$. However, according to linear analysis, the equation (3.11) is unconditionally stable (Fornberg and Withham, (1978)).

3.3 Numerical Test

To illustrate the efficiency and determine the accuracy of the numerical method we are applying, we performed the numerical soluions of $1D$ & $2D$ cubic NLSEs keeping the benchmark of the algorithm against the analytical solutions. After fully testing the algorithm and comparing with the well known results, the algorithm was further modified to solve our model equations (2.22) and (2.23) satisfied by the DAWs.

The $1D$ cubic NLSE is given by

$$i\frac{\partial u}{\partial t} + \frac{\partial^2 u}{\partial x^2} + |u|^2 u = 0, \tag{3.21}$$

for $x \in R, t \geq 0$.

The cubic NLSE is a general envelop wave equation that describes the various nonlinear physical phenomena, such as hydrodynamics, laser beam interactions, nonlinear optics, wave generations etc. Here, u is the complex amplitude and its second spatial derivative $\frac{\partial^2 u}{\partial x^2}$ represents the nonlinearity of the medium and the cubic term, $|u|^2 u$ represents the

dispersion of the medium. When the nonlinear effect is balanced with the dispersion phenomenon, the soliton solution is formed. We choose the following single soliton solution (Mahdy, (2016)) as the exact analytical solution of the cubic $1D$ NLSE to run the current test.

$$u(x,t) = \sqrt{2\alpha} \exp\left\{i\left[\frac{1}{2}cx - \left(\frac{1}{4}c^2 - \alpha\right)t\right]\right\}\text{sech}\{\sqrt{\alpha}(x - ct)\}, \qquad (3.22)$$

where α is a constant and c is the speed of the soliton.

To run the test, the equation (3.22) was solved by pseudo-spectral method in the spatial domain $-30 \leq x \leq 30$ with grid points of 128, and taking $\alpha = 0.01$ and $c = 0.1$ for $t \in [0, 100]$ with $\Delta t = 5 \times 10^{-5}$. For this purpose, the following initial condition of the simulation was used

$$u(x,0) = \sqrt{2\alpha} \exp\left(\frac{1}{2}icx\right)\text{sech}\{\sqrt{\alpha}x\}. \qquad (3.23)$$

The boundary conditions are

$$u(L,t) = u(-L,t) = 0 \qquad for \qquad t \geq 0. \qquad (3.24)$$

To check the efficiency, we compare the analytical solution against the numerical solution. First, we compare the wave amplitude profiles ($|u|$ vs (x,t)) in figure (3.2). Further, in table (3.1) and (3.2), the real and imaginary values of $u(x,t)$ at different locations of x and fixed $t = 10$ are shown for both the analytical solution and numerical solution. The absolute error comes out to be of the order of $\sim 10^{-5}$.

Next, we consider the $2D$ cubic NLSE

$$i\frac{\partial u}{\partial t} + \frac{\partial^2 u}{\partial x^2} + \frac{\partial^2 u}{\partial y^2} + |u|^2 u = 0, \qquad (3.25)$$

which has the analytical solution as (Sweilam, (2007))

$$u(x, y, t) = \sqrt{2\alpha}e^{i(0.5c(x+y)-(0.25c^2-\alpha)t)}\text{sech}[\sqrt{\alpha}(x + y - ct)], \qquad (3.26)$$

where α is a constant and c is the speed of the soliton. The numerical simulation of equation (3.26) was performed using the pseudospectral method with the initial condition of the simulation as

$$u(x, y, 0) = \sqrt{2\alpha}e^{i(0.5c(x+y))}\text{sech}[\sqrt{\alpha}(x + y)] \qquad (3.27)$$

with boundary conditions

$$\frac{\partial u(-L, y, t)}{\partial x} = \frac{\partial u(L, y, t)}{\partial x} = 0 \qquad (3.28)$$

and

$$\frac{\partial u(x, -L, t)}{\partial y} = \frac{\partial u(x, L, t)}{\partial y} = 0, \qquad t \geq 0. \qquad (3.29)$$

For numerical purpose, we took $L = 40$, $c = 0.1$, $\alpha = 0.01$, $\Delta t = 5 \times 10^{-5}$ and the number of grid points as 256×256. The wave amplitude profiles ($|u|$ vs (x, y) at a fixed $t = 10$) are shown in figure (3.3) for both the analytical and numerical solutions. Figure (3.4) shows $|u|$ vs (x, t) at a fixed value of $y = 35$. Table (3.2) and (3.3) represent the comparision of the values of $u(x, y, t)$ (both real and imaginary parts) at $y = 35$ and $t = 10$) between the analytical solution and numerical solution. The absolute error is of the order of $\sim 10^{-5}$. The comparison of the numerical results we generated with the analytical results justifies the efficiency and accuracy of the pseudospectral method.

Fig. 3.2 Wave amplitude profiles ($|u|$ vs (x, t)) of 1D cubic NLSE (a) analytical solution and (b) numerical solution.

x	Analytical solution	Numerical solution	Absolute error
-30	0.001847389	0.001847179	2.1×10^{-7}
-20	0.020537122	0.020526231	1.0×10^{-5}
- 10	0.077218400	0.07722730	8.8×10^{-6}
0	0.140321602	0.140311501	1.0×10^{-5}
10	0.082814068	0.082823057	8.9×10^{-6}
20	0.019685191	0.019676181	9.0×10^{-6}
30	-0.000065223	-0.000054112	1.1×10^{-5}

Table 3.1 Real parts of $u(x, t)$ at different locations of x and fixed $t = 10$ obtained by solving 1D cubic NLSE.

x	Analytical solution	Numerical solution	Absolute error
-30	- 0.0125811	- 0.0125700	1.1×10^{-5}
-20	- 0.0272522	- 0.0272412	1.1×10^{-6}
-10	- 0.0349477	- 0.0349366	1.1×10^{-5}
0	0.0105439	0.0105328	1.1×10^{-5}
10	0.0536673	0.0536562	1.1×10^{-5}
20	0.0363963	0.0363852	1.1×10^{-5}
30	0.0155158	0.0155236	7.7×10^{-6}

Table 3.2 Imaginary parts of $u(x,t)$ at different locations of x and fixed $t = 10$ obtained by solving 1D cubic NLSE.
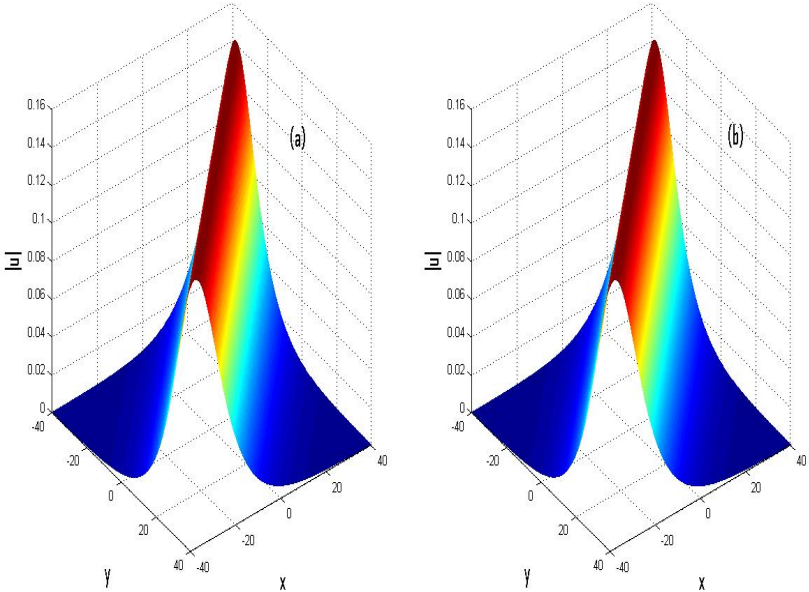
Fig. 3.3 Wave amplitude profiles ($|u|$ vs (x, y) of 2D cubic NLSE at $t = 10$ (a) analytical solution and (b) numerical solution.
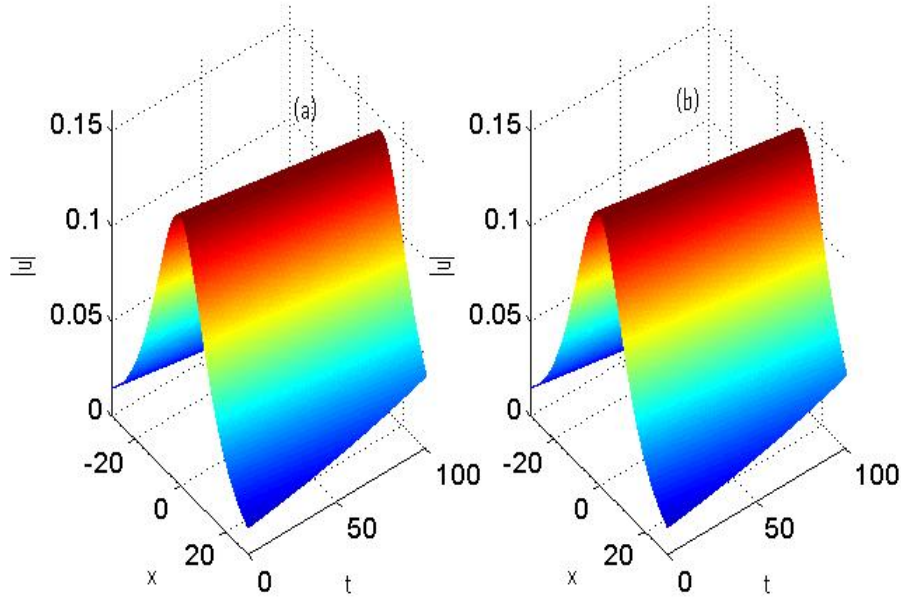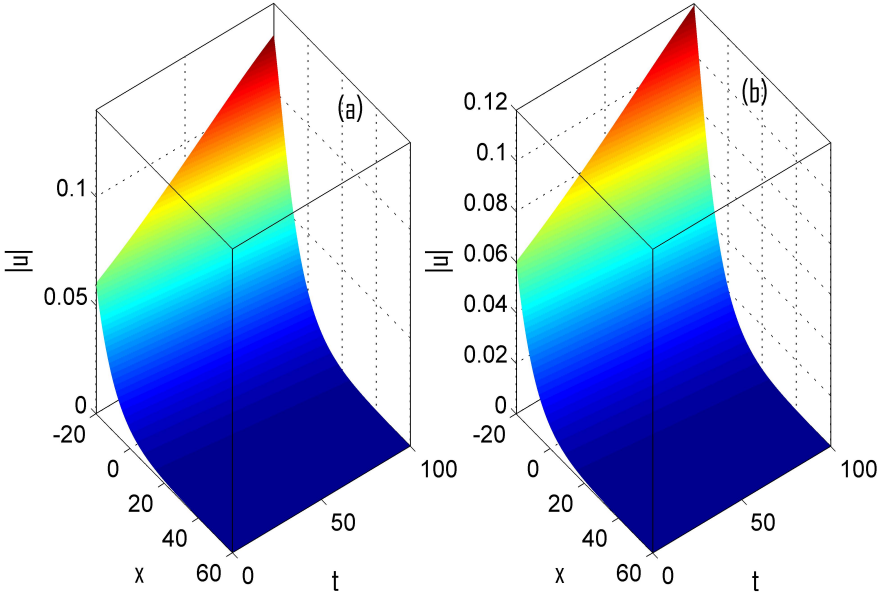

Fig. 3.4 Wave amplitude profiles ($|u|$ vs (x, t)) of 2D cubic NLSE at $y = 35$ (a) analytical solution and (b) numerical solution.

x	Analytical solution	Numerical solution	Absolute error
-30	0.018590	0.018139	2.2×10^{-5}
-20	0.004771	0.004611	5.0×10^{-6}
- 10	-0.001356	-0.001371	1.5×10^{-5}
0	-0.003368	-0.003326	4.2×10^{-5}
10	-0.003462	-0.003406	5.5×10^{-5}
20	-0.002829	-0.002779	4.9×10^{-5}

Table 3.3 Real part of $u(x, y, t)$ at different locations of x and fixed values of $y = 35$ and $t = 10$ obtained by solving 2D cubic NLSE

x	Analytical solution	Numerical solution	Absolute error
-30	0.0415399	0.0408053	8.8×10^{-6}
-20	0.0276667	0.0271411	5.6×10^{-6}
-10	0.0170825	0.0167433	9.2×10^{-6}
0	0.0098585	0.0096555	7.0×10^{-6}
10	0.0052928	0.0051795	1.3×10^{-5}
20	0.0025918	0.0025335	5.8×10^{-5}

Table 3.4 Imaginary parts of $u(x, y, t)$ at different locations of x and fixed values of $y = 35$ and $t = 10$ obtained by solving 2D cubic NLSE.

Chapter 4

Generation of Kinetic Alfvén Wave Turbulence in Solar Wind at 1 AU

4.1 Introduction

From many observations and studies (Li et al. 2015; Tu & Marsch 1993; Bavassano et al. 1998; Neugebauer 2004), it was suggested that the Alfvénicity measured by the correlation of the field and velocity components decreases with solar distances. Alfvénicity of around 3 and 0.7 were found at a solar distance of 0.3 AU, (Tu et al. 1990; Marsch & Tu 1990) and 1AU (Tu & Marsch, 1995) respectively. It shows that the plasma becomes more magnetized as the solar wind expands. However, the existence of large-amplitude Alfvén waves near 1AU, with the Alfvénicity of around 1 were pointed out by Wang et al. 2012. Besides this, various observations (Podesta 2013; Howes et al. 2006; Howes et al. 2008b; Howes et al. 2008c; Howes et al. 2011b; Schekochihin et al. 2008; Schekochihin et al. 2009; Boldyrev and Perez, 2012) have shown the existence of KAWs and its turbulence in the solar wind at 1AU and beyond that extending throughout of the heliosphere . *Polar* spacecraft measurements in the magnetotail region (Wygant et al. 2002) and inner magnetosphere at $6.6R_E$ (Sergeev et al. 2000), observations from UVCS (Ultraviolet Coronograph Spectrometer) on board SOHO (Solar and Heliospheric

Observatory) in the inner heliosphere (Cranmer et al. 1999; Marsch & Tu 2001) showed the existence of KAWs. Since the KAWs can develop field aligned electric fields, the charged particles can be accelerated along the magnetic field direction leading to the heating of the plasma (Hasegawa and Chen, 1975; Wu 2003; Wu & Chao 2004) and anisotropic and mass-dependent energization of heavy ions (Voitenko and Goossens, 2004; Wu & Yang 2006).Hence, the study of KAWs will help to enhance our understanding of the various physical processes, for example solar wind turbulence (Chaston et al. 2005a), coronal heating (Wu & Fang 2003) and auroral particle acceleration (Wygant et al. 2002; Chaston et al. 2003; Chaston et al. 2004; Chaston et al. 2005b).

The *Polar* spacecraft data investigated by Wygant et al. 2002 found magnetic coherent structures of KAWs having transverse scale size near to ion gyro radius. These magnetic coherent structures (filaments) are related with inhomogeneities in magnetic fields, density and temperature (Chen & Liu 1976; Lee et al. 1994; Xu et al. 2008). The magnetic field fluctuations and the ponderomotive force from the nonlinear magnetic pressure results the KAWs to generate the coherent structures of high magnetic field intensity along the magnetic field lines. As the wave propagates, these coherent structures collapse resulting the redistribution of energy from higher wavenumbers to low wavenumbers. This cascade of energy leads to the heating of the plasma.

Many authors (Howes et al. 2008a; Sahraoui et al. 2009; Sahraoui et al. 2010) have reported the evidences for the injection of KAW energy at ion gyroscale and it's dissipation at electron inertial scale resulting to plasma turbulence in many regions of solar plasmas. Two main theories were proposed for this turbulence: non-linear wave-wave or wave-particle interactions and Landau damping. Since the solar wind permeates throughout the heliosphere and solar wind turbulence is also there, it is a good laboratory for theoretical and observational studies (Bruno & Carbone 2013).

In space plasma, it is established that spectral index of the magnetic power spectra at inertial range is nearly the Kolmogorov index of $-5/3$ (Matthaeus et al. 1982; Horbury

et al. 1996; Leamon et al. 1998; Bale et al. 2005). It is followed by another spectral index of -2.5 in the dissipation range (Alexandrova et al. 2008; Chen et al. 2014). This gives the first spectral break at the ion gyroradius or the ion inertial length. The next spectral index is about -5 to -3 at dissipation range (Alexandrova et al. 2009; Sahraoui et al. 2010; Howes et al. 2011a; Chang et al. 2013). This gives the second spectral break at electron scales. The transition region in between the two breaks has the spectral slope either varying from -4 to -2 (Leamon et al. 1998; Smith et al. 2006; Roberts et al. 2013) or complex spectra with no proper spectral index (Bruno & Trenchi 2014). In one of the studies (Lion et al. 2016), the plasma coherent structures are attributed to the steeper spectral slope in the transition region. From the *Cluster* spacecraft data analysis performed by Sahraoui et al. 2013 suggested that the spectral index in the dissipation range to be from -5.5 to -3.5. There is no general consensus regarding the spectral indices of different regions of the magnetic power spectra. In this chapter we try to contribute to the shape of the magnetic power spectra and its spectral index values in the solar wind turbulence by numerically solving the steady state KAW model equation at various types of plasma inhomogeneities represented by the initial conditions of the magnetic fields in the simulations.

Inspite of many studies and investigations (Markovskii et al. 2008; Perri et al. 2010; Bruno & Trenchi 2014), there is no generally accepted theory which can explain the nature of the spectral slopes and break points. The solar wind turbulence and cascade of energy from large scale to small scale in the dissipation range can be explained to some satisfactory level using the KAW (Leamon et al. 2000; Howes et al. 2008b: Schekochihin et al. 2009) or whistler wave (Galtier, 2006: Gary & Smith, 2009; Saito et al. 2010; Podesta et al. 2010; Shaikh 2010), ion cyclotron waves (Goldstein et al. 1994; Leamon et al. 1998; Gary 1999;He et al. 2011), ion Bernstein waves (Howes 2009; Sahraoui et al. 2012), and current sheets (Sundkvist et al. 2007; Osman 2011). In one of the studies of Lion et al. 2016, it was suggested that large amplitude Alfvénic vortex (like

coherent structures) and their collapse could be responsible for the spectral shapes and breaks in the power spectra.

There are many mechanisms that can excite KAWs such as the kinetic fire-hose instability driven by anisotropy in ion and electron temperature (Malovichko 2008; Chen & Wu 2010), field aligned current instability (Chen et al. 2011; Chen et al. 2013; Chen & Wu 2012) and velocity shear instability (Siversky 2005). The field-aligned density perturbations leads to magnetic coherent structures in the plasma. In the past, various authors (Tsiklauri, 2011; Tsiklauri, 2012; Chen et al. 2015; Wu & Chen 2013) have studied the nonlinear propagation of KAWs under density fluctuations and the formation of high intensity magnetic filaments. In a series of studies Tsiklauri, 2011; Tsiklauri, 2012 numerically studied the coronal heating model arising from the KAWs triggered by the density perturbations because of the solar flares. It was concluded that parallel electric fields were generated only in the regions where density fluctuations exist (i.e. at the coronal loop edges). It will effectively accelerate the electrons along the field directions and the ions are effectively accelerated in the transverse direction to the magnetic field by the perpendicular electric fields caused by the KAWs. In the Earth's magnetosphere also similar kind of particle acceleration caused by the KAW dynamics in a perturbed density was found (Tsiklauri, 2011; Chen et al. 2015). Wu & Chen 2013 calculated the growth rate of KAWs driven by transverse density gradient and found that the maximum growth rate for instability occurs when the KAW perpendicular wavelength is near to the spatial characteristic scale of the density fluctuations. Since the KAW perpendicular wavelengths are much shorter than parallel wavelengths, the KAWs are always associated with transverse density fluctuations.

The focus of this chapter is to numerically study the steady state model equation for KAW already derived in the last chapter. The results will be analyzed to understand the role of initial plasma inhomogeneities (fluctuations) to generate magnetic coherent structures and distribution of energy at different wavenumbers and its anisotropy in the

wavevector.

4.2   Model Equation

In this section, we study the dynamics of KAWs in steady state applicable to solar wind at 1 AU. For this purpose we rewrite the governing equation (2.22) in steady state as

$$i\frac{2}{k_{0z}}\frac{\partial B'_y}{\partial z} + \rho_s^2\frac{k_{0x}^2}{k_{0z}^2}\frac{\partial^2 B'_y}{\partial z^2} + \rho_s^2\frac{\partial^2 B'_y}{\partial x^2} + 2ik_{0x}\rho_s^2\frac{\partial B'_y}{\partial x} + \frac{n_1}{n_0}B'_y = 0. \tag{4.1}$$

In an inhomogeneous plasma, a magnetic gradient force known as ponderomotive force acts upon the plasma. The effect of this force and electron Joule heating leads to density perturbation (Shukla & Stenflo 1999). Magnetic field aligned density perturbations in the form of density humps and cavities were found in laboratory and space plasmas (Gekelman et al. 1999).

The particle number density perturbation to the background plasma density was calculated by Shukla & Stenflo, 2000b in adiabatic limit considering slow changes in time with respect to density changes. It is given as

$$n_1 \approx n_0\Big(e^{\xi|B'_y|^2} - 1\Big), \tag{4.2}$$

where $\xi = \{[1 - \Delta(1 + \delta)v_A^2 k_{0z}]/16\pi n_0 T_e\omega^2\}$, $\Delta = \omega^2/\omega_{ci}^2$ and $\delta = m_e k_{0x}^2/m_i k_{0z}^2$. For $\omega(1 + \delta)^{1/2} < \omega_{ci}$, the density profile is a hump. For KAWs since the plasma $\beta >> m_e/m_i$, the particle thermal speed is greater than the Alfvén speed ($v_{ti}, v_{te} >> v_A$). Therefore the electrons or ions move fast enough to respond any adiabatic response in density.

Substituting equation (4.1) to equation (4.2) and reducing it to normalized units, the governing equation for KAW in an inhomogenous plasma becomes

$$i\frac{\partial B'_y}{\partial z} + 2iK\frac{\partial B'_y}{\partial x} + K^2\frac{\partial^2 B'_y}{\partial z^2} + \frac{\partial^2 B'_y}{\partial x^2} + \frac{1}{2g}\Big(e^{2g|B'_y|^2} - 1\Big)B'_y = 0, \qquad (4.3)$$

where $K = k_{0x}\rho_s$ is a dimensionless parameter defining the transverse wave number normalized to the inverse of the ion acoustic gyroradius ρ_s at electron temperature. In substituting the perturbed density, for the sake of generality we have used the dimensionless parameter g that controls the coupling to the density perturbation and magnetic field. When $g = 0$, the equation reduces to well known quadratic nonlinearity. The following normalizing parameters are used: $z_n = 2/k_{0z}$, $x_n = \rho_s$, and $B_n = [\{1 - \Delta(1 + \delta)\}V_A^2 k_{0z}^2/16\pi n_0 T_e \omega^2]^{-1/2}$.

As mentioned above, when $g = 0$ the equation (4.3) resembles cubic nonlinear Schrödinger equation (NLSE). If $g \neq 0$, the governing equation can not be integrated, thereby it may result to spatial chaos.

In order to find out the relationship between the initial KAW pump wave amplitude and the parameter g, we substitute a simpler homogeneous solution as $B_{y0}e^{-iz}$ (Zhou et al. 1992; Zhou & Hi 1994) in equation (4.3) where B_{y0} is the amplitude of the homogenious pump KAW. Further we simplify it by taking $K = 0$ in the model equation to get

$$|B_{y0}| = \sqrt{\frac{ln|1 - 2g|}{2g}}. \qquad (4.4)$$

It gives the range of g as $0 \leq g < 1/2$.

In the next section, we will carry out the numerical solution of equation (4.3) by taking the main KAW as a plain/Gaussian wavefront superimposed with different kinds of perturbations.

4.3   Numerical Simulation

In order to study the role of the different kinds of magnetic field inhomogeneities, the numerical simulation of equation (4.3) was carried out with four different kinds of initial

conditions (ICs) as described below. The first initial condition denoted as IC-1 is

$$B_y'(x, 0) = B_{y0}[1 + \varepsilon \cos(\alpha_x x)] \qquad \text{(IC-1)}$$

where a uniform plane KAW of fixed amplitude is superimposed by a sinusoidal periodic perturbation. The constant ε is the magnitude of the perturbation and α_x which is normalised by x_n^{-1} is the wave number of the perturbation.

The second initial condition denoted as IC-2 is a uniform plain KAW with a Gaussian perturbation

$$B_y'(x, 0) = B_{y0}[1 + \varepsilon \exp\left(-x^2/r_{01}^2\right)] \qquad \text{(IC-2)}$$

where r_{01} normalized by x_n is the scale size of the transverse perturbation.

The third initial condition denoted as IC-3 is a non-uniform KAW of Gaussian wave front with a sinusoidal perturbation

$$B_y'(x, 0) = B_{y0}[\exp(-x^2/r_0^2) + \varepsilon \cos(\alpha_x x)] \qquad \text{(IC-3)}$$

where r_0 normalized by x_n is the transverse scale size of the main KAW initial beam width.

The fourth initial condition denoted as IC-4 is a non-uniform KAW of Gaussian wave front with a random perturbation

$$B_y'(x, 0) = B_{y0}[\exp(-x^2/r_0^2) + \varepsilon \exp(2\pi i\theta(x))] \qquad \text{(IC-4)}$$

where $\theta(x)$ is a random variable uniformly distributed on [0,1].

The numerical code was developed in FORTRAN by applying pseudo-spectral method with Fast Fourier Transform (FFT) for transverse (x-direction) space integration with periodic length $L_x = 2\pi/\alpha_x$ with 2^8 grid points. The numerical method used here, was extensively discussed in chapeter 3. Along the z-direction a finite-difference method with a predictor-corrector scheme with step size $dz = 5 \times 10^{-5}$ was used. In the normalized

model equation, the linear terms appeared as second, third and fourth terms in the equation were solved in Fourier space and the nonlinear term appeared as fifth term in the equation was solved by taking local product in real space first and then it was transformed to k-space by taking FFT. First we developed the programme code for well-known cubic NLSE that can be obtained here by taking $K = 0$ and $g = 0$, which gives the density profile as quadratic to magnetic field i.e. $n_1/n_0 \simeq \xi |B_y'|^2$. Since the cubic NLSE can be integrated, we computed the integration constant i.e. the plasmon number $N = \sum_k |B_k|^2$. This indicates the conservation of wave energy. In our simulation the plasmon number was found to be constant upto the precision of six decimal places. Once the cubic NLSE code was fully tested, the code was modified to numerically solve our given model equation satisfied by the KAWs.
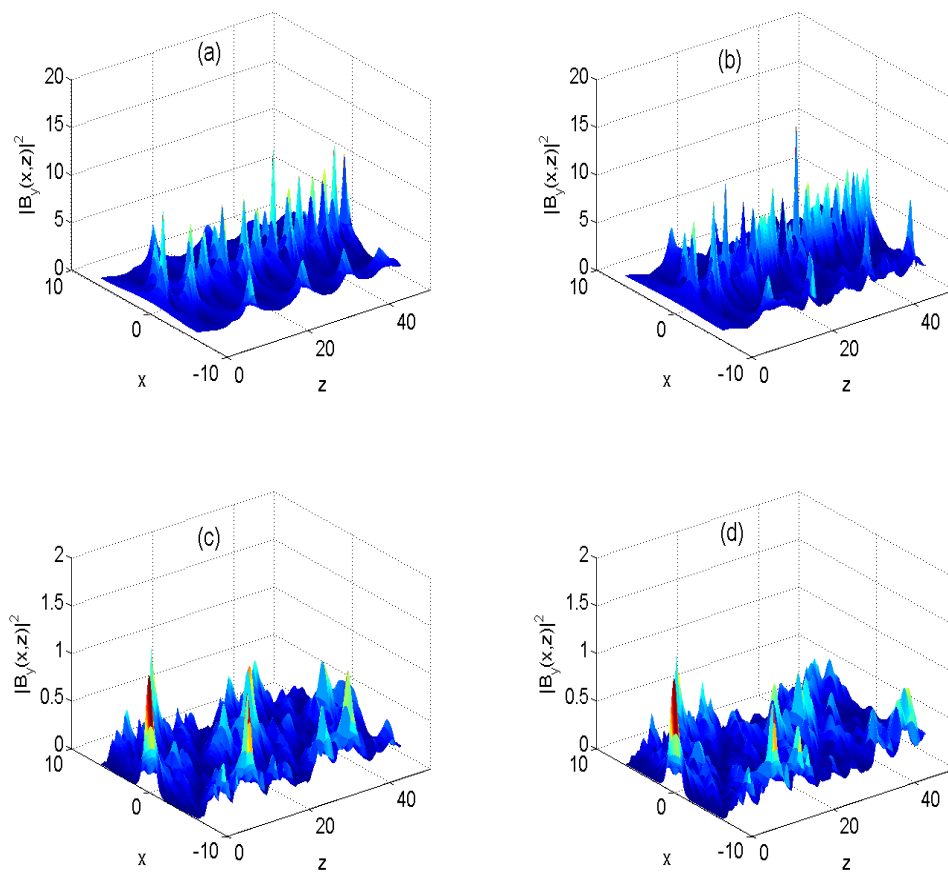
Fig. 4.1 Coherent structures of magnetic field applicable to solar wind at 1 AU: (a) IC-1, (b) IC-2, (c) IC-3 and (d) IC-4.

The values of the parameters we used in numerical simulations are $\varepsilon = 0.1$, $\alpha_x = 0.5$, $r_0 = 1.0$, $r_{01} = 5$. Hence we get $L_x = 2\pi/\alpha_x \simeq 12.5 \simeq 2.5 r_{01}$. We chose the parameter $g = 0.01$. Hence we get the amplitude of the pump KAW $B_{y0} \simeq 1.005$ and the ratio of the magnetic fluctuation to the amplitude of the pump KAW $|\delta B_y/B_{y0}| \simeq 0.1$. Large depressions of magnetic field, $\delta B/B_0 \sim 90\%$ were found from the satellite data analysis in the solar wind (Winterhalter et al. 1994) the cusp, magnetosheath and magnetopause of the earth's magnetosphere (Tsurutani et al. 1982; Savin et al. 1998).

The solar wind data measured at 1AU by *Helios* 2 spacecraft (Cravens, 2004) are: $B_0 \approx 1 \times 10^{-4} G$, $n_0 \approx 5\ cm^{-3}$, $T_e \approx 0.5 \times 10^5 K = 4.31 eV$, $T_i \approx 0.2 \times 10^5 K = 1.72 eV$. In order to substitute the required parameter values in the simulation and it's relevant applications to solar wind, we calculated the other parameters of interest as: $\beta = 0.121$, $v_{te} \approx 8.7 \times 10^7 cm\ s^{-1}$, $V_A \approx 9.8 \times 10^6 cm\ s^{-1}$, $\omega_{ci} \approx 0.95 rad/sec$. $\rho_s = 2.5 \times 10^6 cm$, $\rho_i = (\sqrt{T_i/T_e})\rho_s = 3.75 \times 10^6 cm$, $\rho_e = 4.9 \times 10^4 cm$, $\lambda_i = 9.9 \times 10^6 cm$, $\lambda_e = 2.38 \times 10^5 cm$. Here we redefine the parameters ion gyroradius $\rho_i\ (= v_{ti}/\omega_{ci})$, electron gyroradius ρ_e $(= v_{te}/\omega_{ce})$, ion inertial length (or ion skin depth) $\lambda_i = c/\omega_{pi}$ and ion plasma oscillation frequency $\omega_{pi}(= \sqrt{4\pi n_0 e^2/m_i})$.

For $\omega = 0.01 rad/sec$ and $K = k_{0x}\rho_s = 0.01$; we get $k_{0z} = 6.44 \times 10^{-9}\ cm^{-1}$ and $k_{0x} = 3.98 \times 10^{-9} cm^{-1}$. The values of other normalizing parameters are $B_n \simeq 4.2 \times 10^{-5} G$, $x_n \simeq 2 \times 10^6\ cm$ and $z_n \simeq 3 \times 10^8\ cm$.

Now we start analyzing the numerical simulation results of the model equation solved with the four initial conditions as described earlier. First the magnetic field intensity profiles depicted by the spatial evolution of KAW packets in 2D are shown in figures 4.1(a) - 4.1(d). The localized magnetic coherent structures (filaments) of KAWs are generated. Their sizes vary from the energy injection scale which is comparable to ion gyroradius to dissipation scale which is comparable to electron gyroradius. It is observed from the figures that IC-1 and IC-2 generate almost same pattern of magnetic field intensity profile. The profile peak intensities are nearly at $|B_y|^2 = 12.29$ localized at the

spatial locations of around $z = 31.50$ and $x = 0.29$ for IC-1 and $|B_y|^2 = 14.17$ localized at around $z = 31$ and $x = 0.40$ for IC-2. Most of the filaments are generated at the mid position of the x direction. For IC-3 and IC-4, the magnetic field intensity filaments are very less. The peak intensities for both the initial conditions are almost same, having the value of around 0.96 located at around $x = 6.18$ and $z = 12.50$.

The mechanism for the generation of magnetic coherent structures is similar with the mechanism of laser focusing as explained by Kruer 2003. As the density of the medium is perturbed, the dielectric constant and hence the refractive index of the medium will be changed. The laser beam propagating through the medium of varying refractive index will act as a focusing lens and the wave will be focused. Similarly here also, the parallel ponderomotive force will modify the density. The KAWs propagating through this medium having density perturbations will produce varying phase velocity generating the spatial localization of the wave field.

These magnetic coherent structures enhances in transferring energy from large scales (comparable to ion acoustic gyroradius) to small scales (comparable to electron thermal gyroradius). The plasma inhomogeneities manifested in the magnetic field and density perturbations in our study will take energy from the main KAW by nonlinear interaction and as the KAW propagates, it will generate magnetic filaments. Gershman et al. 2017 have found that local generation of observed KAWs, as observed by NASA's Magnetospheric Multiscale (MMS) mission, are due to the combined effects of nonlinearities arising from inhomogeneities in the magnetic field and particle number density.
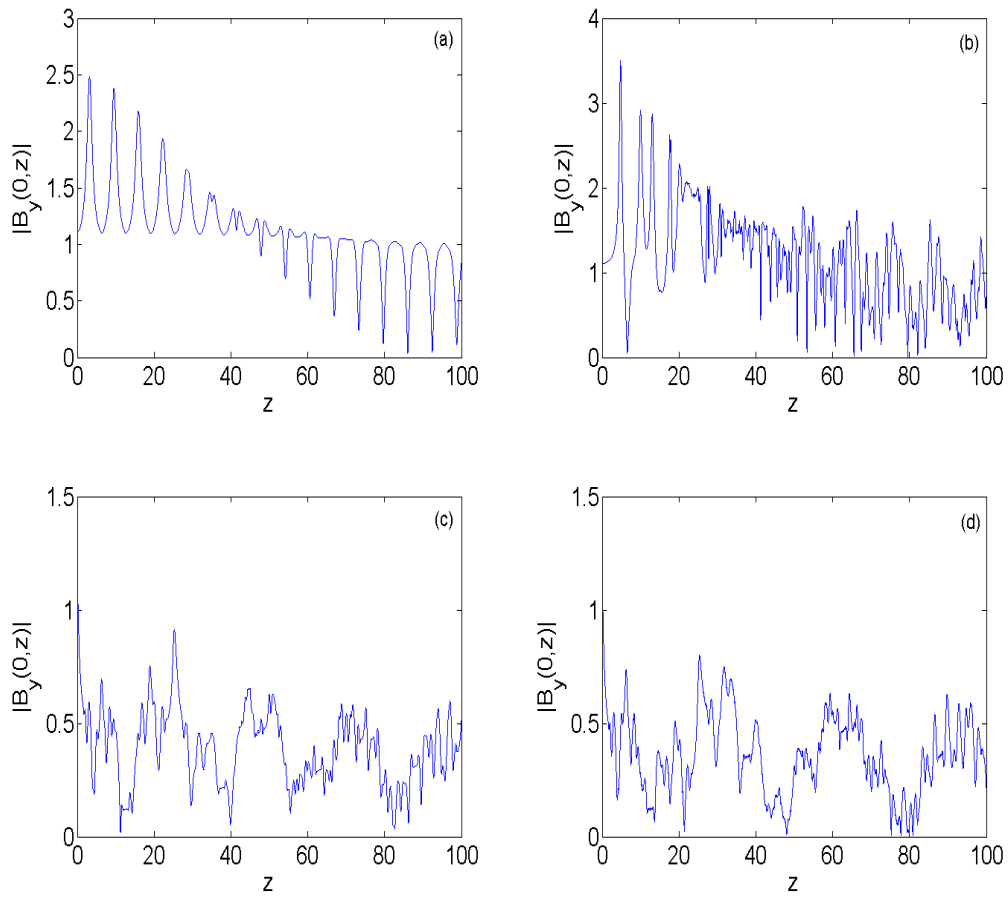
Fig. 4.2 Plot of magnetic field amplitude verses the distance of propagation for KAWs applicable to solar wind at 1AU (a) IC-1, (b) IC-2, (c) IC-3 and (d) IC-4.
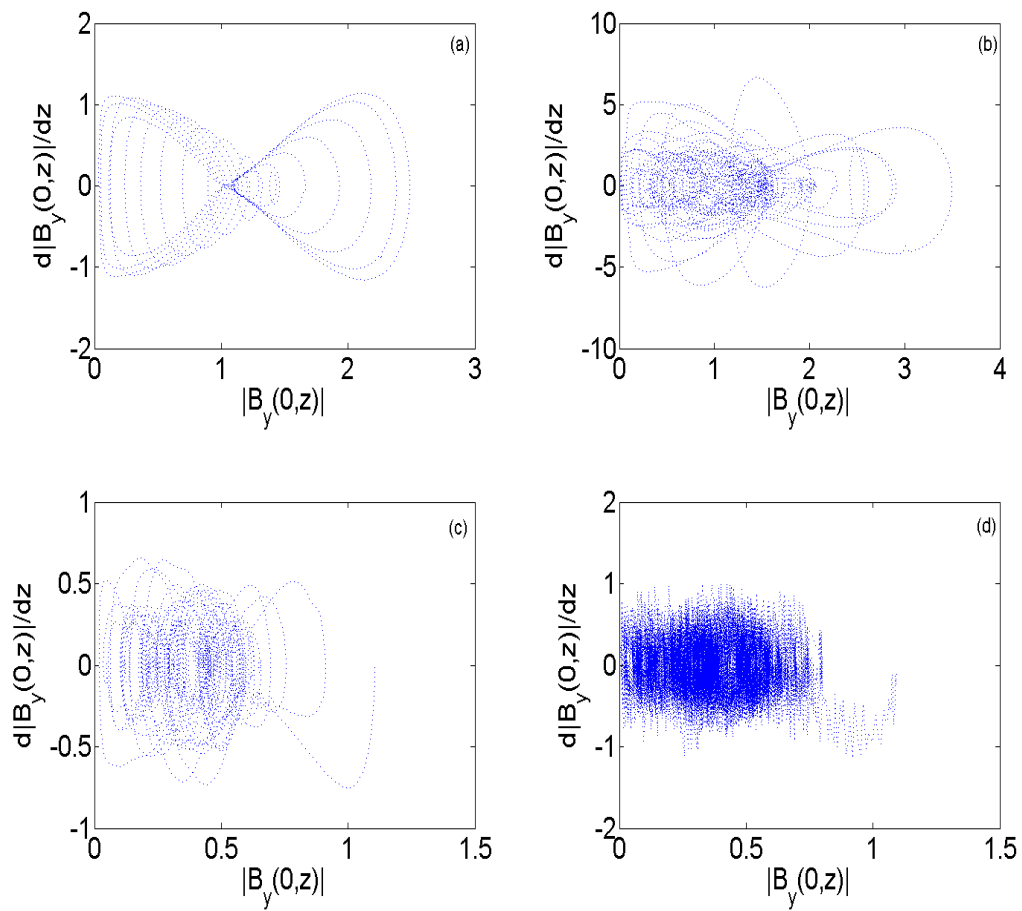
Fig. 4.3 Phase space plots of KAWs applicable to solar wind at 1AU: (a) IC-1, (b) IC-2, (c) IC-3 and (d) IC-4.
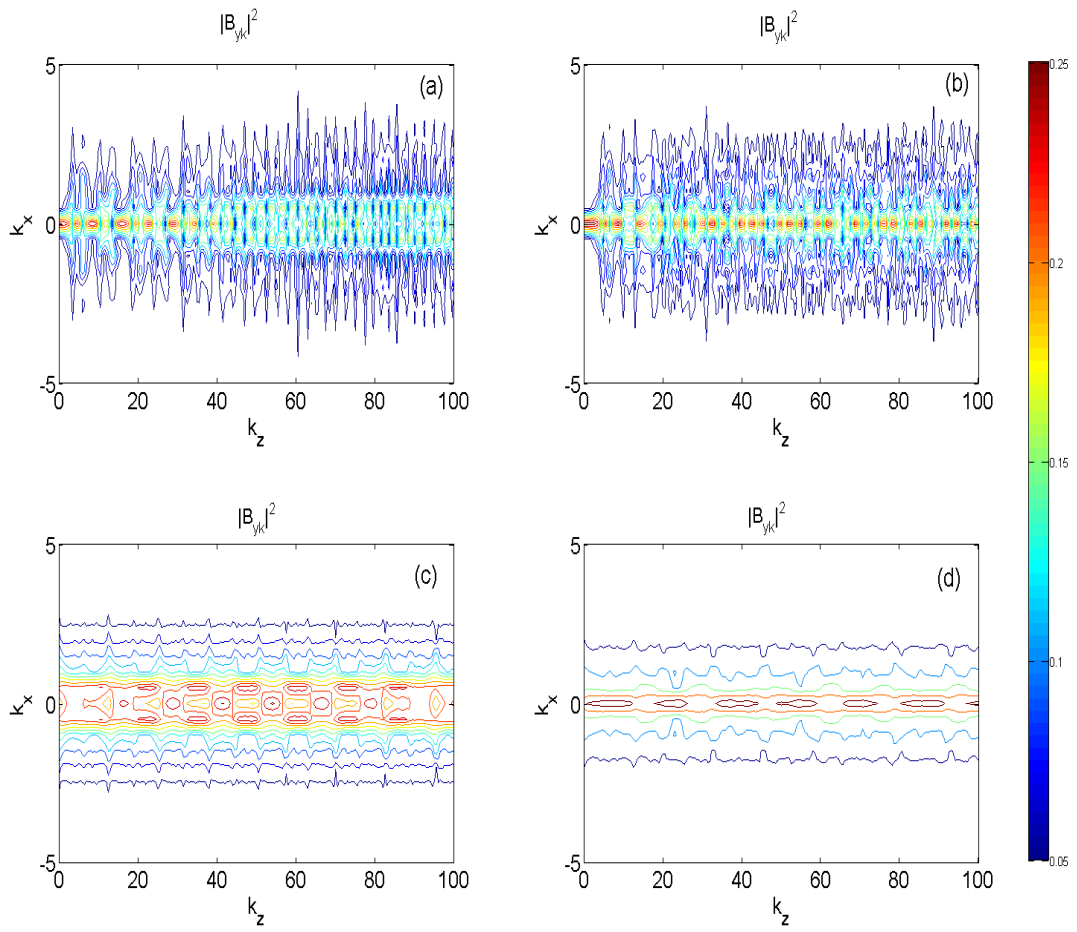
Fig. 4.4 Contour plot of KAWs applicable to solar wind at 1AU: (a) IC-1, (b) IC-2, (c) IC-3 and (d) IC-4.

If the parallel fluctuations in the magnetic fields and current density are sufficiently large in amplitude as happened in the propagation of KAWs, the electrons can be trapped in between the wave packets. The fluctuations in parallel magnetic field will result in transit time damping effects that can be considered as magnetic analog of Landau damping. From the magnetic field intensity profile depicted in figure (4.1), it is observed that when the strength of the magnetic field intensity is sufficient, the collapse of the structures at kinetic scales starts. This will lead heating of the electrons/ions in the plasma. Furthur, if the size of the magnetic structures are less than ion acoustic gyroradius, the ion motions decouple from the electron motions. Our simulation result shows that the largest scale size of the magnetic coherent structures measured at the half of the intensity peak is of the order of ion gyroradius $\approx 6\rho_s = 188.50$ km. Lion et al. 2016 and Chmyrev et al. 1988 also reported almost the same scale size of magnetic coherent structures as we found in our simulation. However, if we increase the pump wave amplitude that can be done here by increasing the parameter g, the filamentary size becomes less than ρ_s (Sharma et al. 2006). When the transverse wavelength is comparable to ρ_s, heating of the plasma particles is more effective by transferring energy from the KAW to electrons/ions.

For furthur investigation, we take the value of the magnetic field amplitude at a fixed $x(x = 0)$ and plotted it at various positions of propagation distance z as shown in figure (4.2). For IC-1, the motion is quasiperiodic. For other initial conditions it tends to chaotic motions. The phase space portraits are shown by plotting $|B_y(0, z)|$ vs $d|B_y(0, z)|/dz$ in figure (4.3). The motion is having irregular homoclinic orbit (HMO) with quasiperiodic oscillations for IC-1. The hyperbolic fixed point was observed at $|B_{y0}| = \sqrt{ln(1 - 2g)/2g}$. For other initial conditions, the motion is spatially chaotic.

Our numerical results showed that all four ICs produce some features of chaotic motions. This can be quantitatively represented by calculating the Lyapunov exponent defined as

$$\lambda = \lim_{z \to \infty} \lim_{b(z=0) \to 0} \left\{ \frac{1}{z} ln \left| \frac{b(z)}{b(z=0)} \right| \right\} \tag{4.5}$$

where b is the first derivative of $B(x, z)$ w.r.t. z at a fixed x. The calculated Lyapunov exponents for IC-1, IC-2, IC-3 and IC-4 were 0.013, 0.028, 0.052 and 0.097 respectively. The positive values of Lyapunov exponents mean that the system is complex and spatially chaotic for all ICs. But their degree of complexity and chaosness are not same. Hence, nature of the inhomogeneties in the magnetic field and density determines the nature of the KAW propagation and its distribution of energy.

To investigate the propagation of energy in Fourier space, we plotted the contour plots of $|B_{yk}|^2$ in k_x, k_z plane (Figure 4.4). Here, the lines in the plot connect the coordinates of k_x and k_z having the same values of $|B_{yk}|^2$. The intensity of the magnetic field represented by the color bar appeared on the right panel of the figure. Initially most of the energy is confined at $k_x = 0$ and it is ditributed to higher wavenumbers as KAW propagates. The distribution of the energy at perpendicular wave number is greater in IC-1 than that of IC-2. It is observed from the contour plots that the energy is already distributed from $k_z = 0$ for IC-3 and IC-4.

Fig. 4.5 Magnetic field spectral intensity $|B_{yk}|^2$ versus $k_\parallel \rho_s$ for solar wind at 1AU: (a) IC-1, (b) IC-2, (c) IC-3 and (d) IC-4.

Next we show the spectral power along the parallel wavenumber by plotting $|B_{yk}|^2$ vs $k_z = k_\parallel$ [Figure 4.5 (a) - 4.5(d)]. Earlier it was predicted theoretically that there was no cascade of energy in parallel wave number space (Kraichnan, (1965a); Shebalin et al. 1983). But Goldreich & Sridhar, 1995 showed that in strong MHD regime there is cascade of energy in the parallel wave number space. In our simulation results, all the initial conditions have spectral indices of Kolmogorov scale $k_\parallel^{-5/3}$ for $k_\parallel \rho_s < 1$ *i.e.* called inertial range. This is in agreement with the observations of many authors such as Champeaux et al. 1998; Lavender et al., (2001) and Sulem & Sulem, 1999. In the transition region from inertial range i.e. ion scale to kinetic range i.e.electron scale, there is no fixed spectral shape. The first spectral break happens at $k_\parallel \rho_s \approx 1$. The transition region having variable spectral shape was reported from many studies (Smith et al. 2006; Sahraoui et al. 2010; Bruno & Trenchi 2014; Jian et al. 2014). After the transition range, the spectral index is more steep (k^{-2} to $k^{-5.5}$) at ion kinetic scale ($k\rho_s > 1$) (Leamon et al. 1998; Bale et al. 2005; Smith et al. 2006; Sahraoui et al. 2009; Sahraoui et al. 2013; Roberts et al. 2013). Our power spectral graph from figure (4.5), shows these slopes as $-3, -4, -2$ and -2 for IC-1, IC-2, IC-3 and IC-4 respectively.
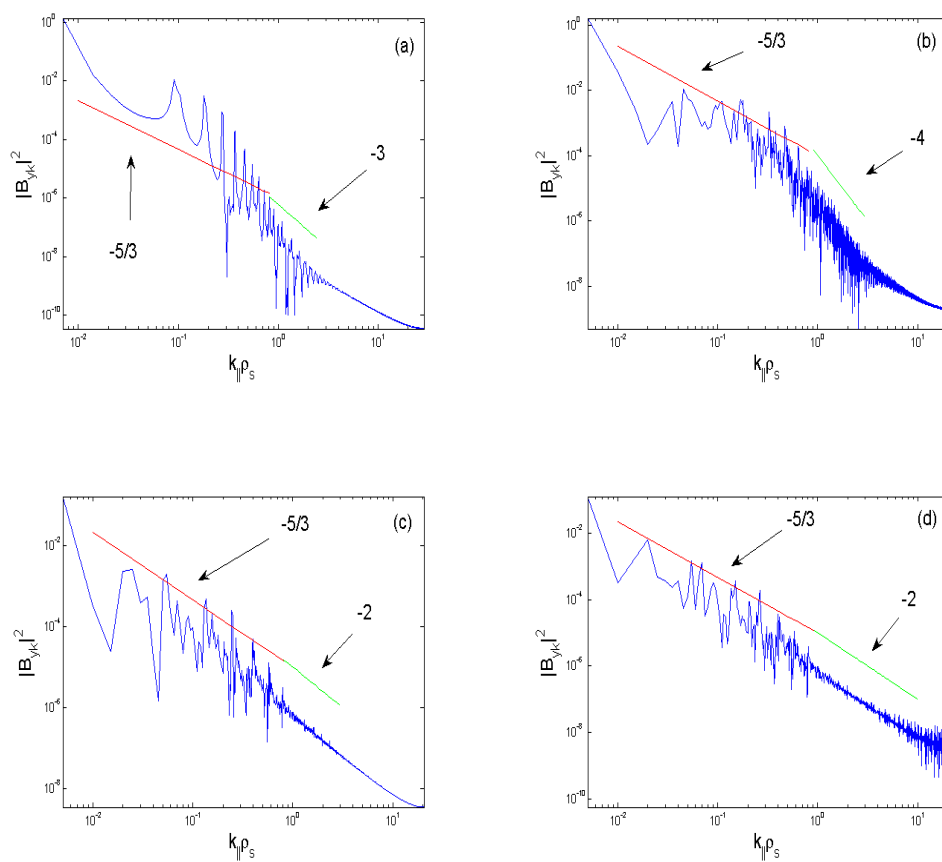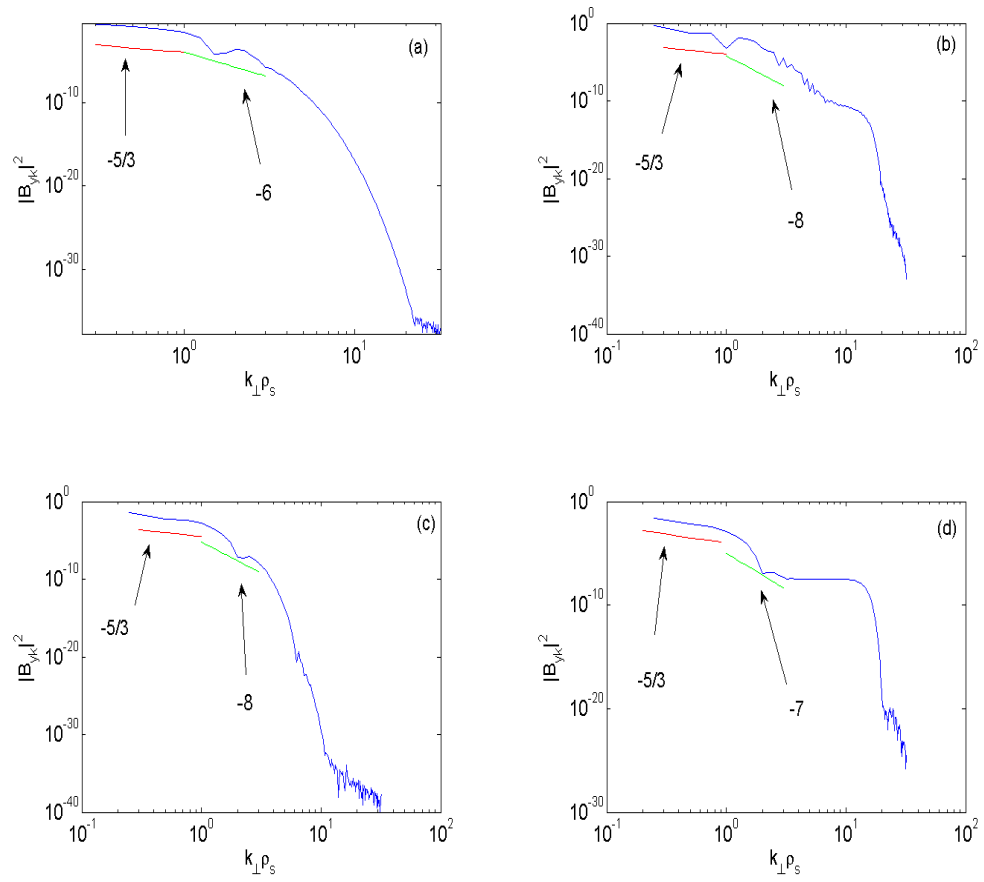
Fig. 4.6 Magnetic field spectral intensity $|B_{yk}|^2$ against $k_\perp \rho_s$ for solar wind at 1AU (a) IC-1, (b) IC-2, (c) IC-3 and (d) IC-4.

The injected energy at inertial scale is redistributing to the various Fourier modes. To witness this we plotted log-log scale of $|B_{yk}|^2$ versus $k_\perp \rho_s$ in figures 4.6(a) - 4.6(d). The usual Kolmogorov scale of $-5/3$ spectral slope is found at inertial scale ($k_\perp \rho_s < 1$). The slopes are much steep at ion scale (i.e. $k_\perp \rho_s > 1$) being -6 for IC-1, -8 for IC-2 & IC-3 and -7 for IC-4. The deepest spectral slopes are at the electron scale *i.e.* $k_\perp \rho_s \geq 10$ or $k_\perp \rho_e \approx 1$.

The second break point in the spectral shape happens at electron inertial scale length, i.e. $k_\perp \rho_s \approx 10$. It should be mentioned here that our present model is not applicable beyond this scale length because of the low frequency $\omega < \omega_{ci}$ approximation we have used in deriving the governing wave equations. From the Cluster spacecraft data analysis, Sahraoui et al., (2009) found that the cascade of energy due to KAWs at low frequency $\omega < \omega_{ci}$ happens down to $k_\perp \rho_i \approx 20$. It corresponds to KAW frequency of around 5 Hz which is the noise level of the instrument. Hence, our model is not fit for the range beyond $k_\perp \rho_s \approx 10$. In this regime, whistler wave models ($\omega > \omega_{ci}$) or the interaction of KAWs with whistler waves are to be taken into consideration.

Anisotropies in magnetic fluctuations in solar plasma at kinetic scales were reported by many investigations (Chen et al. 2010; Sahraoui et al. 2010; Narita et al. 2011). They showed that the turbulence is more anisotropic at large wavenumbers, hence more energy cascade in the perpendicular wavenumber when $k_\perp > k_\parallel$. It is evident from our spectral intensity plots that the magnetic spectral slope is anisotrpic to the field energy producing more deep in $k_\perp$ than in $k_\parallel$ at kinetic scale. The slopes in $k_\perp$ are -6, -8, -8 and -7 for IC-1, IC-2, IC-3 and IC-4 respectively. Sahraoui et al. 2013 found the magnetic power spectra having the slopes from -5.5 to -3.5 at the electron scales.
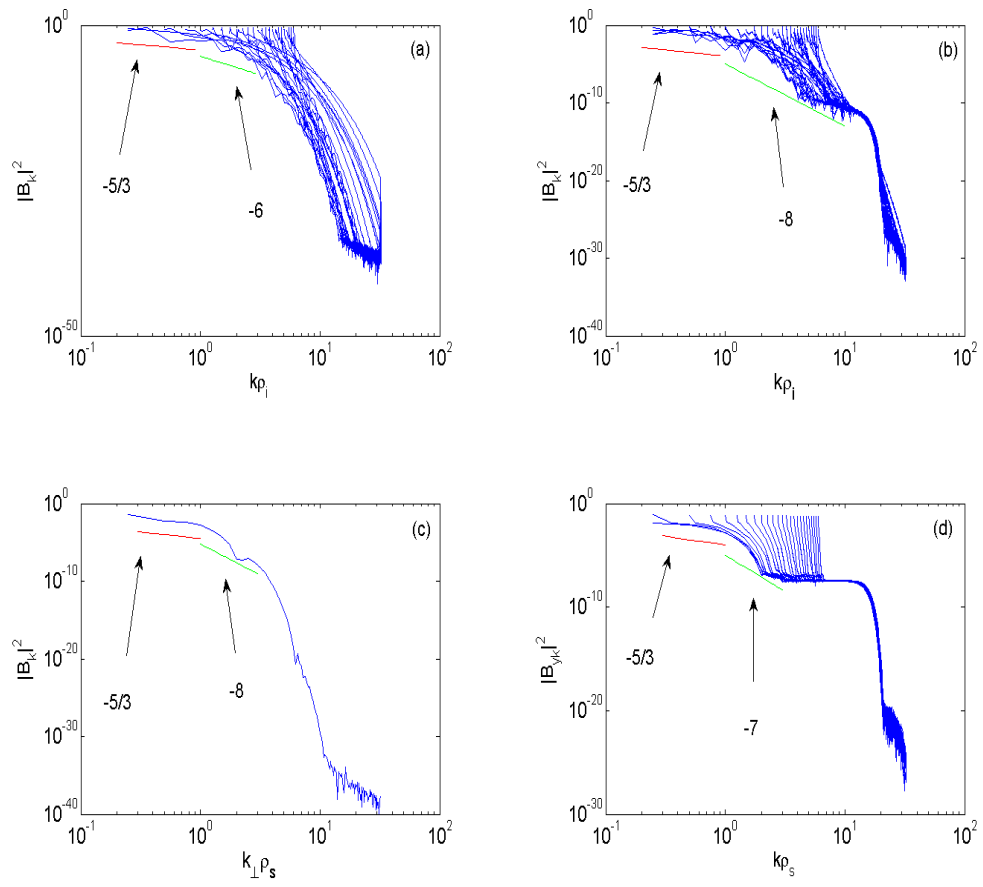
Fig. 4.7 Magnetic field spectral intensity $|B_{yk}|^2$ versus $k\rho_s$ for solar wind at 1 AU: (a) IC-1, (b) IC-2, (c) IC-3 and (d) IC-4.

Figure (4.7) represents $|B_{yk}|^2$ versus $k\rho_s$, where the total wavenumber was calculated as $k = \sqrt{k_\parallel^2 + k_\perp^2}$. It shows the slope of -6 to -8 at $k\rho_s > 1$. Alexandrova et al. 2009 tried to fit the spectral break with that of *Cluster* spacecraft data as $\sim e^{-\sqrt{k\rho_e}}$ for the range of $k\rho_e$ from 0.1 to 1. Howes et al. 2006 and Schekochihin et al. 2009 attributed the dispersive nature of KAWs as the main reason for the steepening of spectral index. Wave particle interaction becomes dominant at the scales near to ion gyroradius or electron inertial length leading to Landau damping to heat the plasma particles (Gary & Nishimura, 2004; Sahraoui et al. 2009). Since the whistler waves and KAWs have similar prroperties, it is not clear whether the small scale fluctuations are due to KAWs or whistler waves or the interaction between them (Gary & Smith, 2009; Salem et al. 2012; Boldyrev et al. 2013; Chen et al. 2013). Many researchers have also studied the interaction of KAWs with other waves such as whistler waves, magnetosonic waves, ion acoustic waves etc as the possible way to understand the solar wind turbulence and particle acceleration. Therefore, our present model will contribute to the knowledge of solar wind turbulence which is not fully understood till now.

The model we are studying in this present chapter is limited to steady state (spatial domain) only. In fact, the transient fluctuations are also to be taken into account. Therefore, we extend the present model in the next chapter to study the transient behaviour of the KAW dynamics in an inhomogenous medium.

4.4   Conclusion

In this chaper, we have presented the numerical simulation results of steady state dynamical KAW propagation in an inhomogenous plasma having the inhomogeneity in transverse magnetic field and density fluctuations. The applications of the results at 1AU solar wind parameters were also discussed. The magnetic filaments of KAWs with high intensity are generated as the wave propagates along the direction of magnetic field. The dynamical motions are dependent on the type of plasma inhomogeneity represented by

four different kinds of initial conditions in our numerical simulation. The perturbation present in the magnetic field gets the energy from the pump KAWs. As the wave propagates magnetic coherent structures are generated when there is a balance between the wave diffraction and nonlinearity effects resulting from plasma inhomogeneity profile. The collapse of the KAW packets will take place when this balance is no more and this leads to the transfer of energy from the wave to the particles in the plasma such as electrons and ions. This transfer of energy at perpendicular wavevector is more for uniform initial pump KAW (IC-1& IC-2) than those for non-uniform initial pump wave of Gaussian wavefront (IC-3 & IC-4). The transfer of energy at kinetic small scales when the wavenumber is less than ion gyroradius and comparable to electron inertial length causes solar wind turbulence and heating of the plasma. In our study we found the spectral index following the Kolmogorov scale of $-5/3$ which is in the inertial range followed by deeper indices varying from -2.5 to -8 in the kinetic dissipation range.

In the magnetized plasma like solar wind, where the particle density is very low, the collision mean free path is of the order of 1AU. Since the collisions among particles are very rear, we can not precisely well defined the scale length of the dissipation process. Some of the spatial characteristic scale lengths in the solar wind turbulence are ρ_s, ρ_i, λ_i, ρ_e and λ_e. As the scale length changes, the mechanism for energy transfer also changes, hence energy transfer rates are also different. Therefore it results in different spectral indices in the magnetic power spectra. Since the formation of magnetic filaments and it's collapse is considered as one of the faster way to transport energy, our present study may provide some clues to understand the phenomenon of energy distribution via dissipation in the solar wind.

Chapter 5

Transient Dynamics of Kinetic Alfvén Waves and Turbulence in Solar Coronal Loops

5.1 Introduction

The solar coronal heating problem, where photosphere near the sun is having temperature of around $5780K$ only and the solar corona at more far away from the Sun having temperature of around $2 \times 10^6 K$, is an unresolved issue in Astrophysical community till now. Recently various spacecraft observations such as Solar and Heliospheric Observatory ($SOHO$), Transition Region and Coronal Explorer ($TRACE$), Hinode and Solar Dynamics Observatory (SDO) have observed that the solar atmosphere is inhomogeneous in magnetic field and density. Therefore, the magnetic fine structures known as magnetic filaments which are the manifestation of field aligned density or temperature gradients play a very significant role in the coronal heating.

Generally, solar corona can be divided as coronal holes (open regions) and coronal loops (closed regions). The solar wind originates from the coronal holes which are cooler and less dense. The solar wind permeates through the space with the associated magnetic

field lines and energetic charged particles. Alfvén, 1942 for the first time, presented the role of Alfvén waves and solar magnetic field lines to understand solar coronal heating. Since then many physical processes were proposed, among them two prominent theories are: heating by waves (Narain and Ulmschneider, 1996; Hood et al. 1997; Goossens, 1994; Priest et al. 2000; Poedts and Goossens, 1989; Ruderman, 1999) and heating by flares or magnetic reconnection (Jain et al. 2005; Hood et al. 2009; Sturrock et al. 1999; Cassak and Shay, 2012). More recently, the role of Alfvén waves in solar coronal heating were reported from spacecraft data analysis and theoretical studies (Parker, 1979; De Pontieu et al. 2007; Okamoto et al. 2007; Cirtain et al. 2007).

Pure Alfvén waves can not sufficiently dissipate to heat the plasma to reach up to the coronal temperature because of the large transverse scale length (Wu & Chen 2013). When AW transverse wavelength is comparable to the main kinetic length scale of the plasma, λ_e or ρ_i or ρ_s (whatever is longer) where λ_e is the electron inertial length, ρ_i is the ion gyroradious and ρ_s is the ion acoustic gyroradius, the AWs become dispersive and known as dispersive AWs (DAWs). DAWs can be classified into two: the inertial Alfvén wave (IAW) when $\lambda_e > \rho_i$ or ρ_s and the kinetic Alfvén wave (KAW) when $\rho_s >$ or $\rho_i > \lambda_e$. Many studies supported that the dispersive property of DAWs are mainly responsible for heating the inhomogeneous plasma such as solar wind and corona (De Azvedo et al. 1994; Voitenko, 1995; Voitenko, 1996; Elfimov et al. 1996; Asgari-Targhi and Van Ballegooijen, 2012; Morton, 2015; Testa et al. 2014). When the low frequency ($\omega < \omega_{ci}$) DAWs propagate in a transversely inhomogeneous plasma, it generates sufficient parallel and perpendicular components of electric fields. Here the transverse density (or/and temperature) inhomogeneity scale length should be comparable to the microscopic scale length of plasma particle motions such as electron inertial or ion gyroradious length. The parallel electric field can sufficiently accelerate the plasma along the ambient magnetic field direction.

The IAWs applicable in low $\beta < m_e/m_i$ plasmas are observed to the auroral region of the Earth's magnetosphere located at altitudes less than 4 Earth radii. However, in solar corona both the plasma β values are applicable; the intermediate β plasma, $m_e/m_i < \beta < 1$, in active regions such as coronal holes coronal loops and low β plasmas at the base of the coronal holes or coronal loops where the heavy particle density $n_0 \sim (10^8 - 10^{10})cm^{-3}$ and ambient magnetic field $B_0 \sim (5 - 150)G$ (Champeaux et al. 1997). Therefore, KAW is applicable to both the solar wind $\beta = 0.121$ at 1AU (Cravens, 2004) and the coronal loops $\beta = 0.01$ (Shukla et al. 1999). For solar wind at 1AU and coronal loops the temperatures ($\approx 10^6 K$) are almost same. However, the magnetic field of the solar wind ($B_0 \approx 1 \times 10^{-4}G$) is very less than that of the coronal loop $B_0 \approx 100G$. Similarly the density of the coronal plasma ($n_0 \approx 5 \times 10^9 cm^{-3}$) are much higher then that of solar wind ($n_0 \approx 5cm^{-3}$).

In a series of studies, Voitenko, 1996, Voitenko, 1998 showed that the KAW magnetic filaments and its collapse is the main candidate for the nonlinear evolution of turbulent saturated spectra in coronal loops and solar flares. Other studies also supported that the dissipation of KAWs can lead to particle energization in bright coronal loops (Wu & Fang, 1999), bright coronal plumes (Wu & Fang 2003), sunspot chromosphere (Wu and Fang, 2007), anisotropic and mass dependent heating in solar corona (Wu & Yang 2006; Wu & Yang, 2007). To model the Freja sattelite data results, auroral particle acceleration and coronal heating, many researchers (Wu et al. 1997; Wang, 1998; Chen et al. 2000) have investigated the propagation of KAWs in an inhomogenous plasma having the density variations in the form of dips, humps and dipoles. Further, Shukla and Stenflo, 2000 using the ponderomotive force relations derived by Bellan & Stasiewicz 1998 showed that KAWs can produce magnetic field aligned quasistationary density humps and dips.

The anisotropic nature of KAW magnetic field energy in wavevector was reported by many authors (Goldreich & Sridhar, 1995; Goldreich and Sridhar, 1997 Marson and Goldreich, 2001; Cho et al. 2002) and spacecraft data (Leamon et al. 1998; Luo and

Wu, 2010; Luo et al., 2012). They suggested that the wave energy is predominantly cascading in the transverse directions to the field lines i.e. $k_\perp >> k_\parallel$, where $k_\perp$ $(k_\parallel)$ is the wave number perpendicular (parallel) to the ambient magnetic field (Howes et al. 2006; Schekochihin et al. 2009). Hence, we will have to take into account the effect of finite $k_\perp \rho_s$ i.e. $\partial/\partial x >> \partial/\partial z$ in the dynamical model equations that we are studying.

The main aim of this chapter is to study the transient KAW dynamics propagating in an inhomogeous plasma. The inhomogeneity in the plasma comes from the field aligned density fluctuations because of ponderomotive force and Joule heating. The governing equations derived in Chapter 2 in the form of modified nonlinear Schrödinger equation (NLSE) was solved numerically in Fourier space with the possible parameters of coronal loop plasma. The numerical results are analyzed to understand the generation of magnetic filaments, distribution of energy among the wave numbers. The role of the plasma inhomogeneity represented by four kinds of initial conditions of simulations is also studied.

Earlier studies (Sharma et al. 2006; Singh & Sharma, 2007; Singh & Jatav, 2019) related to the dynamics KAW in the form of modified NLSE applicable to solar wind turbulence and coronal heating were much limited to steady state. In their studies, the anisotropic character of the magnetic power spectra was not discussed properly. This chapter studies the non-steady state (transient) propagation of 2D-KAWs applicable to coronal loops. How the plasma inhomogeneity affects on the generation of magnetic coherent structures and the wavenumber anisotropy in energy distribution, is also discussed. The generation of 3D KAW vortices from the twisting of the magnetic coherent structures and its effect on plasma heating was studied by Sharma et al. 2014; Sharma et al. 2016. They considered the interactions of 3D-KAWs and 3D-ion acoustic waves and suggested that as the time progresses, the coronal loops are twisted more and more, increasing the flow of current in the plasma channel. When the strength of the current reaches the critical value, it will erupt as solar flares. However, the physical mechanism of the KAW turbulence and

heating has not been solved till now. Some possible theories may be due to dissipation of KAWs or whistler waves or coupling of whistler waves and KAWs as studied by Gary & Smith, 2009; Salem et al. 2012; Boldyrev et al. 2013 and Chen et al. 2013. Again it may be due to interactions of KAWs with ion acoustic or magnetosonic waves as studied by Sharma et al. 2017. Afterall, because of the similarities in the properties of KAWs and whistler waves, it is difficult to distinguish which one will have more role in coronal heating and solar wind turbulence. Therefore, the simulation results of our present KAW dynamics may contribute something to the unsolved problem of space plasma physics.

5.2   Model KAW Dynamics

In this section, we study the transient behaviour of KAWs applicable to solar coronal loops and its heating mechanism. For this purpose, we rewrite the governing dynamical equation (2.22) as

$$i\frac{2\omega}{v_A^2 k_{0z}^2}\frac{\partial B_y'}{\partial t} + i\frac{2}{k_{0z}}\frac{\partial B_y'}{\partial z} + \rho_s^2\frac{k_{0x}^2}{k_{0z}^2}\frac{\partial^2 B_y'}{\partial z^2} + \rho_s^2\frac{\partial^2 B_y'}{\partial x^2} + 2ik_{0x}\rho_s^2\frac{\partial B_y'}{\partial x} + \frac{n_1}{n_0}B_y' = 0. \quad (5.1)$$

In an inhomogeneous plasma, a nonlinear magnetic gradient force called ponderomotive force is developed. When this force combines with Joule heating, it can modify the plasma density (Shukla & Stenflo 1999). This change in particle number density under adiabatic approximation (i.e large density fluctuations) was theoretically calculated by Shukla & Stenflo, 2000b and is given as

$$n_1 \approx n_0\Big(e^{\xi|B_y'|^2} - 1\Big), \quad (5.2)$$

where $\xi = \{[1 - \Delta(1+\delta)v_A^2 k_{0z}]/16\pi n_0 T_e \omega^2\}$, $\Delta = \omega^2/\omega_{ci}^2$ and $\delta = m_e k_{0x}^2/m_i k_{0z}^2$. In case of $\omega\,(1+\delta)^{1/2} < \omega_{ci}$ the density change is a hump. In an intermediate plasma β, since

$v_{ti},, v_{te} > v_A$ the plasma particles move fast enough to respond any adiabatic changes in density.

Substituting equation (5.1) in to equation (5.2) and normalizing the equation we get

$$i\frac{\partial B'_y}{\partial t} + i\frac{\partial B'_y}{\partial z} + 2iK\frac{\partial B'_y}{\partial x} + K^2\frac{\partial^2 B'_y}{\partial z^2} + \frac{\partial^2 B'_y}{\partial x^2} + \frac{1}{2g}\left(e^{2g|B'_y|^2} - 1\right)B'_y = 0, \qquad (5.3)$$

where the constant $K = k_{0x}\rho_s$. In the normalization, we use $t_n = 2\omega/v_A^2 k_{0z}^2$ $z_n = 2/k_{0z}$, $x_n = \rho_s$ and $\quad B_n = [\{1 - \Delta(1+\delta)\}V_A^2 k_{0z}^2/16\pi n_0 T_e \omega^2]^{-1/2}$. In the above equation, we introduced a dimensionless parameter g. It controls the amplitude of the pump KAW, and the coupling between the density perturbation and magnetic field. When we take $g = 0$, the density profile becomes quadratic in magnetic field and the model equation for KAW reduces to modified cubic NLSE.

Considering a homogeneous solution of the form of $B_{y0}e^{-iz}$ (Zhou et al. 1992) and $K = 0$, and substituting it to equation (5.3), we can get a relation of g with the KAW pump amplitude as

$$|B_{y0}| = \sqrt{\frac{ln|1 - 2g|}{2g}}, \qquad (5.4)$$

where $0 \leq g < 1/2$ and B_{y0} is the amplitude of the homogenious pump KAW.

5.3   Numerical Simulation

The dynamical model equation (5.3) was solved numerically by the method of 2-D pseudo-spectral for space integration and forward method with predictor corrector method for evolution in time. Here we took the step size of $dt = 5 \times 10^{-5}$ and system lengths of $L_x = 2\pi/\alpha_x$ and $L_z = 2\pi/\alpha_z$, where α_x (α_z) is the perturbation wave number in x (z). Both the system lengths were divided with 2^7 grid points each. First the numerical code was developed for well-known 2D-cubic NLSE as mentioned in Chapter 3. The Fast

Fourier Transform (FFT) was directly applied to linear terms. For nonlinear term, we took the local product in real space first and then FFT was applied. After fully testing the code for 2D cubic NLSE, it was modified to solve our present model equation (5.3).

In the numerical simulation we used four kinds of initial conditions as listed below. First initial condition (IC-1) is a uniform plane KAW of fixed amplitude superimposed by a sinusoidal periodic perturbation.

$$B'_y(x, z, t = 0) = B_{y0}[1 + \varepsilon \cos(\alpha_x x)][1 + \varepsilon \cos(\alpha_z z)] \qquad \text{(IC-1)}$$

where ε is the magnitude of the perturbation, α_x (α_z) is the wave number perturbation normilised by x_n^{-1} (z_n^{-1}).

Next initial condition is a Gaussian perturbation superimposed on a uniform plain KAW

$$B'_y(x, z, t = 0) = B_{y0}[1 + \varepsilon \exp\left(-x^2/r_{01}^2\right)][1 + \varepsilon \exp\left(-z^2/r_{02}^2\right)] \qquad \text{(IC-2)}$$

where r_{01} (normalized by x_n) and r_{02} (normalized by z_n) are the transverse and longitudinal scale sizes of the perturbations respectively.

The IC-3 is a pump KAW of Gaussian wavefront with a sinusoidal perturbation

$$B'_y(x, z, t = 0) = B_{y0}[\exp(-x^2/r_0^2) + \varepsilon \cos(\alpha_x x)][\exp(-z^2/r_0^2) + \varepsilon \cos(\alpha_z z) \qquad \text{(IC-3)}$$

where r_0 (normalized by x_n) represents the transverse scale size of the main KAW initial beam width.

The last initial condition (IC-4) is a random perturbation superimposed on the Gaussian wavefront.

$$B'_y(x, z, t = 0) = B_{y0}[\exp(-x^2/r_0^2) + \varepsilon \exp(2\pi i\theta(x))]$$
$$[\exp(-z^2/r_0^2) + \varepsilon \exp(2\pi i\theta(z))] \qquad \text{(IC-4)}$$

where $\theta(x)$ and $\theta(z)$ are the random variables uniformly distributed on [0,1].

In the simulation we used the value of the parameter $\varepsilon = 0.1$ and the values of the perturbation wavenumbers $\alpha_x = \alpha_z = 0.5$. The perturbation wavenumbers are chosen so that all fields may be allowed to represent as discrete Fourier series with integral wave vector components. Furthur, we set $r_0 = 1.0$, $r_{01} = r_{02} = 5$. Now we get $L_x = L_z \simeq 12.5 \simeq 2.5r_{01} \simeq 2.5r_{02}$. The value of $g = 0.01$ was chosen, so it gives $B_{y0} \simeq 1.005$. With all these parameters, the magnetic fluctuation comes out to be $|\delta B_y/B_{y0}| \simeq 0.1$.

In the coronal loops the possible plasma parameters are (Shukla et al. 1999): $B_0 \approx 100G$, $n_0 \approx 5 \times 10^9 \ cm^{-3}$, $T_e \approx 6 \times 10^6 K$, $T_i \approx 2 \times 10^6 K$. Now we calculated other parametrs required as $\beta = 0.01$, $v_{te} \approx 2 \times 10^9 cm \ s^{-1}$, $V_A \approx 3 \times 10^8 cm \ s^{-1}$, $\rho_s = 22cm$, $\rho_i = (\sqrt{T_i/T_e})\rho_s = 68cm$. By taking $\omega/\omega_{ci} \approx 0.02$ and for $k_{0x}\rho_s \approx 0.01$, we get $k_{0x} \approx 1.9 \times 10^{-5} cm^{-1}$, $k_{0z} \approx 1.5 \times 10^{-5} cm^{-1}$. The normalizing values are $x_n = 22cm$, $z_n = 1.3 \times 10^5 cm$, $t_n = 1.4 \times 10^{-3} sec$ and $B_n = 0.91G$.

Fig. 5.1 Snapshots of normalized magnetic field intensity profiles (upper panel) and spectral contour plots of magnetic field intensity (lower panel) at $t = 2, 3$ and 4 for IC-1.

Fig. 5.2 Snapshots of normalized magnetic field intensity profiles (upper panel) and spectral contour plots of magnetic field intensity (lower panel) at $t = 3, 4$ and 6 for IC-2.

Fig. 5.3 Snapshots of normalized magnetic field intensity profiles (upper panel) and spectral contour plots of magnetic field intensity (lower panel) at $t = 6.5, 8$ and 9.5 for IC-3.
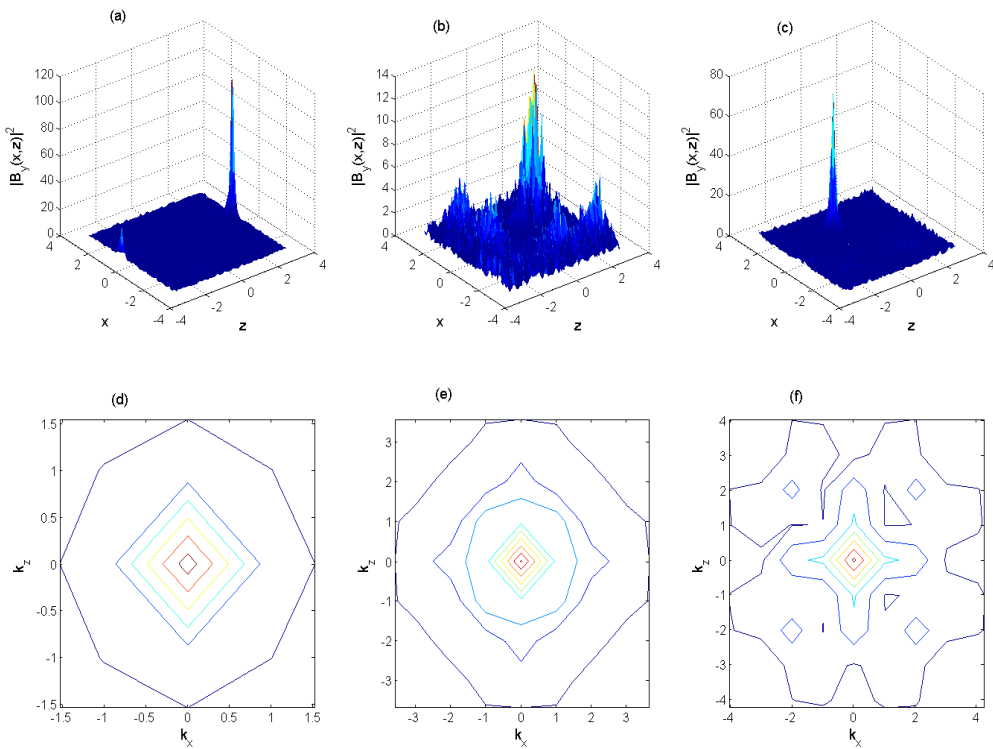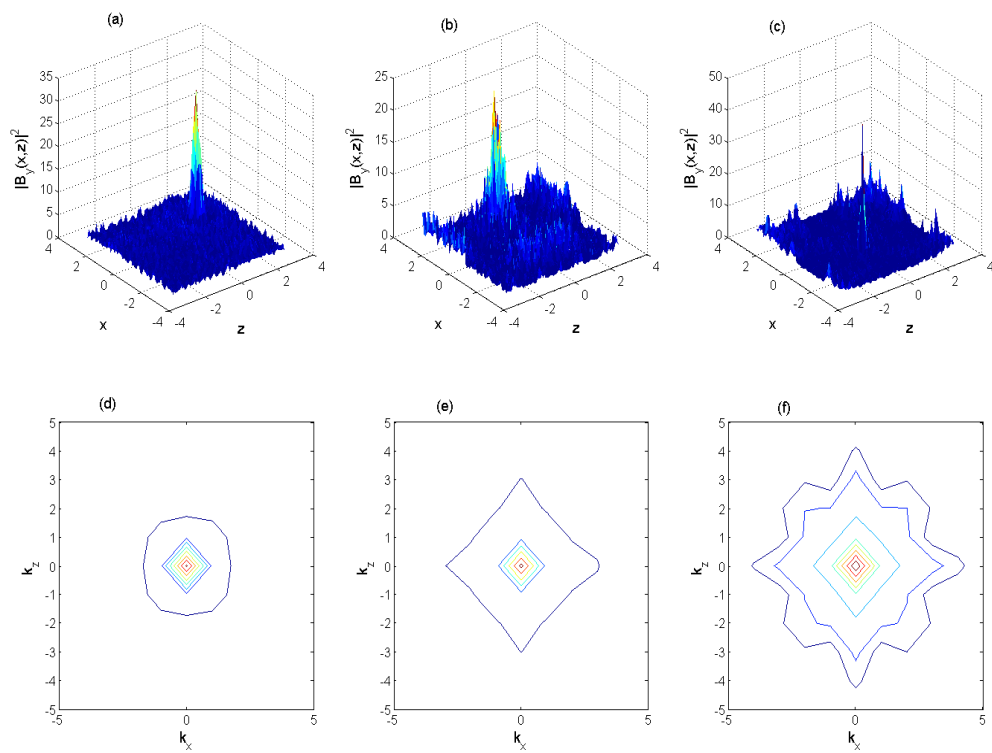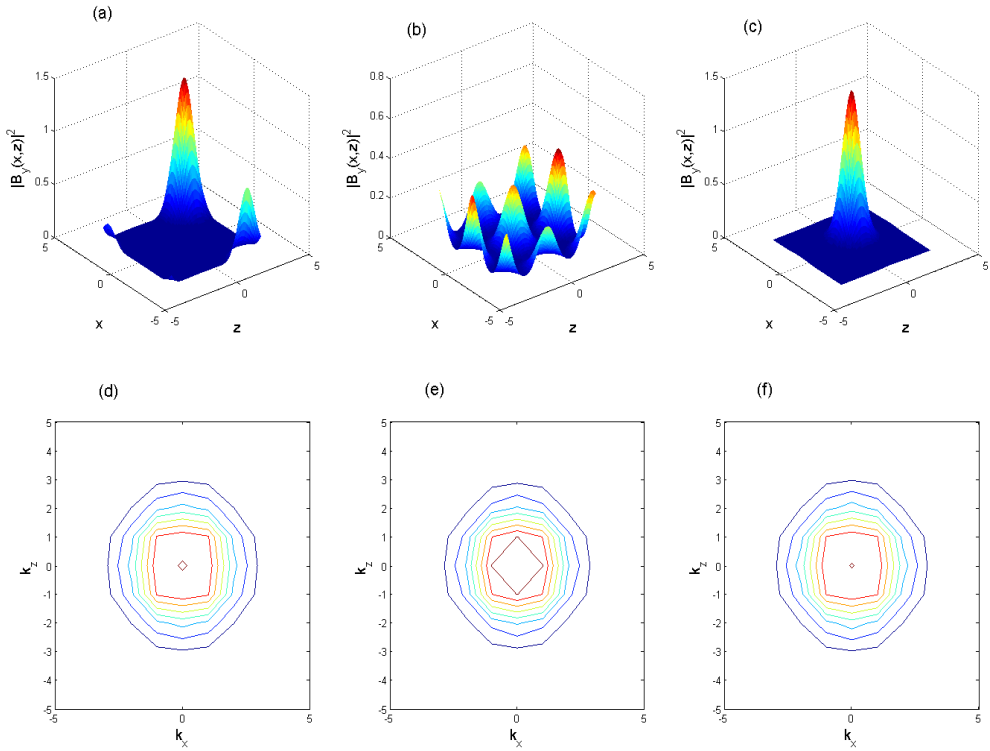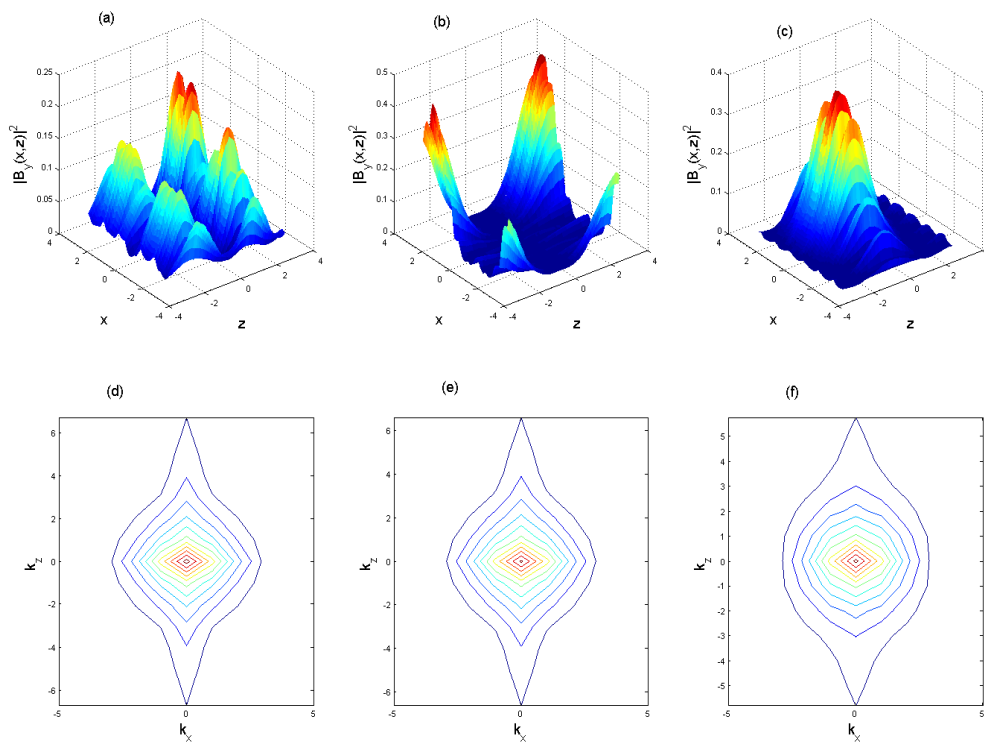
Fig. 5.4 Snapshots of normalized magnetic field intensity profiles (upper panel) and spectral contour plots of magnetic field intensity (lower panel) at $t = 5, 6$ and 10 for IC-4.
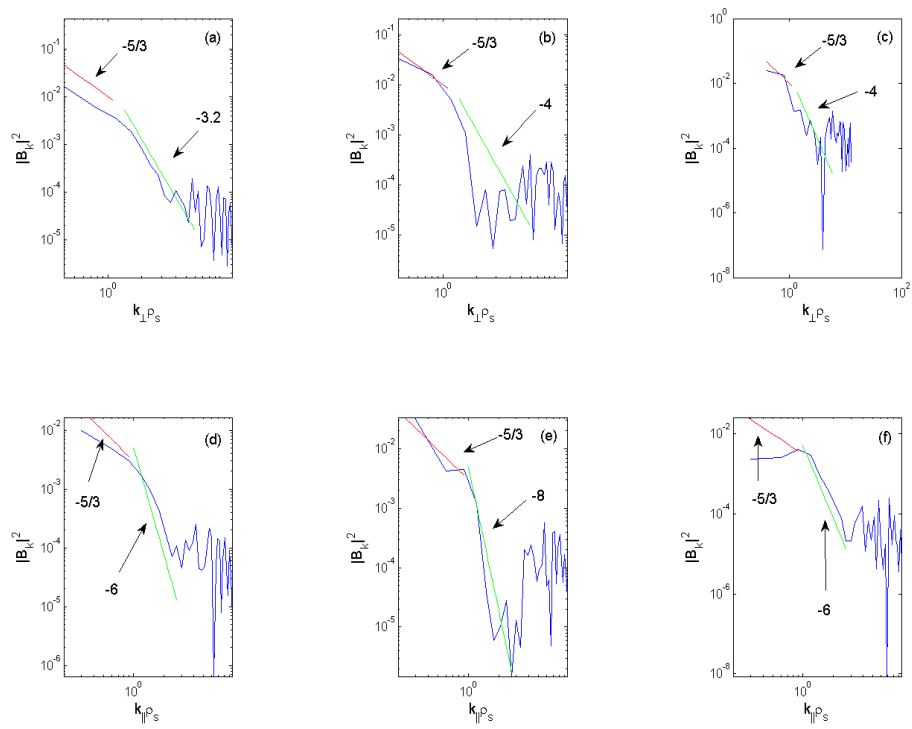
Fig. 5.5 Spectra of magnetic field fluctuations for IC-1 in $k_\perp$ space (upper panel) and $k_\parallel$ space (lower panel) at $t = 2, 3$ and 4.

Now, we start presenting the numerical simulation results of equation (5.3) for coronal loops. Figure (5.1) represents the 2D snapshots of the time evolution of transverse KAW field intensity at three instants of time. The plasma density is modified due to the ponderomotive force acting on the plasma. Due to this, the phase velocity of KAWs change and it gives the magnetic fields localized in space as the wave propagates. The inhomogeneity of the field in the form of the perturbation represented here takes the energy away and the localized magnetic structures collapse with the progress of time. The nonlinear interactions between density and magnetic fields will regroup the collapsed structures.

The magnetic field intensity profiles for KAWs for IC-2 are almost same as that of IC-1 except the values of the time and locations where filaments are formed. At time $t = 3, 4$ and 6 the filaments of highest intensities are around 30, 23 and 13 respectively. The contour plots in Fourier wavenumber modes connecting the same magnetic field energies are plotted in figures $5.2(d) - 5.2(f)$. Figures $5.3(a) - 5.3(c)$ show the the snapshots of the magnetic field intensity profiles for IC-3. The values of the magnetic field intensities are $1.30, 0.40$ and 1.36 at $t = 6.5, 8$ and 9.5 respectively. It is evident that it is not possible for IC-3 to generate very high intensity filaments. Therefore, distribution of energy from lower wavenumber to higher wavenumber is not possible, as evident from figures $5.3(d) - 5.3(f)$. Hence, we can conclude that the kind of magnetic field inhomogeneity represented as IC-3 may not be appropriate to sufficienly accelerate the ions and electrons in the plasma. The initial condition of random perturbation superimposed to a Gaussian wavefront (IC-4) also shows almost similar results as shown for IC-3 [figure (5.4)]. Overall summary is that the magnetic field localization for KAWs is more dependent on the nature of the pump KAW rather than the perturbation. If the pump KAWs are same, then the magnetic field intensity profiles are almost same irrespective of the perturbating waveforms.

The mechanism for the generation of magnetic coherent structures is similar with the mechanism of laser focusing as explained by Kruer 2003. As the density of the medium is perturbed, the dielectric constant and hence the refractive index of the medium will be changed. The laser beam propagating through the medium of varying refractive index will act as a focusing lens and the wave will be focused. Similarly here also, the parallel ponderomotive force will modify the density. The KAWs propagating through this medium having density perturbations will produce varying phase velocity generating the spatial localization of the wave field.

These magnetic coherent structures help in enhancing the transfer of energy from large scales (comparable to ion acoustic gyroradius) to small scales (comparable to electron thermal gyroradius). The plasma inhomogeneities manifested in the magnetic field and density perturbations in our study will take energy from the main KAW by nonlinear interaction and as the KAW propagates, it will generate magnetic filaments. Gershman et al. 2017 have found that local generation of observed KAWs, as observed by NASA's Magnetospheric Multiscale (MMS) mission, are due to the combined effects of nonlinearities arising from inhomogeneities in the magnetic field and particle number density.

Fig. 5.6 Spectra of magnetic field fluctuations for IC-2 in $k_\perp$ space (upper panel) and $k_\parallel$ space (lower panel) at $t = 3, 4$ and 6.

Fig. 5.7 Spectra of magnetic field fluctuations for IC-3 in $k_\perp$ space (upper panel) and $k_\parallel$ space (lower panel) at $t = 6.5, 8$ and 9.5.

If there is large fluctuations in the parallel magnetic fields as well as high current density, then the lighter particles (electrons) can be sufficiently trapped in between the wave packets. In this way, the wave energy is converted to particle energy. Therefore, it gives magnetic analog of Landau damping and can heat the plasma. We can measure the transverse scale size of the magnetic coherent structures from the magnetic field intensity profile. At early times, it comes out to be of the order of ion gyroradius $\approx 6\rho_s = 188.50$ km (measured at the half of the peak intensity). As the time progresses, this scale size becomes smaller because of the transverse collapse. When this size reaches kinetic scales of KAWs, enough electron or ion heating occurs. Lion et al. 2016 and Chmyrev et al. 1988 reported the scale size of KAW filament structures of the order of ρ_s. Further by increasing the pump wave amplitude of the KAW, which can be achieved with increasing the value of g, we get the scale size of the filaments at micro kinetic scales and it leads to chaotic motion. The transfer of wave energy to particle energy is sufficiently happening at this stage.

Next, we present the spectral energy $|B_{yk}|^2$ at various wavenumber space, first in $k_x(k_\perp)$ direction and then to $k_z(k_\parallel)$ direction. From the spectral plots (figures $(5.5) - (5.8)$), we see that the spectral indices of energy cascade follow the Kolmogorov scale of $-5/3$ in the so called inertial range i.e. when $k_\perp \rho_s < 1$ and $k_\parallel \rho_s < 1$. This is in agreement with the results of many authors (Champeaux et al. 1998; Lavender et al., (2001); Sulem & Sulem, 1999). There are observational evidences from solar flares Dennis, (1985); Hudson, (1991) showing spectral index of solar flares to be approximately -1.6. Many authors (Dennis, 1985; Hudson, 1991). Hollweg, 1984 calculated the energy flux density in the plasma turbulence in the coronal loops applying $-5/3$ spectral index. The results were in agreement with many observations. However, how this high energy flux in the coronal loops are achieved and what is the mechanism for turbulence leading to heating the corona have been still debating. The generation of KAW magnetic filaments and it's
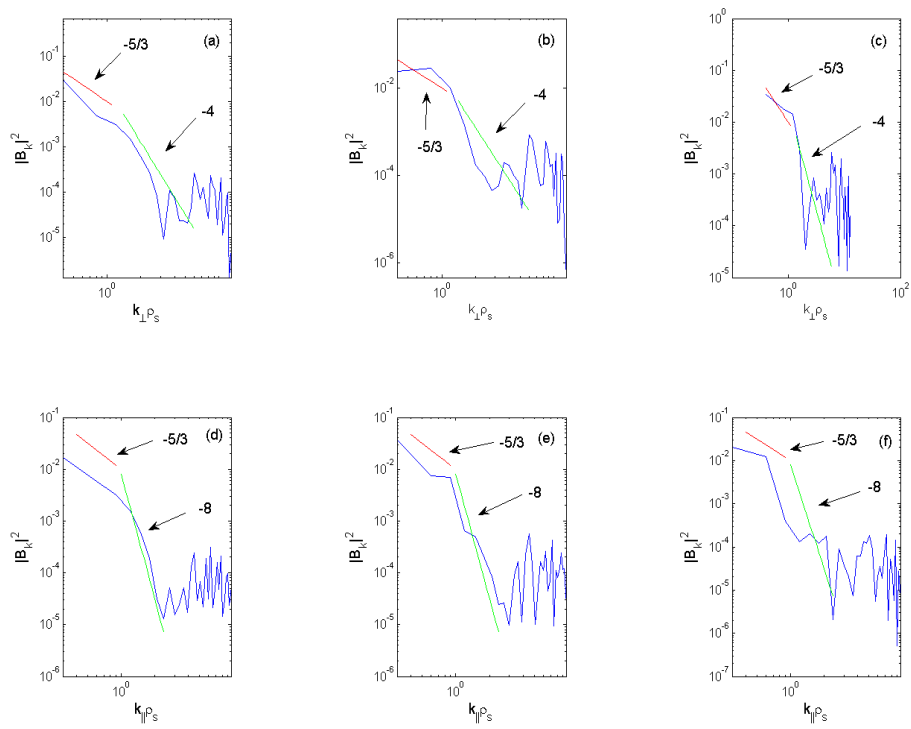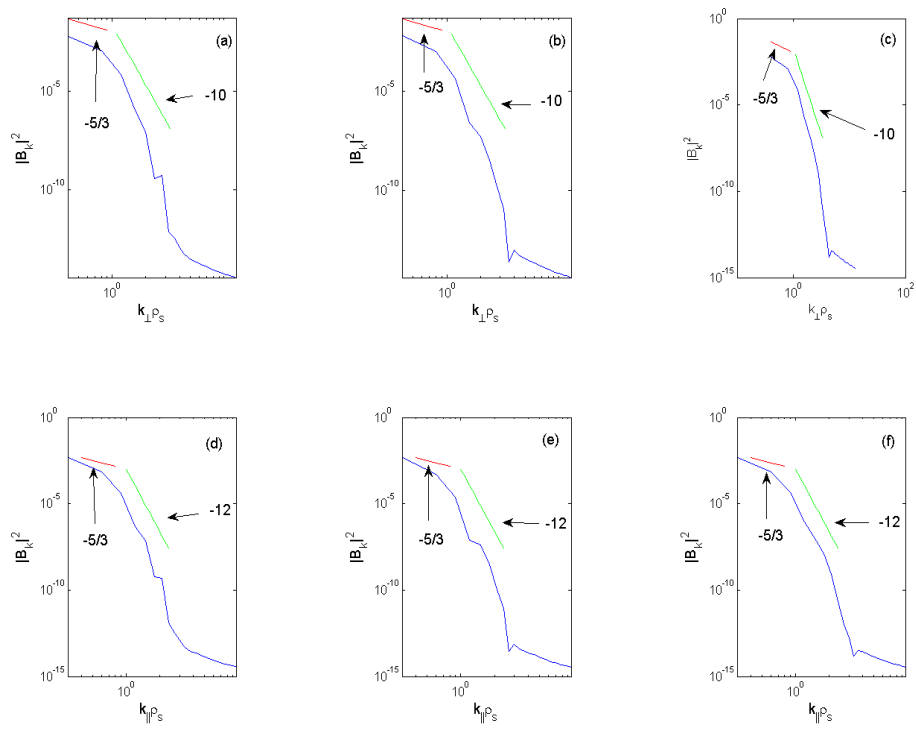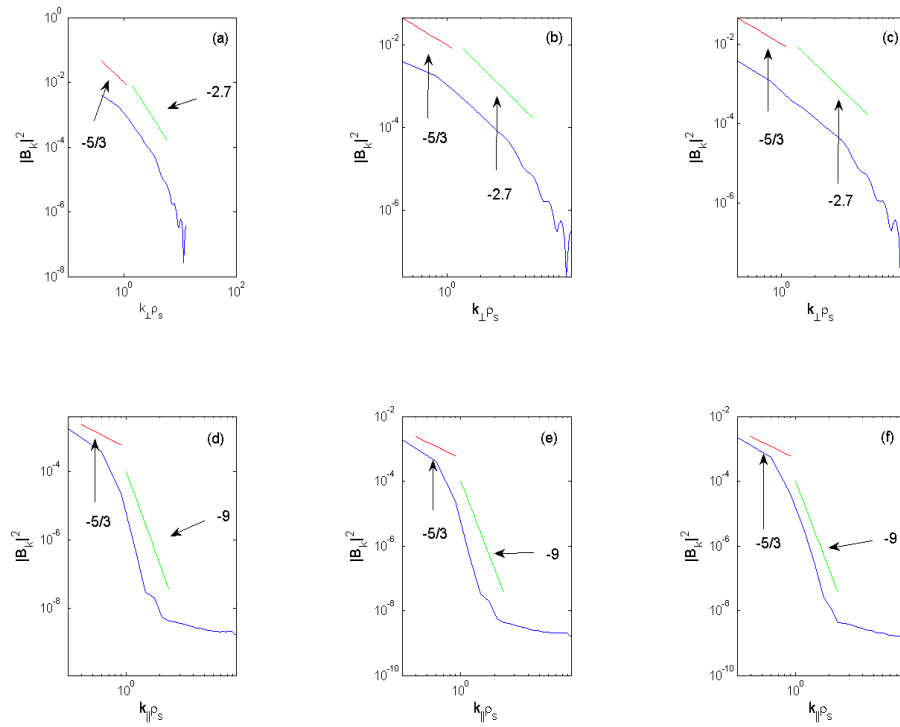
Fig. 5.8 Spectra of magnetic field fluctuations for IC-4 in $k_\perp$ space (upper panel) and $k_\parallel$ space (lower panel) at $t = 5, 6$ and 10.

transverse collapse are proposed in this chapter as one of the candidates to explain the coronal heating.

We find from the magnetic power spectra that the first spectral break takes place at $k_\perp \rho_s \approx 1$ and $k_\parallel \rho_s \approx 1$. Further, it shows no fixed spectral shapes for all the initial conditions of the simulation. The first spectral break signifies a transition region from ion scale known as inertial range to electron scale known as kinetic range. In the transition range, our simulation results show the spectral indices in $k_\perp$ to be -3.2 and -4 for IC-1, -4 for IC-2, -10 for IC-3 and -2.7 for IC-4. In $k_\parallel$ direction, they are -6 and -8 for IC-1, -8 for IC-2, -12 for IC-3 and -9 for IC-4. Hudson, 1991 suggested that to sufficiently heat the solar corona by small scale burst like solar flares; the negative spectral magnetic energy slope of at least -2 is required. Many spacecraft observational results reported the spectral index deeper than -2 in the coronal loops (Aschwanden & Parnell, 2002). We also find here the anisotropy in spectral energy showing the spectral index more deep in $k_\parallel$ direction than that of $k_\perp$ direction. Therefore, we can say that more energy is cascading in perpendicular wavenumber space. Anisotropy in magnetic fluctuations in solar plasma at kinetic scales were reported by many investigations (Chen et al. 2010; Sahraoui et al. 2010; Narita et al. 2011). They showed that the turbulence is more anisotropic at large wavenumbers, hence more energy cascade in the perpendicular wavenumber when $k_\perp > k_\parallel$. By analyzing the figures $(5.5) - (5.8)$ and also comparing the upper and lower panel of the figures, we confirm that there is spectral anisotropy in our results for KAW dynamics applicable to coronal plasma. Therefore, the cascade of energy in transverse wavenumber is more prominent than that of parallel wavenumber. Among the four initial conditions, the third one shows the lowest energy cascade. The anisotropic spectra of solar plasma has been verified by many authors (Marson and Goldreich, 2001; Cho et al. 2002; Leamon et al. 1998; Luo and Wu, 2010; Luo et al., 2012). Anisotropic scaling correlation reported was $k_\parallel \propto k_\perp^{1/3} (= k_\perp^{0.33})$ (Schekochihin et al. 2009; Cho & Lazarian, 2004; Cho & Lazarian, 2009). From our results this correlation is $k_\parallel \propto k_\perp^{0.53}$ and $k_\parallel \propto k_\perp^{0.50}$ for first two initial and $k_\parallel \propto k_\perp^{0.83}$ for third initial condition and $k_\parallel \propto k_\perp^{0.30}$ for fourth initial condition.
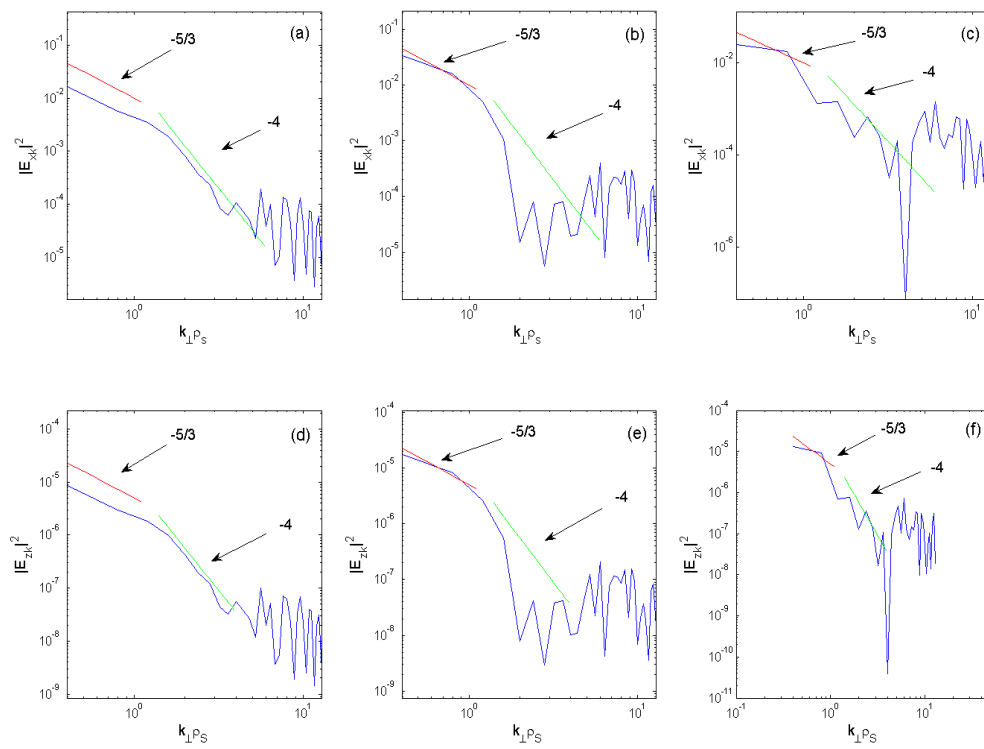
Fig. 5.9 Spectra of electric field fluctuations for IC-1 in $k_\perp$ space: perpendicular electric field (upper panel) and parallel electric field (lower panel) at $t = 2, 3$ and 4.

In our study, we can not finalize the role of different initial conditions in the wave-vector anisotropy. One possible way to study it furthur may be to solve the KAW dynamics semi analytically by taking the initial conditions used here as *ansatz* and compare it with the fully solved numerical solutions. Moreover, the filamentaion process can lead to other kinds of plasma instabilities which can further contribute to energization of particles. The wave-vector anisotropy and turbulence in space plasma is a complex phenomena. More in depth studies are required to understand properly.

Lastly, the electric field spectra are presented at different values of perpendicular and parallel wave numbers. From equations (2.13) and (2.14), the dimensionless electric field components are found as $E_x = (2 - e^{|B_y|^2})B_y$ and $E_z = B_y/Q$. Here the constant $Q = v_A^2/(v_{te}^2 \lambda_e^2 k_{0x} k_{0z})$ and the electric field is normalized by $E_N = B_N k_{0z} v_A^2/(\omega c)$. From Figure (5.9), we find the spectral indices of $-5/3$ in the inertial range and -4 in the dissipation range. Electric spectra show the same shape as that of magnetic spectra except that the field intensities are lower in case of electric spectra. Therefore, we are showing the electric spectra for the first initial condition only. Theoretically Zhao et al 2016 modeled the kinetic Alfvenic turbulence of scaling law $k_\perp^{-5/3}$ and $k_\perp^{-1/3}$ for $E_\perp$ spectra and $k_\perp^{4/3}$ and $k_\perp^{-1/3}$ for $E_\parallel$ spectra. For scales smaller than the ion kinetic scales, $k\rho_i > 1$, spectral scaling of $k_\perp^{-1/3}$ was modeled (Schekochihin et al. 2009; Zhao et al 2013; Bian & Kontar, 2010). However for strong turbulence Boldyrev and Perez, 2012 modeled it to be $-2/3$. For parallel electric spectrum, Zhao et al 2016 found the spectral indices of $k_\perp^{4/3}$ and $k_\perp^{-1/3}$ in the inertial and kinetic scales respectively. In the inertial regime, the $E_\parallel$ spectral energy increases with $k_\perp$ (Zhao et al 2013; Bian & Kontar, 2011). By analyzing the *THEMIS* and *Cluster* data Mozer and Chen, 2013 found that both the electric spectra have almost the same power and scaling law of $-5/3$ at ion scales and -2.1 to -2.8 at electron scales. In contrast to this, some researchers (Zhao et al 2013; Bian & Kontar, 2010; Bian & Kontar, 2011; Mozer and Chen, 2013) predicted that the spectral power is much higher in $E_\perp$ spectrum. Hence, the total energy is contributed

mainly from $E_\perp$ energy. In our simulation results also, by comparing the two electric spectra, we find that $E_\perp$ spectral energy is higher of the order of 3 times than that of $E_\parallel$ spectral energy. It should be mentioned here that $E_\parallel$ is the actual force which mediates the wave-particle interaction and it is important in accelerating the charged particles (Wu & Fang, 1999; Fletcher & Hudson, 2008; McClements and Fletcher, 2009) via Landau resonance. Particle heating takes place when the electric thermal speed and the magnitude of wave phase velocity are comparable. This stochastic heating problem can be treated by considering a distribution function in velocity phase space and solving the quasilinear diffusion equation (Fokker-Plank equation). This stochastic heating problem will be addressed in chapter 6 when we consider the inertial AWs applicable to space plasma.

From the electric spectra we presented, it is found that $E_\parallel$ and $E_\perp$ spectra show more negative spectral indices in the dissipative region as compared to some of the studies (Bian & Kontar, 2010; Bian et al. 2010; Mozer and Chen, 2013). However, our spectral results are qualitatively matching with the results of Valentini et al. 2017 using hybrid Vlasov-Maxwell simulations, and Howes et al. (2008) and Howes et al. (2011) using gyrokinetic continuum simulations. Furthur, in the electron inertial length scale, i.e. $k_\perp \rho_s$, $k_\parallel \rho_s \approx 5$, we find a second spectral break point in the spectra. We can not explain the second spectral break point and the following spectral index, because our model equations satisfied by DAWs were derived for low frequency DAWs by assuming $\omega < \omega_{ci}$. Therefore, the present study can not be applied in the dissipation regime of electron kinetic scale length. Whistler waves $\omega > \omega_{ci}$ can be one of the possible candidates to study in this region. The nonlinear interactions arising from whistler waves and KAWs were numerically investigated by Dwivedia & Sharma, 2013. In spite of all the attempts, the physics behind small scale fluctuations in the dissipation range is not fully developed. Hence, our present model may be able to provide some possible explanation to understand the physics of wavevector anisotropy and heating of solar corona.

5.4 Conclusion

We have carried out the numerical simulation for modified NLSE modeled for the transient KAW dynamics in an inhomogeous plasma. The nonlinearity term in the equation arises because of the couping of the magnetic field and the density perturbations arising on account of ponderomotive force and Joule heating. Because of this nonlinear interactions, coherent structures of magnetic fields in the form of solitons are generated. Furthur, with the advancement of time, these structures break down to smaller scale size, which are the main source of the plasma kinetic turbulence. The turbulence was studied by plotting the power spectral graphs. The power spectral indices in the perpendicular and parallel wavenumber Fourier space are not same, indicating the wavevector anisotropy in energy cascade. The wavevector anisotropy in turbulence are important to study the energization of plasma particles. The anisotropy in the dissipation range follows the following relations: $k_\parallel \propto k_\perp^{0.53}$, $k_\parallel \propto k_\perp^{0.50}$, $k_\parallel \propto k_\perp^{0.83}$ and $k_\parallel \propto k_\perp^{0.30}$ for different kinds of of initial conditions used in the simulation to represent the plasma inhomogeneity.

Chapter 6

Inertial Alfvén Wave Turbulence and Particle Heating in Space Plasma

6.1 Introduction

The low-frequency (compared to the ion gyrofrequency) inertial Alfvén waves (IAWs) play very important role in laboratory, space and astrophysical plasmas (Hasegawa & Uberoi (1982); Shukla et al., (1996); Wang et al. (1998)). The space and astrophysical plasma examples include some more intense auroral arcs at the Earth's northern and southern poles (Wahlund et al., (1994); Chaston et al. (2000); Stasiewicz et al., (2000)), solar corona (Hollweg, (1999)) and extragalactic jets (Jafelice & Opher, (1987)). The laboratory plasma examples includes Large Plasma Device (LAPD) (Gekelman et al., (1994)), beam-in-plasma interaction at the SLAC National Accelerator Laboratory, the ultra-cold, highly correlated plasma studied in CERN (European Organisation for Nuclear Research) etc.

The IAWs can be driven by equilibrium sheared plasma flows, in which the large-amplitude IAWs are produced (Shukla & Stenflo, (1997)). The parallel electric field of

large-amplitude IAWs is responsible for the electron acceleration to higher energy in the Earth's ionosphere (Thompson & Lysak, (1996)). On the other hand the finite-amplitude IAWs are responsible for the generation of nonlinear effects in plasma (Petviashvili & Pokhotelov, (1992)). The IAWs are observed at the Earth's magnetosphere, leading to play a key role in the magnetosphere-ionosphere coupling (Hasegawa, (1976); Goertz et al., (1979); Chaston, (2006)). These IAWs are also observed at the lower region (base) of the solar corona (Fletcher & Hudson, (2008); Escande et al., (2019)), which can energize the electrons and ions to reach upto the coronal temperature.

The aurora formation in the visible space is one of the prominent manifestation of highly energetic charged particles. This is generated due to the electrons impinging onto the electromagnetically upper atmosphere of the Earth. The neutral particles available in the lower atmosphere of the Earth are partially ionized by the ultraviolet light of the Sun and it is known as ionosphere. The magnetosphere is produced by the ionosphere and the solar wind, which is magnetized by the geomagnetic field. In this region due to the the Lorenz force, the charged particles move into the spiral shape around the magnetic field lines. The charged particles in the magnetosphere are susceptible to accelerate along the geomagnetic field and funneled toward northern and southern polar of the Earth where they generate the aurora's glowing light. The particle acceleration in the magnetosphere is one of the reasons that motivates to study in this chapter.

The observational study of the electron acceleration by FAST, Freja, Polar, Geotail and Cluster missions in the auroral region have been a new era of measurement from the past three decades. The Polar spacecraft observations of Alfvénic poynting flux at 4-7 *Re* in the plasma sheet boundary layer are correlated with the auroral structures. The studies of Polar and FAST spacecraft observations demonstrated that the Alfvénic poynting flux dominates over the electron energy flux at Polar spacecraft orbit while the electron energy flux is greater than the Alfvénic poynting flux at the FAST spacecraft altitude. The observed studies suggested that the IAWs are losing their energy via

wave-particle interaction to accelerate the electrons when they propagate toward the ionosphere. These studies also suggested that the IAWs may be responsible for particle acceleration in the ionosphere.

The auroral particle acceleration due to parallel electric field of IAWs was first demonstrated by Hasegawa, (1976). In 1979, Goertz et al., (1979) demonstrated that the auroral electron acceleration occurs in the lower magnetosphere where the shear Alfvén waves are described by the IAW limit. Kletzing, (1994) studied the resonant process that affects the superthermal electrons in aurora. These resonant electrons travelled slower than the Alfvén waves and interact with the parallel electric fields of the Alfvén waves. The resonant electrons are picked up by the IAWs and pushed it into the front of the waves. This resonant interaction can accelerate electrons nearly to twice of the AW speed and energize it to 600-1000 eV. Kletzing & Hu, (2001) repeated the calculations of Kletzing, (1994), with density and magnetic field gradients that are applicable for the auroral magnetosphere. It was found that the Alfvén waves move toward the ionosphere leading to change the Alfvén speed and amplitude of the Alfvén waves. Chaston, (2006) used test-particle calculation with similar approach of Kletzing & Hu, (2001) and focused only on individual particle orbits instead of focusing on the dynamics of the entire distribution function of IAWs. It predicted two different acceleration mechanisms for electrons. The first one is, the high speed electrons move along the geomagnetic field lines through the parallel electric fields of IAWs, thus the parallel electric field is the electrostatic. These electrons move faster than the Alfvén wave speed and are accelerated to greater speeds by electrostatic effect. This mechanism occurs at around 2-Re where the parallel electric field is strong. The second mechanism shows the resonance of test particles with the phase velocity of the Alfvén waves and this condition is called as the Landau resonance. In this mechanism the electron receives the energy from the Alfvén waves through the collisionless damping. The electron acceleration by Landau resonance mechanism affects the superthermal electrons as proposed by Kletzing & Hu, (2001)

theoretically. Furthur, Chaston, (2006) suggested that the electron acceleration by Landau resonance is more effective because of the Earth's magnetic field.

Turbulence in the form of temporal or/and spatial magnetic or electric field fluctuations exists in space plasmas (Tu & Marsch, (1995); Matthaeus & Velli, (2011)). Several spacecrafts like FAST, THEMIS and CLUSTER observations have demonstrated the presence of magnetic field fluctuations in geospace plasma region (Zimbardo et al., (2010)), the Earth's plasma sheet region (Borovsky & Funsten, (2003)), the magnetosheath region (Alexandrova, (2008)) and the auroral region (Chaston, (2006)).

6.2 Model Equation

The dynamical model equation satisfied by IAWs applicable to auroral region and solar corona as derived in equation (2.23) is

$$2i\frac{\omega}{v_A^2 k_{0z}^2}(1 + k_{0x}^2\lambda_e^2)\frac{\partial B_y'}{\partial t} + \frac{2i}{k_{0z}}\frac{\partial B_y'}{\partial z} + \frac{1}{k_{0z}^2}\frac{\partial^2 B_y'}{\partial z^2} - \frac{2ik_{0x}\lambda_e^2\omega^2}{k_{0z}^2 v_A^2}\frac{\partial B_y'}{\partial x} - \frac{\lambda_e^2\omega^2}{k_{0z}^2 v_A^2}\frac{\partial^2 B_y'}{\partial x^2} + \frac{n_1}{n_0}B_y' = 0.$$
(6.1)

In an inhomogeneous plasma, a nonlinear magnetic gradient force known as ponderomotive force is developed. This force, in combination with Joule heating, can modify the plasma density. This change in particle number density under adiabatic approximation (i.e large density fluctuations) was theoretically calculated by Shukla & Stenflo 1999 and found as

$$n_1 \approx n_0\left(e^{-\xi_2|B_y'|^2} - 1\right),$$
(6.2)

where $\xi_2 = (1 + 8k_{0x}^2\lambda_e^2)/48\pi n_0 T_e$.

Substituting equation (6.2) in equation (6.1) we get

$$i\frac{\partial B'_y}{\partial t} + i\frac{\partial B'_y}{\partial z} + 4\frac{\partial^2 B'_y}{\partial z^2} - iC\frac{\partial B'_y}{\partial x} - \frac{\partial^2 B'_y}{\partial x^2} + \frac{1}{2g}\left(e^{-2g|B'_y|^2} - 1\right)B'_y = 0, \qquad (6.3)$$

where the dimensionless parameters used in the normalization are $t_n = 2\omega/v_A^2 k_{0z}^2$, $z_n = 2/k_{0z}$, $x_n = \lambda_e\omega/v_A k_{0z} = \lambda_e/\sqrt{1+k_{0x}^2\lambda_e^2}$, $C = 2k_{0x}\lambda_e\omega/v_A k_{0z} = 2k_{0x}\lambda_e/\sqrt{1+k_{0x}^2\lambda_e^2}$ and $B_n = [(1+8k_{0x}^2\lambda_e^2)/48\pi n_0 T_e]^{-1/2}$.

In substituting the perturbed density, for the sake of generality we have used the dimensionless parameter g that controls the coupling to the density perturbation and magnetic field. When $g = 0$, the equation (6.3) reduces to the form of cubic NLSE. If we increase the value of g, the system reaches to chaotic state. This was studied earlier by some authors (Sharma et al. 2006; Singh & Sharma, 2007), but those were limited in steady states only. Therefore, the time evolution of IAWs applicable to auroral region is studied here.

In order to find out the relationship between the initial IAW pump wave amplitude and the parameter g, we substitute a simpler homogeneous solution as $B_{y0}e^{-iz}$ (Zhou et al. 1992; Zhou & Hi 1994) in equation (6.3) where B_{y0} is the amplitude of the homogenious pump IAW. Further we simplify it by taking $C = 0$ and we get

$$|B_{y0}| = \sqrt{\frac{ln|1-2g|}{2g}}, \qquad (6.4)$$

where the value of g is limited as $0 \leq g < 1/2$ and B_{y0} is the amplitude of the homogenous pump IAW.

6.3 Numerical Simulation

The numerical simulation of equation (6.3) was carried out by using 2-D pseudo-spectral method for space integration with periodic spatial domain of $L_x = 2\pi/\alpha_x$ and $L_z = 2\pi/\alpha_z$ (where α_x and α_z are the perturbation of IAW wave numbers in x and z directions

respectively) with $2^7 \times 2^7$ grid points. The modified version of Gazdag predictor-corrector method for evolution in time with a step size of $dt = 5 \times 10^{-5}$ was employed

First, we wrote the algorithm for well-known 2D-cubic NLSE as described in Chapter 3. The linear terms were transformed to Fourier space by performing Fast Fourier Transform (FFT) whereas for the nonlinear term the local product in real space was taken first and then applied FFT to transform it into Fourier space. If the linear evolution is fully integrable, then the plane wave solution is the possible solution. After fully testing the algorithm for 2D-cubic NLSE, the algorithm was modified to solve equation (6.3).

To understand the role of the initial conditions of the simulation which represents the inhomogenous magnetic field, we used two different types of initial conditions of simulation. The first initial condition we used is a uniform plane IAW at fixed amplitude which is superimposed by a sinusoidal periodic perturbation. It is represented as IC-1.

$$B_y'(x, z, t = 0) = B_{y0}[1 + \varepsilon \cos(\alpha_x x)][1 + \varepsilon \cos(\alpha_z z)] \qquad \text{(IC-1)}$$

where ε is the magnitude of the wave perturbation. The wave numbers of the perturbations α_x and α_z are normalized by x_n^{-1} and z_n^{-1} respectively. In fact, IAWs are more complicated than the sinusoidal waves. But any type of waves can be represented by the sum of the components of sinusoidal waves.

When a Gaussian perturbation is superimposed on a uniform plain IAW, we represent the second initial condition as IC-2.

$$B_y'(x, z, t = 0) = B_{y0}[1 + \varepsilon \exp(-x^2/r_{01}^2)][1 + \varepsilon \exp(-z^2/r_{02}^2)] \qquad \text{(IC-2)}$$

where r_{01} (normalized by x_n) is the transverse scale size of the perturbation and r_{02} (normalized by z_n) is the longitudinal scale size of the perturbation. The parameter values we used in the simulation are $\varepsilon = 0.1$ and $\alpha_x = \alpha_z = 0.5$ so that all fields of the wave may be allowed to denote as discrete Fourier series with integral wave vector components. For $r_0 = 1.0$ and $r_{01} = r_{02} = 5$, we get $L_x = L_z \simeq 12.5 \simeq 2.5r_{01} \simeq 2.5r_{02}$.

Here we have chosen fixed value of $g = 0.01$ which provides the amplitude of the pump wave $B_{y0} \simeq 1.005$.

To express the normalized units of the simulation results to absolute units as well as to substitute the values of the constants appeared in the model equation and make a relevant application to the regions of interest in space plasma, we choose two regions: solar coronal holes and auroral region in the Earth's magnetosphere. First the possible solar coronal hole parameters as reported by Champeaux et al. (1998) are: for $\beta = 2 \times 10^{-4}$, $B_0 \approx 32G$, $n_0 \approx 108cm^{-3}$, $T_e \approx 0.4 \times 10^6 K$, $T_i \approx 0.2 \times 10^6 K$. Now we calculate $v_A \approx 7 \times 10^8 cms^{-1}$, $v_{Te} \approx 2.5 \times 10^8 cms^{-1}$, $\omega_{ci} = 3 \times 10^5 Hz$. For $\omega = 13.8 \times 10^3 Hz$ and $k_{0x}\lambda_e = 0.01$ we get $k_{0x} = 1.9 \times 10^{-4}cm^{-1}$, $k_{0z} = 2 \times 10^{-5}cm^{-1}$.

The values of the normalizing parameters are: $x_n \approx 2.6 \times 10^3 cm$, $z_n \approx 2.5 \times 10^7 cm$, $t_n \approx 0.362s$, $n_N \approx 4 \times 10^4 cm^{-3}$ and $B_n \approx 2.56G$.

In the auroral ionosphere located at the altitude of $1700km$, the possible plasma parameters (Wu et al., (1996)) are $B_0 \approx 0.3G$, $n_0 \approx 5 \times 10^3 cm^{-3}$, $T \approx 1eV$; then $\beta \approx 2.2 \times 10^{-6}$, $v_A \approx 9.3 \times 10^8 cms^{-1}$, $v_{Te} \approx 4.2 \times 10^7 cms^{-1}$, $\omega_{ci} \approx 2.9 \times 10^3 Hz$, $\lambda_e \approx 7.5 \times 10^3 cm$. For these parameters at $\omega/\omega_{ci} = 0.02$ and $k_{0x}\lambda_e = 0.1$, we get $k_{0x} \approx 1.3 \times 10^{-5}cm^{-1}$, $k_{0z} \approx 6.2 \times 10^{-8}cm^{-1}$.

The values of the normalizing parameters are $x_n \approx 3.8 \times 10^4 cm$, $z_n \approx 8.1 \times 10^8 cm$, $t_n \approx 0.90cm^{-3}$ and $B_n \approx 0.24G$.

Our simulation results are applicable for both solar coronal holes and auroral region of the Earth. For detailed application purpose, we need to use the values of the normalizing parameters calculated from the possible plasma parameters in the two regions. The 2D snapshots of the time evolution of transverse IAW field intensity for two types of initial conditions are shown in figures $6.1(a)$ - $6.1(c)$ and $6.2(a)$ - $6.2(c)$ (upper panels) at three instants of times. Whereas the distribution of magnetic field intensity patterns in Fourier modes (k_x, k_z) are shown in figures $6.1(a) - 6.1(c)$ and $6.2(a)$ - $6.2(c)$ (lower panels). These pattern lines connect the coordinates of k_x and k_z having the same values of $|B_{yk}|^2$.

Fig. 6.1 Snapshots of normalized magnetic field intensity profiles (upper panel) and spectral contour plots of magnetic field intensity (lower panel) for IAWs at $t = 3, 3.5$ and 4 for IC-1.

When the ponderomotive force acts on the plasma, the density gets modified. Due to this, the phase velocity of IAWs changes. When the IAWs propagate, the magnetic fields are localized in space. The inhomogeneity of the field in the form of the perturbation represented here takes the energy away and the localized magnetic structures collapse with the advancement of time. The nonlinear interactions between density and magnetic fields try to regroup the collapsed structures.

The mechanism for the generation of magnetic coherent structures is similar with the mechanism of laser focusing as explained by Kruer 2003. As the density of the medium is perturbed, the dielectric constant and hence the refractive index of the medium will be changed. The laser beam propagating through the medium of varying refractive index will act as a focusing lens and the wave will be focused. Similarly here also, the parallel ponderomotive force will modify the density. The KAWs propagating through this medium having density perturbations will produce varying phase velocity generating the spatial localization of the wave field.

These magnetic coherent structures enhance the transferring of energy from large scales (comparable to ion acoustic gyroradius) to small scales (comparable to electron thermal gyroradius). The plasma inhomogeneities manifested in the magnetic field and density perturbations in our study will take energy from the main IAW by nonlinear interaction and as the IAW propagates, it will generate magnetic filaments. Gershman et al. 2017 have found that local generation of observed IAWs, as observed by NASA's Magnetospheric Multiscale (MMS) mission, are due to the combined effects of nonlinearities arising from inhomogeneities in the magnetic field and particle number density.
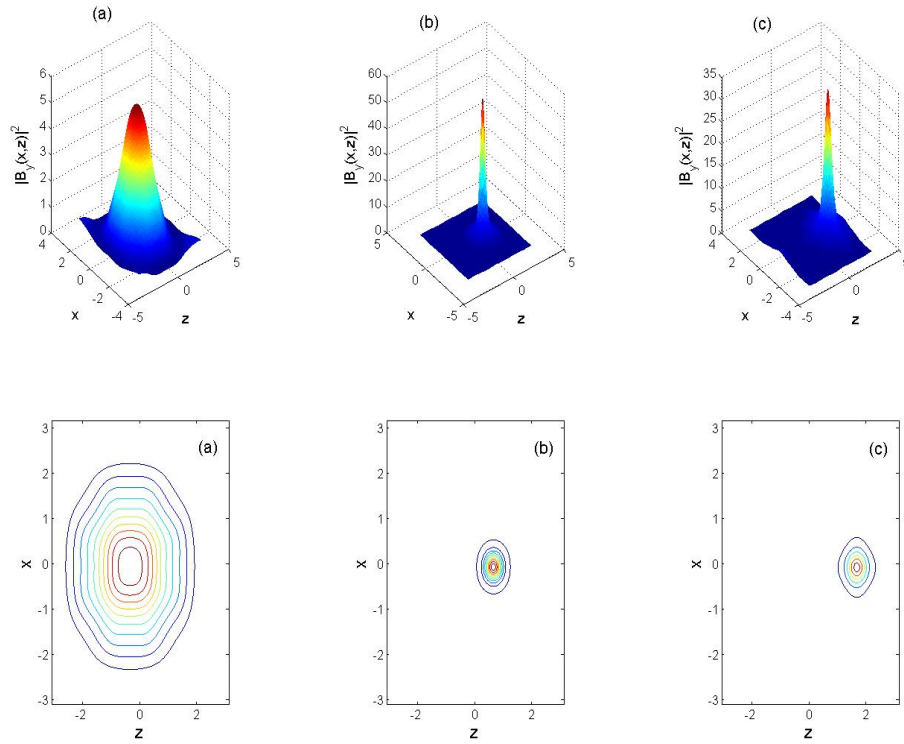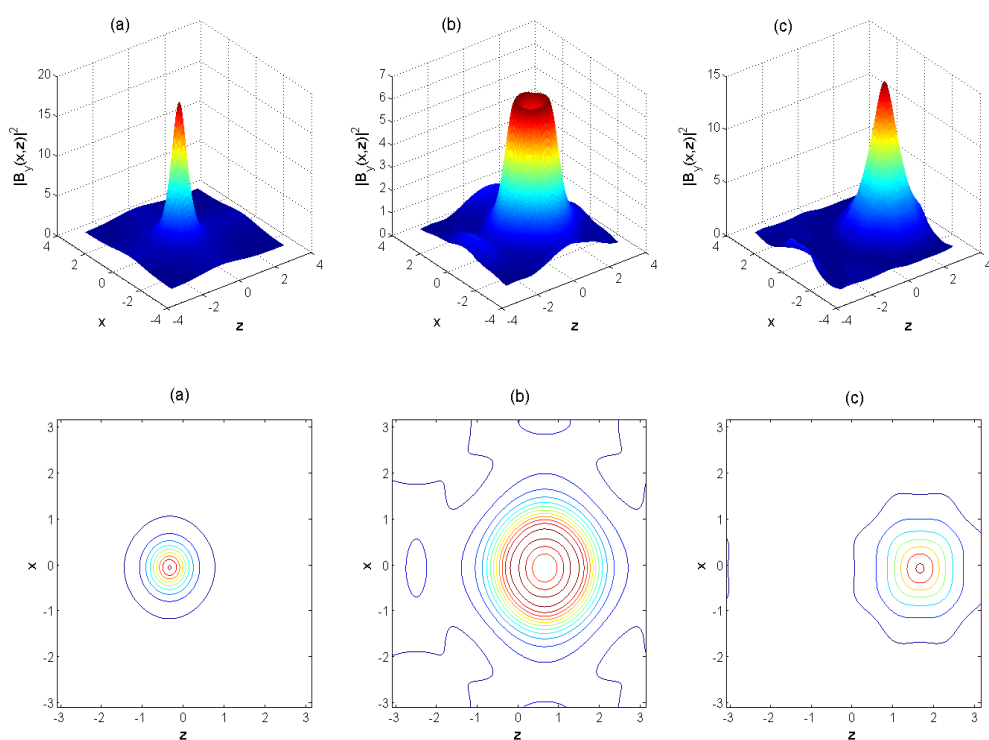
Fig. 6.2 Snapshots of normalized magnetic field intensity profiles (upper panel) and spectral contour plots of magnetic field intensity (lower panel) for IAWs at $t = 3, 3.5$ and 4 for IC-2.
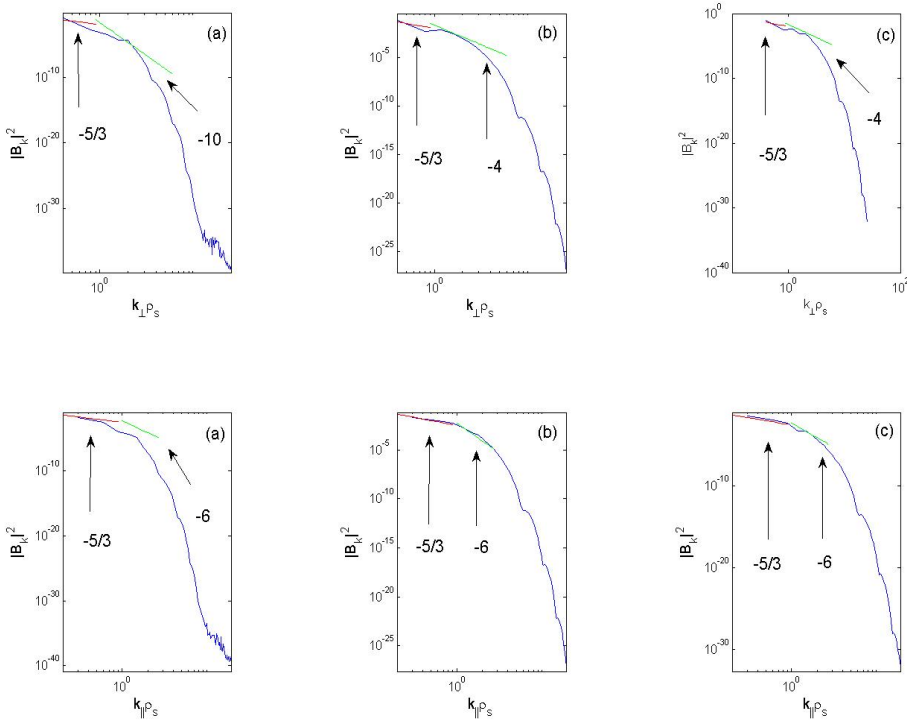
Fig. 6.3 Spectra of IAW magnetic field fluctuations for IC-1 in $k_\perp$ space (upper panel) and $k_\parallel$ space (lower panel) at $t = 3, 3.5$ and 4

If there is large fluctuations in the parallel magnetic fields as well as high current density, then the lighter particles (electrons) can be sufficiently trapped in between the wave packets. In this way, the wave energy is converted into particle energy. Therefore, it gives magnetic analog of Landau damping and can heat the plasma. We can measure the transverse scale size of the magnetic coherent structures from the magnetic field intensity profile. At early times, it comes out to be of the order of ion gyroradius $\approx 6\rho_s = 188.50$ km (measured at the half of the peak intensity). As time progresses, this scale size becomes smaller because of the transverse collapse. When this size reaches kinetic scales of IAWs, enough electron or ion heating takes place. Lion et al. 2016 and Chmyrev et al. 1988 reported the scale size of IAW filament structures of the order of ρ_s. Further by increasing the pump wave amplitude of the IAW which can be attained with increasing the value of g, we get the scale size of the filaments at micro kinetic scales and it leads to chaotic motion. The transfer of wave energy to particle energy is sufficiently happening at this stage.

Next, we present the spectral energy $|B_{yk}|^2$ at various wavenumber spaces, first in $k_x(k_\perp)$ direction [Figure 6.3(a)- 6.3(c) (upper panel)] and then to $k_z(k_\parallel)$ direction [Figure 6.3(a) - 6.3(c) (lower panel)] for first initial condition. For the second initial condition, the same is shown in figure (6.4). From the spectral plots, we see that the spectral index of energy cascade follows the Kolmogorov scale of $-5/3$ in the inertial range i.e. when $k_\perp \rho_s < 1$ and $k_\parallel \rho_s < 1$. This is in agreement with the results of many authors (Champeaux et al. 1998; Lavender et al., (2001); Sulem & Sulem, 1999). Hollweg, 1984 calculated the energy flux density in the plasma turbulence in the coronal holes by applying $-5/3$ spectral index. The results were in agreement with many observations. However, how this high energy flux in the coronal holes is achieved and what is the mechanism for turbulence leading to heating the corona have been still debating. The generation of IAW magnetic filaments and it's transverse collapse have been proposed in this chapter as one of the candidates to understand the coronal heating.
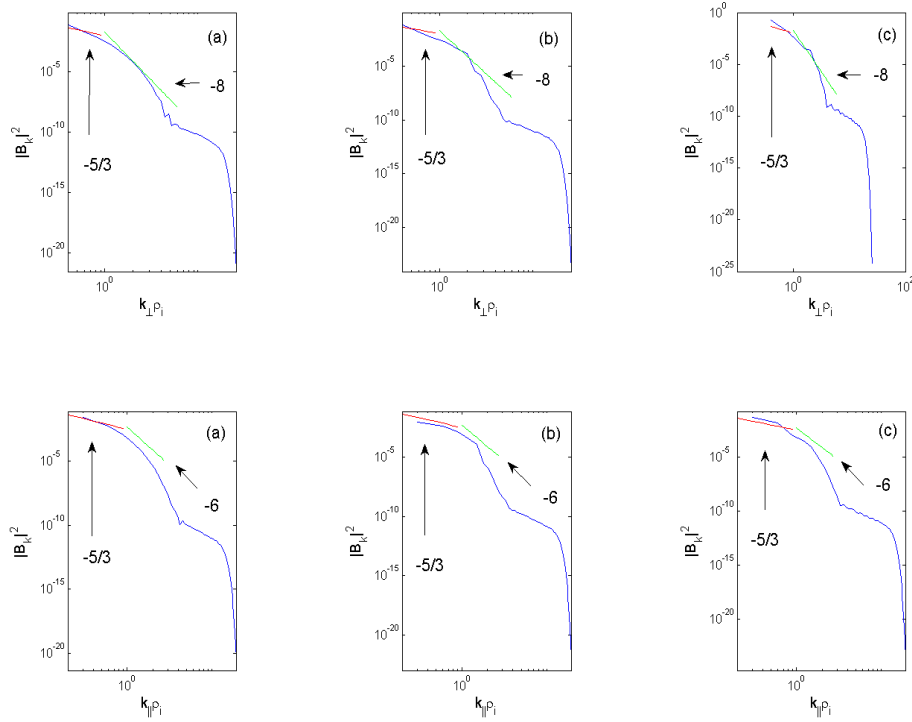
Fig. 6.4 Spectra of IAW magnetic field fluctuations for IC-2 in $k_\perp$ space (upper panel) and $k_\parallel$ space (lower panel) at $t = 3, 3.5$ and 4

It is found from the power spectra that the first spectral break happens at $k_\perp \rho_s \approx 1$ and $k_\parallel \rho_s \approx 1$. The first spectral break signifies a transition region from ion scale known as inertial range to electron scale known as kinetic range. In the transition range, our simulation results show the spectral indices in $k_\perp$ to be -10 and -4, and in $k_\parallel$ to be -6 for first initial condition. For second initial condition, these are -8 in $k_\perp$ and -6 in $k_\parallel$. Hudson, 1991 suggested that to sufficiently heat the solar corona by small scale burst like solar flares, the negative spectral magnetic energy slope of at least -2 is required. Many spacecraft results reported the spectral index deeper than -2 in the coronal region (Aschwanden & Parnell, 2002).

Finally, the electric field spectra are presented in Fourier space (6.5). From Chapter 2 equations (2.13) and (2.14), the dimensionless electric field components are found as $E_x = (2 - e^{|B_y|^2})B_y$ and $E_z = B_y/Q$. Here the constant $Q = v_A^2/(v_{te}^2 \lambda_e^2 k_{0x} k_{0z})$ and the electric field is normalized by $E_N = B_N k_{0z} v_A^2/(\omega c)$. From figure (6.5), we find the spectral indices of $-5/3$ in the inertial range for all instants of time. In the dissipation range, the slopes are different: -8 at $t = 3$, and -6 at $t = 3.5$ and $t = 4$. Electric spectra showed the same shape as that of magnetic spectra except that the field intensities are low in case of electric spectra. Therefore, we show here the electric spectra for the first initial condition only. Theoretically, Zhao et al 2016 modeled the inertial Alfvénic turbulence of scaling law $k_\perp^{-5/3}$ and $k_\perp^{-1/3}$ for $E_\perp$ spectra, and $k_\perp^{4/3}$ and $k_\perp^{-1/3}$ for $E_\parallel$ spectra. For scales smaller than the ion kinetic scales $k\rho_i > 1$, spectral scaling of $k_\perp^{-1/3}$ was modeled (Schekochihin et al. 2009; Zhao et al 2013; Bian & Kontar, 2010). However, for strong turbulence Boldyrev and Perez, 2012 modeled it to be $-2/3$. For parallel electric spectrum, Zhao et al 2016 found the spectral indices of $k_\perp^{4/3}$ and $k_\perp^{-1/3}$ in the inertial and kinetic scales respectively. In the inertial regime, the $E_\parallel$ spectral energy increases with $k_\perp$ (Zhao et al 2013; Bian & Kontar, 2011). By analyzing the *THEMIS* and *Cluster* data Mozer and Chen, 2013 found that both the electric spectra have almost the same power and scaling law of $-5/3$ at ion scales and -2.1 to -2.8 at electron scales. In contrast to this, some authors (Zhao et al 2013; Bian & Kontar, 2010; Bian & Kontar, 2011; Mozer and Chen, 2013) predicted that the spectral power is much higher in $E_\perp$ spectrum. Hence, the total energy is contributed mainly from $E_\perp$ energy. In our simulation also, by comparing the two electric spectra, we found that $E_\perp$ spectral energy is higher of the order of 3 than that of $E_\parallel$ spectral energy. It should be mentioned here that $E_\parallel$ is the actual force which mediates the wave-particle interaction and it is important in accelerating the charged particles (Wu & Fang, 1999; Fletcher & Hudson, 2008; McClements and Fletcher, 2009) via Landau resonance. Particle heating occurs when the electric thermal speed and the magnitude wave phase velocity are comparable. This stochastic heating problem can be

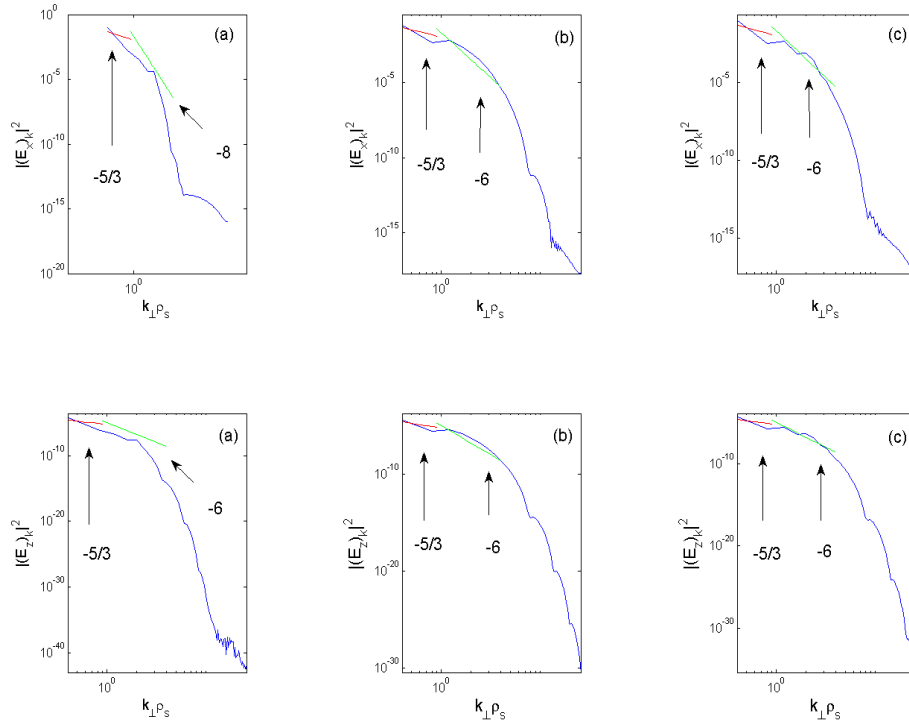Fig. 6.5 Spectra of IAW electric field fluctuations in $k_\perp$ space for IC-1: perpendicular electric field (upper panel) and parallel electric field (lower panel) at $t = 3, 3.5$ and 4.

treated by considering a distribution function in velocity phase space and solving the quasilinear diffusion equation (Fokker-Plank equation). This stochastic heating problem will be addressed in the next section.

6.4 Particle Acceleration

In this section, we will study the evolution of the velocity distribution function due to the fluctuating magnetic/electric spectra at dissipation region. It can be carried out by using the Quasi-Linear Theory (QLT) using the Fokker–Planck diffusion equation (Fuchs et al. (1985))

$$\frac{\partial f_e}{\partial t} = \frac{\partial}{\partial v_{ez}}\left(D(v_{ez})\frac{\partial f_e}{\partial v_{ez}}\right), \tag{6.5}$$

where $f(v_{ez}, t)$ is the velocity distribution function and $D(v_{ez})$ is the diffusion coefficient given as (Rozmus et al., (1987))

$$D(v_{ez}) = \frac{1}{4}\left(\frac{e}{m_e}\right)^2 l_A \frac{|E_{zk_{min}}|^2}{v_{ezk_{min}}} \tag{6.6}$$

where l_A is the periodicity length and e is the charge of the electron. Further, $|E_{zk}| = |E_{zk_{min}}|[|k_{min}/k|]^{S/2}$ with k_{max} and k_{min} as the wavenumbers at the edges of the fluctuating field region, $k_{min} \leq k \leq k_{max}$, and S as the slope of the power spectrum.

We can take the steady state form of the equation (6.5) i.e. $\frac{\partial f}{\partial t} = 0$, if the distribution function is independent of time when it reaches a constant value. This can be achieved if the observation time is much longer than the characteristic time of the nonlinearity that arises due to ponderomotive force. This characteristic time of nonlinearity is of the order of r_0/c_s, where r_0 is the transverse scale size of the magnetic filaments and c_s is the ion sound speed. Considering the steady state situation, we can write equation (6.5) in dimensionless form as

$$\frac{\partial f}{\partial v_{ez}} = \frac{C_1}{D(v_{ez})}, \tag{6.7}$$

where C_1 is a constant.

Now substituting $|E_{zk}|$ as given above, we get

$$D(v_{ez}) = \left[\frac{1}{4}\left(\frac{e}{m_e}\right)^2 \frac{l_A}{|v_{ez}|}|E_{k_{min}}|^2\left|\frac{k_{min}}{k}\right|^S\right]_{k=\omega_A/v}.$$ (6.8)

Substituting the relevent relations, equation (6.7) becomes

$$\frac{\partial f}{\partial v_{ez}} = \frac{C_1}{D_0}\left(\frac{v_p(k_{min})}{v_{ez}}\right)^{S-1}$$ (6.9)

where

$$D_0 = \frac{1}{4}\left(\frac{e}{m_e}\right)^2 l_A \frac{|E_{zk_{min}}|^2}{v_p(k_{min})}.$$ (6.10)

Performing integration on equation (6.9), we get its solution as

$$f = \frac{C_1 v_p(k_{min})}{D_0(2-S)}\cdot\left(\frac{v_p(k_{min})}{v_{ez}}\right) + C_2.$$ (6.11)

Here, the two constants C_1 and C_2 have to be evaluated using the boundary conditions. First boundary condition is that the total number of particles n_c in the distribution tail is equal to the initial number of particles with velocities $v_{max} \leq v_{ez} \leq v_{min}$. It can be represented mathematically as

$$n_c = \int_{v_{min}}^{v_{max}} f_m dv$$ (6.12)

where

$$f_m = n_e\left(\frac{m_e}{2\pi k_B T_e}\right)exp\left(-\frac{1}{2}\frac{m_e v_{ez}^2}{k_B T_e}\right)$$ (6.13)

The last boundary condition is: $f(v_{ez}) = f(v_{min})$. These two conditions are used two calculate C_1 and C_2 as

$$C_1 = \left(\frac{D_0(2-S)}{v_p(k_{min})}\right).[n_c - (v_{max} - v_{min}).f(v_{min})].\left[\frac{v_p(k_{min})}{3-S}\left\{\left(\frac{v_p(k_{min})}{v_{max}}\right)^{(S-3)}\right.\right.$$

$$\left.\left. - \left(\frac{v_p(k_{min})}{v_{min}}\right)^{(S-3)}\right\} - \left(\frac{v_p(k_{min})}{v_{max}}\right)^{(S-2)}.\left(v_{max} - v_{min}\right)\right]^{-1} \tag{6.14}$$

and

$$C_2 = f_m(v_{min}) - \frac{C_1 v_p(k_{min})}{D_0(2-S)}\left(\frac{v_p(k_{min})}{v_{max}}\right)^{(S-2)}. \tag{6.15}$$

It is evident from equation (6.11) that the distribution function is dependent on the slope of the wavenumber power spectra. The distribution function thermal tail will be enhanced for the dissipative range of spectra than the inertial range. So we can conclude that for more deep spectral index in the power spectra, the thermal tail of the distribution function is elongated and the particles gain more energy.

6.5 Conclusion

To encapsulate this chapter, we have presented the numerical simulation results of the nonlinear dynamical equation of IAWs in low β plasma applicable to solar coronal holes and magnetospheric auroral region. These results showed the generation of coherent structures of magnetic field intensity and turbulent spectra of magnetic and electric field fluctuations. The magnetic coherent structures of high intensity peaks can generate other waves and it can be the source of collapse of IAWs. The turbulent magnetic spectra are proportional to $k_\perp^{-4}$ and $k_\parallel^{-6}$ in the dissipation range. But in the inertial range (energy injection region) it follows $k^{-5/3}$ scaling. For the fluctuating electric/magnetic fields, the distribution function of the charged particles satisfy the Fokker-Plank equation. By solving the distribution function in steady state condition, we showed that the extension of the distribution thermal tail depends on the wavenumber spectral index of the electric/magnetic field power spectra. The charged particles at the end of the

distribution function thermal tail will have higher velocity and thereby energizing the solar coronal or auroral plasma particles.

Chapter 7

Conclusions and Future Outlooks

7.1 Conclusions

In this thesis we explore some of the magnetohydrodynamic and kinetic properties of nonlinear Alfvén waves in the context of solar wind, solar corona and the magnetospheric turbulence as well as the heating of the plasma particles. It studies about the formation of coherent, filamentary Alfvén structures, their decay processes, their role in particle heating and acceleration, and their relevance for creating the power-law spectra of turbulence observed in solar wind. The numerical results tried to contribute some knowledge and understanding to resolve the yet unsolved problems of heating and acceleration of particles in solar wind, corona and magnetosphere. The problems in these research areas remain at the top of interest of many physicists working with magnetospheric plasma and solar physics. This is stimulated by new experimental results from satellites, scanning the magnetosphere and observing the Sun. After several decades of worldwide research concerned with acceleration of solar and magnetospheric plasma, there is still no consensus about the fundamental processes to fully understand in this direction.

Chapter 1 of this thesis contains a comprehensive review of the present knowledge of the role of dispersive Alfvén wave (DAW) in acceleration processes in the terrestrial magnetosphere and solar plasma. Chapter 2 derives the governing equations of DAWs

by using the two fluid model when the plasma background density is modified by ponderomotive force and Joule heating. Chapter 3 describes the algorithm of the numerical method and its testing. Chapter 4 to Chapter 6 contain highlights and review of the publications that are basis of the thesis, with a final summary in this present Chapter 7.

The dynamical governing equations satisfied by DAWs follow the modified nonlinear Schrödinger equation. The equations were solved by pseudo-spectral method of simulation by taking Fast Fourier Transform and forward difference method. The numerical correctness and accuracy of the solver was checked by applying it to known solutions. By assuming an energy inputs in the form of pump waves in the kinetic range (KAW), or electron inertial range (IAW) the author studies numerically the evaluation of these waves that lead to filamentary nonlinear structures, or to creation of spatio-temporal turbulence. The magnetic filaments of DAWs with high intensity are generated as the wave propagates along the direction of magnetic field. The transverse modulation of Alfvén waves resulting in coherent structure formation has a significant effect on the evaluation of the spectra of the turbulent magnetic and density fluctuations. The perpendicular characteristic scale is found to be the ion Larmor radius for the kinetic Alfvén wave and the electron skin depth for the inertial Alfvén wave.

The applications of the results of KAWs at 1AU solar wind parameters and coronal loops, and IAWs at solar coronal holes were also discussed. The dynamical motions are dependent on the type of plasma inhomogeneity represented by four different kinds of initial conditions in our numerical simulations. The perturbation present in the magnetic field takes the energy from the pump DAWs and as the wave propagates magnetic coherent structures are generated when there is a balance between the wave diffraction and nonlinearity effects resulting from plasma inhomogeneity profile. The collapse of the DAW wave packets takes place when this balance is no more and this leads to transfer of energy from the wave to the particles in the plasma such as electrons and ions. This

transfer of energy at perpendicular wavevector is more for uniform initial pump DAW rather than those for non-uniform initial pump wave of Gaussian wavefront. The transfer of energy at kinetic small scales when the wavenumber is less than ion gyroradius and comparable to electron inertial length causes solar wind turbulence and heating of the plasma. In our study we found the spectral index following the Kolmogorov scale of $-5/3$ which is in the inertial range followed by deeper index varying from -2.5 to -8 in the kinetic dissipation range.

The solar coronal heating has been an open problem in solar physics in spite of having proposed many theoretical models to explain it. Dispersive Alfvén waves (DAWs) have been proposed by many authors to be responsible for inhomogeneous heating of solar coronal plasmas. By use of the pseudo-spectral method, the present thesis numerically studied the turbulent power spectra of magnetic fluctuations associated with DAWs based on the fluid model including the effects of the ponderomotive force and Joule heating. The results showed that the steady magnetic power spectra follow the Kolmogorov scaling in the inertial region and exhibit evidently anisotropy in the kinetic scale range, in similar with the results obtained by many previous works cited in this thesis. Meanwhile the present thesis also presented some interesting and important new results that the anisotropic scaling law of the magnetic power spectra in the kinetic scales obviously depends on the initial conditions of simulations, specifically, the distribution and component of initial pump waves. The scaling anisotropy of turbulent power spectra in the kinetic scales of plasma particles can importantly influence the plasma heating and turbulent energy transferring processes. For the heating of plasma particles via the wave-particle interactions, in general, the electric power spectra of the turbulent waves are more important than the magnetic power spectra. For the fluctuating electric/magnetic fields, the distribution function of the charged particles satisfy the Fokker-Plank equation. By solving this distribution function in steady state condition, we showed that the extension of the distribution thermal tail depends on the wavenumber spectral index

of the electric/magnetic field power spectra. Hence, charged particles at the end of the distribution function thermal tail have higher velocity and thereby energizing the solar coronal or auroral plasma. Since the formation of magnetic filaments and it's collapse are considered as one of the faster way to transport energy, our present study may provide some clues to understand the phenomenon of energy distribution via dissipation in the solar wind, solar corona and other relevant plasma environments.

7.2   Future Outlooks

In addition to bringing out a theoretical framework to explain the solar wind turbulence and coronal heating, the thesis also has explicitly brought out the simplicities involved in existing models. We identify at least four areas that need to be incorporated in the future work to enhance the conclusions presented here: three dimensional DAW dynamics, considerations of arbitrary plasma β, elliptical polarization, and compact expression for the density perturbations.

Three-dimensional considerations:- The simulations in this work are two-dimensional by assuming the DAWs propagating in $x - z$ plane i.e. $\vec{k}_0 = \vec{k}_{0x} + \vec{k}_{0z}$. Generalizing the model to a fully three-dimensional simulation can be proceeded by considering the wave vector $\vec{k}_0 = \vec{k}_{0x} + \vec{k}_{0y} + \vec{k}_{0z}$. The numerical simulation in $3D$ by pseudo-spectral method will be time consuming and require high end machines.

Arbitrary plasma- β:- Two-fluid equations under assumption of plane propagation describe all branches of waves: Alfven, slow/fast magnetosonic, acoustic, kinetic Alfven (KAW) and electron inertial Alfven (IAW). However, our model equation for KAW/IAW was obtained after decoupling the solutions of two fluid equations together with Maxwells equations where plasma β is very much less than unity. Removing this condition, one can find out the general dynamical equation for arbitrary plasma β value. This will be useful to study the role of nonlinear Alfven waves in many parts of the heliosphere such as the heliospheric current sheets located at around $5 A.U.$.

Consideration of elliptical polarization:- The KAW is generally elliptically polarized having the magnetic field into two components B_x and B_y. When $\omega \ll \omega_{ci}$, the wave is nearly linearly polarized giving only one component of transverse magnetic field. In our study, we took linearly polarized waves resulting the dynamical model equation involving only B_y, other components (B_x, B_z) can be obtained from Faraday's law. Our study can be improved by considering the elliptical polarization by defining two modes, left and right circularly polarized waves as $E_x + iE_y$ and $E_x - iE_y$ respectively.

Compact density perturbation:- We used the z-component of the ponderomotive force to get the modified density (Bellan & Stasiewicz (1998); Shukla & Stenflo, (2000a)) which is valid for an adiabatic case when the ion acoustic wave is propagating along the field line. The density perturbation can also be obtained from the normal momentum conservation equation, which leads to a completely different equation than we used in our study. However, it is difficult to obtain the compact expression for the modified density. To the best of our knowledge, we have not seen this type of density expression in the literature. So, it can be a challenging work to carry out.

References

Agrawal, G. P., Nonlinear Fibre Optics, 2013, 2nd Ed. Academic Press, 5th edition.

Alexandrova, O., Mangeney, A., Maksimovic, M., Lacombe, C., Cornilleau-Wehrlin, N., Lucek, E. A., Decreau, P. M. E., Bosqued, J.-M., Travnicek, P., Fazakerley, A. N., 2004, J. Geophys. Res. 109, A05207.

Alexandrova O., Carbone V., Veltri P., Sorriso-Valvo L. 2008, Apj, 674, 1153-1157.

Alexandrova, O., 2008, Nonlinear Processes Geophys. 15, 95.

Alexandrova O., Saur J., Lacombe C., Mangeney A., Mitchell J., Schwartz S. J., Robert P. 2009, Phys. Rev. Lett., 103, 165003.

Alfven, H., 1942, Nature, 150, 405.

Antoine, X., Bao, W., Besse, C., 2013, Computational methods for the dynamics of the nonlinear Schrodinger/Gross-Pitaevskii equations, Comput. Phys. Comm. 184, 2621-2633.

Aschwanden, M. J., Parnell, C. E. 2002, Astrophys. J., 572, 1048.

Asgari-Targhi, M., Van Ballegooijen, A. A. 2012, Astrophys. J. 746, 81.

Bale, S.D., Kellogg, P.J., Mozer, F.S., Horbury, T.S., Reme H. 2005, Phys. Rev. Lett., 94, 215002.

Bame, S. J., Asbridge, J. R., Feldman, W. C., Gosling, J. T., 1977, J. Geophys. Res., 82, 1487–1492.

Bao, W., Jaksch, D., Markowich, P. A., 2003, Numerical solution of the Gross-Pitaevskii equation for Bose-Einstein condensation, J. Comput. Phys. 187, 318-342.

Bareford, M. R., Hood, A. W., 2015, Phil. Trans. R. Soc. A 373, 20140266.

Bavassano B., Pietropaolo E., Bruno R. 1998, J. Geophys. Res., 103(A4), 6521-6529.

Bellan, P.M., Stasiewicz, K. 1998, Phys. Rev. Lett. 80, 3523.

Belcher, J. W., Davis, L., 1971, J. Geophys. Res. 76, 3534.

Beresnyak, A., Lazarian, A., 2009, Astrophys. J., 702, 460–471.

Bian, N. H., Kontar, E. P., 2011, Astron. Astrophys., 527, A130.

Bian, N. H., Kontar, E. P., 2010, phy. plasmas, 17, 062308.

Bian, N. H., Kontar, E. P., Brown, J. C. 2010, Astron. Astrophys., 519, A114.

Bieber, J. W., Wanner, W., Matthaeus, W. H., 1996, J. Geophys. Res., 101, 2511–2522.

Birn, J., Artemyev, A. V., Baker, D. N., Echim, M., Hoshino, M., Zelenyi, L. M., 2012, Space Science Review, 173, 102.

Birn, J., Priest, E. R., 2007, Reconnection of Magnetic Fields. Cambridge: Cambridge University Press.

Bittencourt, J. A., 2004, Fundamentals of plasma physics, 3rd edition, Springer, p-318.

Bloxham, J., Zatman, S., Dumberry, M., 2002, Nature, 420, 65–68.

Bohr, T., Jensen, M. H., Paladin, G., Vulpiani, A., Dynamical Systems Approach to Turbulence. Oxford University Press, 1998.

Boldyrev, S., Horaites, K., Xia, Q., Perez, J. C. 2013, Astrophys. J., 777, 41.

Boldyrev, S., Perez, J. C. 2012, Astrophys. J., 758, L44.

Borovsky, J. E., Funsten, H. O., 2003, J. Geophys. Res. 108, 1284.

Brandt, J. C., 1970, Introduction to the Solar Wind. W. H. Freeman and Company, San Francisco.

Bruno, R. and Carbone, V. 2013, Living Rev. Solar Phys., 10, 2.

Bruno, R., Carbone, V., 2005, Living Rev. Solar Phys., 2.

Bruno, R., Trenchi, L. 2014, Astrophys. J. Lett., 787, L24.

Burlaga, L. F., Ness N. F., Acuña, M. H., Lepping, R. P., Connerney, J. E. P., Richardson, J. D., 2008, Nature, 454, 75–77.

Burt, J., Smith, B., 2012, in IEEE Aerospace Conference, 1.

Cairns, Iver H., McMillan, B. F., 2005, Physics of Plasmas, 12.

Carter, T., Dorfman, S., 2014, URSI General Assembly and Scientific Symposium, IEEE Conference, Volume 5, p. 3216.

Cassak, P.A., Shay, M.A. 2012 Space Sci. Rev. 172, 283.

Champeaux, S., Gazol, A., Passot, T., Sulem, P.-L. 1997, Astrophys. 486, 477-483.

Champeaux, S., Passot, T., Sulem, P. -L. 1998, Phys. Plasmas 5, 100.

Champeaux, S., Passot, T., Sulem, P. L., 1997, J. Plasma Phys. 58, 665.

Chandran, B. D. G., 2008, Astrophys. J., 685, 646–658.

Chang, O., Gary, S.P., Wang, J. 2013, J. Geophys. Res., 118, 2824-2833.

Chaston, C. C., 2006, ULF-Waves and Auroral Electrons, in Magnetospheric ULF-Waves: Synthesis and New Directions, edited by Takahashi, K., Chi, P. J., Denton, R. E., Lysak, R. L., volume 169 of Washington DC American Geophysical Union Geophysical Monograph Series, p. 239.

Chaston, C. C., Carlson, C. W., Ergun, R. E., McFadden, J. P., 2000, Phys. Scr., T T84, 64.

Chaston, C. C., Bonnell, J. W., Carlson, C. W., McFadden, J. P., Ergun, R.E., Strangeway, R. J. 2003, J. Geophys. Res., 108, 8003.

Chaston, C. C., Bonnell, J. W., Carlson, C. W., McFadden, J. P., Ergun, R.E., Strangeway, R. J., Lund, E. J. 2004, J. Geophys. Res., 109, A04205.

Chaston C C., Phan T. D., Bonnell J. W., Mozer F. S., Acuna M., Goldstein M. L., Balogh A., Andre M., Reme H., Fazakerley A. 2005a, Phys. Rev. Lett., 95, 065002.

Chaston C. C., Peticolas L. M., Carlson C. W., McFadden J. P., Mozer F., Wilber M., Parks G. K., Hull A., Ergun R. E., Strangeway R. J., Andre M., Khotyaintsev Y., Goldstein M. L., Acuna M., Lund E. J., Reme H., Dandouras I., Fazakerley A. N., Balogh A. 2005b, J. Geophys. Res., 110, A02211.

Chen, Y., Li, Z.-Y., Liu, W., Shi Z.-D. 2000, Phys. Plasmas, 7, 371.

Chen C. H. K., Horbury T. S., Schekochihin A. A., Wicks R. T., Alexandrova O., Mitchell J. 2010, Phys. Rev. Lett., 104, 255002.

Chen C. H. K., Boldyrev S., Xia Q., Perez J. C. 2013, Phys. Rev. Lett., 110, 225002.

Chen, L., Wu, D. J., Huang, J. 2013, J. Geophys. Res. Space Phys., 118, 2951–2957.

Chen, F.F., Plasma Physics and Controlled Fusion, 2nd ed. (Springer, New York, 2006).

Chen H. -H., Liu C. -S. 1976, Phys. Rev. Lett., 37, 693.

Chen, L., Wu, D. J. 2010, Phys. Plasmas, 17, 062107.

Chen, L., Wu, D. J. 2012, APJ, 754, 123.

Chen, L., Wu, D. J., Hua, Y. P. 2011, Phys. Rev. E, 84, 046406.

Chen C.H.K., Leung L., Boldyrev S., Maruca B. A., Bale S.D. 2014, Geophys. Res. Lett. 41(22), 8081-8088.

Chen, L., Wu, D. J., Zhao, G. Q., Tang, J. F., Huang, J. 2015, J. Geophys. Res., 120, 61-69.

Chang, Q., Jis., E., Sun., W., 1999, Journal of Computational Physics, 148(2):397415.

Chmyrev V.M., Bilichenko S.V., Phokhotelov O. A., Marchenko V. A., Lararev V.I., Streltsov A. V., Stenfo L. 1988, Phys. Scr., 38, 841-854.

Cho, J. , Lazarin, A., 2002, Phys. Rev. Lett. 88, 245001.

Cho, J., Lazarian, A., Vishniac, E. T. 2002, Astrophys. J., 564, 291.

Cho, J., Lazarian, A. 2004, Astrophys. J. 615, L41–L44.

Cho, J., Lazarian, A. 2009, Astrophys. J. 701, 236–252.

Cirtain, J. W., Golub, L., Lundquist, L., van Ballegooijen, A., Savcheva, A., Shimojo, M., DeLuca, E., Tsuneta, S., Sakao, T., Reeves, K., Weber, M., Kano, R., Narukage, N., Shibasaki, K. 2007, Science, 318, 1580.

Coleman, P. J., 1966, Phys., Rev. Lett. 17, 207.

Coleman, Jr., P. J., 1968, Astrophys. J., 153, 371.

Coleman, P. J., 1967, Planet. Space Sci. 15, 953.

Conde, L., An Introduction to Plasma Physics and its Space Applications, Volume 1, (p. 1-15), 2018 IOP.

Cravens T.E., 2004, Physics of Solar System Plasma, 2nd ed., 345 pp., Cambridge Univ. Press, New York.

Cranmer S. R., Field G. B., Kohl J. L. 1999, Astrophys. J., 518, 937-947.

Dai, C., Wang, Y., Zhang, J., 2010, Analytical spatiotemporal localizations for the generalized (3+1)-dimensional nonlinear Schrodinger equation, Opt. Lett. 35, 1437-1439.

Dasso, S., Milano, L. J., Matthaeus, W. H., Smith, C. W., 2005, Astrophys. J. Lett., 635, L181–L184.

Davidson, P. A., 2001, An introduction to Magnetohydrodynamics, Cambridge University Press.

De Azvedo, C. A., Elfimov, A. G., de Assis, A. S. 1994 Sol. Phys. 153, 205.

Dennis, B. R. 1985, Sol. Phys., 100, 465.

De Pontieu, B., McIntosh, S. W., Carlsson, M., Hansteen, V. H., Tarbell1, T. D., Schrijver1, C. J., Title, A. M., Shine1, R. A., Tsuneta, S., Katsukawa, Y., Ichimoto, K., Suematsu, Y., Shimizu, T., Nagata, S. 2007, Science, 318, 1574.

Domingo, V., Fleck, B., Poland, A. I., 1995, Sol. Phys., 162, 1.

Dwivedia, N. K., Sharma, R. P. 2013, Phys. Plasmas, 20, 042308.

Ebert, R. W., McComas, D. J., Elliott, H. A., Forsyth, R. J., Gosling, J. T., 2009, J. Geophys Res, 114, A01109.

Elfimov, A. G., de Azvedo, C. A., de Assis, A. S. 1996, Phys. Scr. T63, 251.

Escande, D. F ., Gondret, V., Sattin, F., 2019, Nature, 9, 14274.

Feldman, W. C., Anderson, R. C., Bame, S. J., Gary, S. P., Gosling, J. T., McComas, D. J., Thomsen, M. F., Paschmann, G., Hoppe, M. M., 1983, Journal of Geophysical Research, 88, 110.

Fletcher, L., Hudson, H. S. 2008, Astrophys. J., 675, 1645.

Fornberg B., Whitham G.B., 1978, Philos. Trans. R. Soc. Lond. A 289, 373–404.

Forsyth, R. J., Horbury, T. S., et al., 1996, Geophys. Res. Lett., 23, 595.

Fox, N. J., Velli, M. C., Bale, S. D., et al. 2016, Space Sci. Rev., 204, 7.

Fuchs, V., Krapchev, V., Ram, A., Bers, A., 1985, Physica D, 14, 141-160.

Galtier, S., 2006, J. Plasma Phys., 72, 721–769.

Galtier, S., Nazarenko, S. V., Newell, A. C., Pouquet, A., 2000 Plasma Physics, 63, 447.

Gary, S. P. 1999, J. Geophys. Res., 104, 6759-6762.

Gary, S. P., Nishimura, K. 2004, J. Geophys. Res., 109, A02109.

Gary S. P., Smith C. W. 2009, JGRA, 114, A12105.

Gary, S. P., Nishimura, K. 2004, J. Geophys. Res., 109, A02109.

Gary S. P., Smith C. W. 2009, J. Geophys. Res., 114, A12105.

Gekelman, W., 1999, J. Geophys. Res. 104, 14417.

Gekelman, W., Leneman, D., Maggs, J., Vincena, S. 1994, Phys. Plasmas, 1, 3775.

Gekelman W., Pribyl P., Palmer N., Vincena S., Mitchell C. 1999, Bull Am. Phys. Soc., 44, 71

Gershman, D.J., F-Vinas, A., Dorelli, J. C., Boardsen, S. A., Avanov, L. A., Bellan, P.M., Schwartz, S.J., Lavraud, B., Coffey, V. N., Chandler, M.O., Saito, Y., Paterson, W. R., Fuselier, S. A., Ergun, R. E., Strangeway, R. J., Russell, C. T., Giles, B. L., Pollock, C. J., Torbert, R. B., Burch, J. L. 2017, Nat. Commun., 8, 14719.

Goertz, C. K., Boswell, R. W., 1979, J. Geophys. Res., 84, 7239–7246.

Gogoberidze, G., Mahajan, S. M. , Poedts, S., 2009, Physics of Plasmas, 16:072304.

Goldstein, B. E., Neugebauer, M., Smith, E. J., 1995, Geophys Res Lett, 22, 3389–3392.

Goldstein M. L., Roberts, D.A., Matthaeus, W. H., 1995, Ann. Rev. Astron. Astrophys. 33, 283–326.

Goldreich, P., Sridhar, S., 1995, Astrophys. J., 438, 763-775.

Goldstein, M. L., Roberts, D. A., Deane, A. E., Ghosh, S., Wong, H. K., 1999, J. Geophys. Res. 104(A7), 14,437.

Goldreich, P., Sridhar, S. 1997, Astrophys. J., 485, 680.

Goldstein, M. L., Roberts, D. A., Fitch, C. A. 1994, J. Geophys. Res, 99, 11519.

Goldstein, M. L., Roberts, D. A., 1999, Phys. Plasmas, 6, 4154.

Goossens, M. 1994, Space Sci. Rev. 68, 51.

Gourlay, A., 1971, Proceeding of the Royal Socity of London. A Mathematical and Physical Sciences, 323 (1553):219235.

Gringauz K.I., Bezrokikh V. V., Ozerov, V. D., Rybchinskii, R. E., 1960, Sov Phys Dokl 5:361.

Gurnett, D. A., Anderson, R. R., Odem, D. L., 1975, Raumfahrtforschung, 19, 245–247.

Gurnett, D. A., Huff, R. L., Menietti, J. D., Burch, J. L., Winningham, J. D., Shawhan, S. D., 1984, J. Geophys. Res. 89, 8971.

Hasegawa A., Chen L. 1975, Phys. Rev. Lett. 35, 370.

Hasegawa, A., 1976, J. Geophys. Res. 811, 5083–5090.

Hasegawa, A., Uberoi, C., The Alfven Wave, National Technical Information Service, Springfield, VA, 1982.

He, J., Marsch, E., Tu, C., Yao, S., Tian, H. 2011, Astrophys. J., 731, 85.

Herlofson, N., 1995, Nature 165, 1020.

Hilfer, R., 1999, Applications of Fractional Calculus in Physics, World Scienti c, Singapore.

Hollweg, J. V., 1999, J. Geophys. Res. 104, 14811.

Hollweg, J. V. 1984, Astrophys. J. 277, 392.

Hollweg, J. V., Bird, M. K., Volland, H., 1982, J. Gophys. Res. 87, 1.

Hollweg, J. V., 1985, in B. Buti (ed.), Advances in Space Plasma PhYSics, World Scientific, Singapore, p. 77.

Hood, A.W., Browning, P.K., Linden, R.A.M. 2009 Astron. Astrophys., 506, 913.

Hood, A.W., Ireland, J., Priest, E.R. 1997 Astron. Astrophys. 318, 957.

Horbury, T. S., Balogh, A., Forsyth, R. J., Smith, E. J., 1996, J. Geophys. Res. 101, 405.

Horbury T.S., Balogh A., Forsyth R.J., Smith E.J. 1996, Astron. and Astrophys., 316, 333-341.

Hoshino, M., Goldstein, M. L. 1989, phys. Fluids. B1, 1405.

Howes G.G., Cowley S.C., Dorland W., Hammett G.W., Quataert E., Schekochihin A.A. 2006, Astrophys. J. 651, 590-614.

Howes, G. G., Dorland, W, Cowley, S. C., Hammett, G. W., Quataert, E., Schekochihin, A. A., Tatsuno, T., 2008, Phys. Rev. Lett. 100, 065004.

Howes G.G. 2009, Nonlinear Processes Geophys. 16, 219.

Howes, G. G., Dorland, W., Cowley, S. C., Hammett, G. W., Quataert, E., Schekochihin, A. A., Tatsuno, T., 2008, Phys. Rev. Lett., 100(6), 065004.

Howes, G. G., Dorland, W., Cowley, S. C., Hammett, G. W., Quataert, E., Schekochihin, A. A., Tatsuno, T. 2008a, Phys. Rev. Lett., 100, 065004.

Howes, G.G., Cowley, S.C., Dorland, W., Hammett, G.W., Quataert, E., Schekochihin, A.A. 2008b, J. Geophys. Res., 113, A05103.

Howes, G.G., Cowley, S.C., Dorland, W., Hammett, G.W., Quataert, E., Schekochihin, A.A., Tatsuno, T. 2008c, Phys. Rev. Lett., 100, 065004.

Howes, G. G., TenBarge, J. M., Dorland, W, Quataert, E., Schekochihin, A. A., Numata, R., Tatsuno, T. 2011, Phys. Rev. Lett. 107, 35004.

Howes, G. G., TenBarge, J.M., Dorland, W. 2011a, Phys. plasmas, 18, 102305.

Howes, G. G., Tenbarge, J. M., Dorland, W., Quataert, E., Schekochihin, A. A., Numata, R., Tatsuno, T. 2011b, Phys. Rev. Lett., 107, 035004.

Hoz, F.D., Vadillo, F., 2008, Comput. Phys. Commun. 179, 449-456.

Hoz, F.D., Vadillo, F., 2016, J. Comput. Appl. Math., 295, 175-184.

Hu, J., Xin, J., Lu, H.,2011, Comput. Math. Appl. 62, 1510-1521.

Hundhausen, A. J., 1972, Solar wind and Coronal Expansion, Physics and Chemistry in Space Vol. 5, edited by J. G. Roederer, Springer-Verlag, New York.

Hudson, H. S., 1991, Sol. Phys., 133, 357.

Iroshnikov, P. S., 1963, As-tronomicheskii Zhurnal, 40(4), 742.

Iroshnikov, P. S., 1964, Turbulence of a Conducting Fluid in a Strong Magnetic Field, 7, 566.

Jackson, B. V., 1985, Solar Phys. 100, 563–574.

Jain, R., Browning, P., Kusano, K. 2005 Phys. Plasmas 12, 012904.

Jian, L.K., Wei, H.Y., Russell, C. T., Luhmann, J. G., Klecker, B., Omidi, N., Isenberg, P.A., Goldstein, M. L., Figueroa-Vinas, A., Blanco-Cono, X. 2014, Astrophys. J., 786, 123.

Jafelice, L. C., Opher, R., 1987, Astrophys. Space Sci. 137, 303.

Kadomstev, B. B., Academic, New York, 1965.

Kletzing, C.A., 1994, J. Geophys. Res. 99, 11095.

Kletzing, C. A., Hu, S., 2001, Geophys. Res. Lett., 28, 693–696.

Klimchuk, J. A., 2006, Sol. Phys. 234, 41–77.

Klimchuk, J. A., 2015, Phil. Trans. R. Soc. A 373, 20140256.

Kolmogorov, A. N., 1991, Proc R Soc A, 434, 9–13. first published in Russian in Dokl. Akad. Nauk. SSSR, 30, 299–303, (1941).

Kraichnan, R., 1965a, Phys Fluids 8, 1385–1387.

Kraichnan, R., 1965b, Phys Fluids, 8, 575–598.

Kruer W. L. 2003, The Physics of Laser Plasma Interactions , Westview Press, Boulder.

Lanchester, B. S., Rees, M. H., Lummerzheim, D., Otto, A., Sedgemore-Schulthess, K. J. F., Zhu, H., McCrea, I. W., 2001, J. Geophys. Res. 106, 1785.

Lavender, D., Passot, T., Sulem, P. L., 2001, Physica D 152-153, 694.

Lavender, D., Passot, T., Sulem, P. L., 2002, Phys. Plasmas, 9, 293.

Lehnert, B., 1954 Phys. Rev. 94, 815.

Leamon, R.J., Smith, C. W., Ness, N. F., Matthaeus, W. H., Wong, H. K. 1998, J. Geophys. Res. 103, 4775

Leamon, R. J., Matthaeus, W. H., Smith, C. W., Zank, G. P., Mullan, D. J., Oughton, S., Astrophysical. J., 537, 1054.

Lee, L. C., Johnson, J. R., Ma, Z. W. 1994, J. Geophys. Res., 99, (A9)17405-17411.

Li, H., Wang, C., Chao, J.K., Hsieh, W.C. 2015, J. Geophys. Res., 121, 42-55.

Lion, S., Alexandrova, O., Zaslavsky, A. 2016, Astrophys. J., 824, 47.

Lithwick, Y., Goldreich, P., Sridhar, S., 2007, Astrophysical Journal, 655:269.

Longcope, D. W., Tarr, L. A., 2015, Phil. Trans. R. Soc. A 373, 20140263.

Louarn, P., Wahlund, J. E., Chust, T., Feraudy, H. D., Roux, A., Holback, B., Dovner, P. O., Eriksson, A. I., Holmgren, G., 1994, Geophys. Res. Lett. 21, 1847.

Lundquist, S.,1949 Phys. Rev. 76, 1805.

Luo, Q. Y., Wu, D. J. 2010, ApJL, 714, L138.

Luo, Q. Y., Wu, D. J., Yang, L. 2012, Astrophys. J. Lett., 733, L22.

Lysak, R. L., Lotko, W., 1996, J. Geophys. Res. 101, 5085.

Luhr, H., Warnecke, J., et al., 1994, Geophys. Res. Lett. 21, 1883.

Mahdy, A. I., 2016, J. Applied Mathematics and Physics, 4, 2186-2202.

Malovichko, P. P. 2008, Kinemat. Phys. Celest. Bodies, 24, 236.

Markovskii, S.A., Vasquez, B.J., Smith, C.W. 2008, Astrophys. J., 675, 1576-1583.

Marsch, E., Tu, C.Y. 1990, J. Geophys. Res., 95, 8211-8229.

Marsch, E., Tu, C.-Y. 2001, J. Geophys. Res., 106, 277-238.

Marson, J., Goldreich, P. 2001, Astrophys. J., 554, 1175.

Matthaeus, W. H., Zank, G. P., Oughton, S., Mullan, D. J., Dmitruk, P., 1999, Astrophys. J. Lett., 523, L93–L96.

Matthaeus, W. H., Velli, M., 2011, Space Sci. Rev. 160, 145.

Matthaeus, W. H., Goldstein, M. L., Roberts, D. A., 1990, J. Geophys. Res. 95, 20673.

Matthaeus, W. H., Goldstein, M. L., Smith, C. 1982, Phys. Rev. Lett., 48, 1256.

McClements, K. G., Fletcher, L. 2009, Astrophys. J., 693, 1494.

McComas, D. J., Bame, S. J., Barraclough, B. L., Feldman, W. C., Funsten, H. O., Gosling J. T., Riley, P., Skoug, R., Balogh, A., Forsyth, R., Goldstein, B. E., Neugebauer, M., 1998, Geophys Res Lett, 25, 1–4.

McComas, D. J., Barraclough, B. L., Funsten, H. O., Gosling, J. T., Santiago-Muñoz, E., Skoug, R. M., Goldstein, B. E., Neugebauer, M., Riley, P., Balogh, A., 2000, J Geophys Res, 105, 10419–10434.

McComas, D. J., Elliott, H. A., Schwadron, N. A., Gosling, J. T., Skoug, R. M., Goldstein, B. E., 2003, Geophys Res Lett, 30, 1517.

Melrose, D.B., 1992, Astrophys. J. 387, 403–413.

Morton, R. J., Tomczyk, S., Pinto, R. 2015, Nature Commun. 6, 7813.

Mozer, F. S., Chen, C. H. K. 2013, Astron. Astrophys., 768, L10.

Muller, W. C., Grappin, R., 2005, Physical Review Letters, 95, 114502.

Nakariakov, V. M., Ofman, L., DeLuca, E.E., Roberts, B., and Davila, J. M., 1999, Science, 285: 862-864.

Narain, U., Ulmschneider, P. 1996 Space Sci. Rev. 75, 453.

Narita Y., Gary S. P., Saito S., Glassmeier K.-H., Motschmann U. 2011, Geophys. Res. Lett., 38, L05101.

Nariyuki, Y., Hada, T., 2006, Nonlinear Process Geophys, 13, 425–441.

Neugebauer, M. 2004, J. Geophys. Res., 109, A02101.

Neugebauer, M., Snyder, C. W., 1962, Solar plasma experiment. Science 138, 1095–1097.

Ogilvie, K. W., Chornay, D. J., Fritzenreiter, R. J., Hunsaker, F., Keller, J., Lobell, J., Miller, G., Scudder, J. D., Sittler Jr., E. C., Torbert, R. B., Bodet, D., Needell, G., Lazarus, A. J., Steinberg, J. T., Tappan, J. H., Mavretic, A., Gergin, E., 1995, Space Sci. Rev., 71, 55.

Okuda, H., Dawson, J., 1973, Phys. Fluids, 16, 408.

Okamoto, T. J., Tsuneta, S., Berger, T. E., Ichimoto, K., Katsukawa, Y., Lites, B. W., Nagata, S., Shibata, K., Shimizu, T., Shine, R. A., Suematsu, Y., Tarbell, T. D., Title, A. M. 2007, Science, 318, 1577.

Osman,K. T., Matthaeus, W. H., Greco, A., Servidio, S. 2011, Astrophys. J., 727, L11.

Oughton, S., Matthaeus, W. H., 2005, Nonlinear Proc. Geophys., 12, 299.

Parnell, C. E., De Moortel, I., 2012, Phil. Trans. R. Soc. A 370, 3217–3240.

Parker, E. N. 1979, Cosmical Magnetic Fields: Their Origin and Their Activity (Oxford: Clarendon).

Parker, E.N., 1991, Astrophys, J. 376, 355.

Passot, T., Sulem, P. L., 2003, Phys. Plasmas, 10, 3914.

Perri, S., Carbone, V., Yordanova, E., Bruno, R., Balogh, A., 2011, Planet. Space Sci. 59, 575–9.

Perez, J. C., Boldyrev, S., 2009, Phys. Rev. Lett., 102(2), 025003.

Perri S., Carbone V., Veltri P. 2010, Astrophys. J. Lett., 725, L52-L55.

Petviashvili, V. I., Pokhotelov, O. A., 1992, Solitary Waves in Plasmas and in the Atmosphere, Gordon and Breach, Reading, Birkshire, UK.

Petelski, E. F., Fahr, H. J., Ripken, H. W., 1980, Model Calculations of Solar Wind Expansion Including an Enhanced Fraction of Ionizing Electrons, in Solar and Interplanetary Dynamics, edited by M. Dryer and E. Tandberg-Hanssen, volume 91 of IAU Symposium, p. 159.

Phillips, J. L., Bame, S. J., Barnes, A., Barraclough, B. L., Feldman, W. C., Goldstein, B. E., Gosling, J. T., Hoogeveen, G. W., McComas, D. J., Neugebauer, M., Suess, S. T., 1995, Geophys Res Lett, 22, 3301–3304.

Pitaevskii, L., Stringari, S., 2003, Bose-Einstein Condensation, Oxford University Press, Oxford.

Poedts, S., Goossens, M. 1989 Sol. Phys. 123, 83.

Podesta, J.J. 2013, Solar Phys., 286, 529-548.

Podesta, J. J., Borovsky, J. E., Gary, S. P. 2010, Astrophysical J., 712, 685-691.

Podesta, J. J., Bhattacharjee, A., 2010, Astrophys. J., 718, 1151– 1157.

Press, W. H., Teukolsky, S. A., Vetterling, W. T., Flannery, B. P., 1996, "Numerical Recipes in Fortran 77: the Art of Scientific Computing. Second Edition", vol. 1.

Priest, E.R., Foley, C.R., Heyvaerts, J., Arber, T.D., Mackay, D., Culhane, J.L., Acton, L.W. 2000 Astrophys. J. 539, 1002.

Reale, F., 2014, Living Rev. Sol. Phys. 11, 4.

Retinò, A., Nakamura, R., Vaivads, A., Khotyaintsev, Y., Hayakawa, T., Tanaka, K., Kasahara, S., Fujimoto, M., Shinohara, I., Eastwood, J. P., André, M., Baumjohann, W., Daly, P. W., Kronberg, E. A., Cornilleau-Wehrlin, N., 2008, Journal of Geophysical Research: Space Physics, 113, A12.

Roberts, O. W., Li X., Li B. 2013, APJ, 769, 58.

Roberts, D. A., Goldstein, M. L., Matthaeus, W. H., Ghosh, S., 1992, J. Geophys. Res., 97, 17,115.

Rosenbauer, H., Schwenn, R., Marsch, E., Meyer, B., Miggenrieder, H., Montgomery, M. D., Muehlhaeuser, K. H., Pilipp, W. G., Voges, W., Zink, S., 1977, J. Geophys. 42, 561–580.

Rozmus, W., Sharma, R. P., Samson J. C., Tighe, W., 1987, Phys. Fluids, 30, 2181 - 2193.

Ruderman, M.S.1999, Astrophys. J. 521, 851.

Ruderman, M. S., Goldstein, M. L., Roberts, D. A., Deane, A., Ofman, L., 1999, J. Geophys. Res., 104, 17057 – 17068.

Russell, C. T., 1972, NASA Special Publication, 308, 365.

Sabine E., 1851, On periodical laws discoverable in the mean effects of the larger magnetic disturbances, Philos Trans R Soc London 141, 123–139.

Sahraoui, F., Goldstein, M. L., Robert, P., Khotyaintsev, Y. V., 2009, Phys. Rev. Lett., 102(23), 231102.

Sahraoui, F., Pincon, J. L. et al., 2003, J. Geophys. Res. 108, 1335.

Sahraoui, F., Belmont, G., Goldstein, M. L. 2012, Astrophys. J. 748, 100.

Sahraoui, F., Huang, S. Y., Belmont, G., Goldstein, M. L., Robert, P., De Patoul, J. 2013, Astrophysical J. 777, 15.

Sahraoui, F., Goldstein, M. L., Robert, P., Khotyaintsev, Yu. V. 2009, Phys. Rev. Lett., 102, 231102.

Sahraoui, F., Goldstein, M. L., Belmont, G., Canu, P., Rezeau, L. 2010, Phys. Rev. Lett., 105, 131101.

Saito, S., Gary, S. P., Narita, Y., Phys. Plasmas, 2010, 17, 122316.

Salem, C. S., Howes, G. G., Sundkvist, D., Bale, S. D., Chaston, C. C., Chen, C. H. K., Mozer, F. S. 2012, Astrophys. J. Lett., 745, L9.

Sari, J. W., Valley, g. C., 1976, J. Geophys. Res., 81, 5489.

Savin, S. P., Romanov, S. A., Fedorov, A. O., Zelenyi, L., Klimov, S. I., Yermolaev, Y. I., Budnik, E. Y., Nikolaeva, N. S., Russel, C. T., Zhou, X-W., Urquhart, A. L., Reiff, P. H. 1998, Geophys. Res. Lett., 25, 2963-2966.

Schekochihin, A. A., Cowley, S. C., Dorland, W., Hammett, G. W., Howes, G. G., Quataert, E., Tatsuno, T. 2009, Astrophys. J. Ser., 182, 310.

Schmelz J. T, Winebarger, A. R., 2015, Phil. Trans. R. Soc. A 373, 20140257.

Schmelz, J. T., 2003, Adv. Space Res. 32, 895.

Schekochihin, A.A., Cowley, S.C., Dorland, W., Hammett, G.W., Howes, G.G., Plunk, G.G., Quataert, E., Tatsuno, T. 2008, Plasma Phys. Control. Fusion, 50, 124024.

Sergeev, V. A., Sauvaud, J.-A., Popescu, D., Kovrazhkin, R. V., Liou, K., Newell, P. T., Brittnacher, M., Parks, G., Nakamura, R., Mukai, T., Reeves, G.D. 2000, Geophys. Res. Lett., 27, 851-854.

Singh, H. D., Sharma, R. P. 2007, Phys. Plasmas, 14, 102304.

Singh, H. D., Jatav, B. S. 2019, Research in Astron. Astrophys., 19,7.

Siversky, T., Voitenko, Y., Goossens, M. 2005, Space Sci. Rev., 121, 343–351.

Sharma, R.P., Singh, H.D., Malik, M. 2006, J. Geophys. Res., 111, A12108.

Shebalin, J.V., Matthaeus, W. H., Montgomery, D. 1983, J. Plasma Phys., 29, 525.

Shaikh, D. 2010, Mon. Not. R. Astron. Soc. , 405, 2521.

Sharma, R.P., Singh, H.D., Malik, M. 2006, J. Geophys. Res., 111, A12108.

Sharma, R. P., Kumar, S. 2011, J. Geophys. Res. 116, A03103.

Sharma, R. P., Gaur, N., 2014, JGR space physics. 199, 7061-7073.

Sharma, R. P., Yadav, N., Pathak, N. 2014, Astrophys Space Sci., 351, 75-80.

Sharma, P., Yadav, N., Sharma, R. P. 2016, Phys. Plasmas, 23, 052304.

Sharma, R. P., Sharma, P., Yadav, N. 2017, Phys. Plasmas, 24, 012905.

Shukla, P. K., Bingham R., Eliasson, B., Dieckmann, M. E., Stenflo, L., 2006, Plasma Phys. Control. Fusion, 48, B249-B255.

Shukla, P. K., Birk, G. T., Dreher, J., Stenflo, L., 1996, Plasma Phys. Rep. 22, 818.

Shukla, P. K., Stenflo, L., 1997, Phys. Plasmas 4, 3445.

Shukla, P. K., Bingham, R., Mckenzie, J. F., Axford, W.I. 1999, Sol. Phys. 186, 61.

Shukla, P. K., Stenflo, L. 1999, Phys. Plasmas, 6, 4120.

Shukla, P. K., Stenflo, L., Bingham, R. 1999, Phys. Plasmas, 6, 1677.

Shukla, P.K., Stenflo, L., 1989, Astrophys. Space Sci. 155, 145.

Shukla, P. K., Stenflo, L. 1999, Phys. Plasmas, 6, 4120.

Shukla, P. K., Stenflo, L. 2000, Phys. Plasmas, 7, 2738.

Shukla, P. K., Stenflo, L. 2000a, Phys. Plasmas, 7, 2738.

Shukla, P. K., Stenflo, L. 2000b, Phys. Plasmas, 7, 2747.

Shukla, P. K., Stenflo, L. 2005, Phys. Plasmas, 12, 084502.

Shukla, A., Sharma, R. P. 2002, J. Geophys. Res., 107, 1338.

Shukla, A., Sharma, R. P., Malik, M., 2004, Phys. Plasmas, 11, 2068.

Shukla, A., Sharma, R. P., 2001, Phys. Plasma 8, 3759.

Smith, C. W., Hamilton, K., Vasquez, B. J., Leamon, R. J. 2006, APJ Lett., 645, L85-L88.

Srivastava, N., Schwenn, R., 2000, The origin of the solar wind: an overview. In: Scherer K, Fichtner H, Marsch E (eds) The outer heliosphere: beyond the planets. Copernicus, Katlenburg-Lindau, pp 12–40.

Stasiewicz, K., Bellan, P., Chaston, C., Kletzning, C., Lysak, R., Maggs, J., Pokhotelov, O., Seyler, C., Shukla, P., Stenflo, L., Streltsov, A., Wahlund, J. E., 2000, Space Sci. Rev., 92, 423.

Stone, E. C., Cummings, A. C., McDonald, F. B., Heikkila, B. C., Lal, N., Webber, W. R., 2005, Voyager 1 explores the termination shock region and the heliosheath beyond. Science 309, 2017–2020.

Shebalin, J. V., Matthaeus, W. H., Montgomery, D., 1983, J. Plasma Phys, 29, 525–547.

Stefant, J. R., 1970, Phys. Fluids, 13, 440.

Stewart, B., 1861, Philos. Trans. R. Soc. London Ser I, 151, 423–430.

Stasiewicz, K., Gustafsson, G., Marklund, G., Lindqvist, P.-A., Clemmons, J., Zanetti, L., 1997, J. Geophys. Res. 102, 2565.

Sturrock, P.A., Roald, C.B., Wolfson, R. 1999 Astrophys. J. 524, L75.

Stone, E. C., Frandsen, A. M., Mewaldt, R. A., Christian, E.R., Margolies, D., Ormes, J.F., Snow, F., 1998, Space Sci. Rev., 86, 1.

Sulem, C., Sulem, P. L., The Nolinear Schrödinger Equation: Self-Focusing and wave collapse, Applied Mathematical Sciences, vol. 139 (Springer, New York, 1999).

Sundkvist, D., Retino, A, Vaivads, A., Bale, S. D. 2007, Phys. Rev. Lett., 99, 025004.

Sun, C., Barsi, C., Fleischer, J.W., 2008, Peakon proles and collapse-bounce cycles in self-focusing spatial beams, Opt. Exp. 16.

Sweilam, N., H., 2007 J. Comput. Appl. Math., 207 155-163.

Tessein, J.A., Smith, C. W., MacBride, B. T., Matthaeus, W. H., Forman, M. A., Borovsky, J. E., 2009, Astrophysical Journal, 692, 684.

Testa, P., De Pontieu, B., Allred, J., Carlsson, M., Reale, F., Daw, A., Hansteen, V., Martinez-Sykora, J., Liu, W., DeLuca, E. E., Golub, L., McKillop, S., Reeves, K., Saar, S., Tian, H., Lemen, J., Title, A., Boerner, P., Hurlburt, N., Tarbell, T. D., Wuelser, J. P., Kleint, L., Kankelborg, C., Jaeggli, S. 2014, Science 346, 6207.

Thompson, B. J., Lysak, R. L., 1996, J. Geophys. Res. 101, 5359.

Tomczyk, S., McIntosh, S. W., Keil, S. L., Judge, P. G., Schad, T., Seeley, D. H., Edmondson, J., 2007, Science.

Treumann, R. A., Baumjohann, W., Narita, Y., 2015, Front. Phys., 3, 22.

Tsiklauri, D., Sakai, J. I., Saito, S., 2005, Astron. Astrophys. 435, 1105.

Tsiklauri, D. 2011, Phys. Plasmas 18, 092903.

Tsiklauri, D. 2012, Phys. Plasmas, 19, 082903.

Tsurutani B. T., Ho C. M., 1999, Rev. Geophys. 37, 517.

Tsurutani, B. T., Smith, E. J., Anderson, R. R., Ogilvie, K .W., Scudder, J. D., Baker, D. N., Bame, S. J. 1982, J. Geophys. Res., 87, (A8)6060-6072.

Tu, C.Y., Marsch, E., 1995 Space Sci. Rev. 73, 1.

Tu, C.-Y., Zhou, C., Marsch, E., Xia, L.-D., Zhao, L., Wang, J.-X., Wilhelm, K., 2005, Science, 308, 519– 523.

Tu, C.-Y., Marsch, E., 1995, Space Sci. Rev., 73, 1–210.

Tu, C.Y., Marsch, E., Rosenbauer, H. 1990, J. Geophys. Res., 283-286.

Tu C.Y., Marsch E. 1993, J. Geophys. Res., 98, 1257-1276.

Unti, J. W., Neugebauer, N., 1968, Phys. Fluids 11, 563.

Valentini, F., Vasconez, C. L., Pezzi, O., Servidio, S., Malara, F., Pucci, F. 2017, Astro. Astrophys. 599, A8.

Van Ballegooijen, A. A., Asgari-Targhi, M., Cranmer, S. R., DeLuca, E. E., 2011, Astrophys. J. 736, 3.

Van Ballegooijen, A. A., Astrophys. J., (2004) 612, 519.

Velli, M., Pucci, F., Rappazzo F., Tenerani, A., 2015, Phil. Trans. R. Soc. A 373, 20140262.

Vinas, A. F., Goldstein, M. L., Acuna, M. H., 1984, J. Geophys. Res. 89, 3762.

Vincena, S., Gekelman, W., Maggs, J., 2004, Phys. Rev. lett. 93(10).

Vlad, G., Zonca, F., Briguglio S. 1999, Riv. Nuovo Cim., 22,1.

Voigt, J., 2002, Surveys in Geophysics, 23: 335-377.

Voitenko, Y., Goossens, M. 2004, Astrophys. J., 605, L149.

Voitenko, Yu. M. 1995, Sol. Phys. 161, 197.

Voitenko, Yu. M., 1996, Sol. Phys. 168, 219.

Voitenko, Y., Goossens, M. 2004, Astrophys. J., 605, L149.

Voitenko, Y. 1998, Sol. Phys., 182, 411.

Wahlund, J.-E., Louarn, P., Chust, T., de Feraudy, H., Roux, A., Holback, B., Dovner, P. O., Holmgren, G., 1994, Geophys. Res. Lett. 21, 1831–1834.

Wang, X. Y., Liu, Z. X., Li, Z. Y., Zhang, X. B., 1998, Phys. Plasmas 5, 836.

Wang, X.-Y. 1998, Phys. Plasmas, 5, 4395.

Wang, X., He, J.S., Tu, C.Y., Marsch E.m Zhang, L., Chao, J.K. 2012, J. Geophys. Res., 746, 147.

Winterhalter D., Neugebauer M., Goldstein B. E., Smith E. J., Bame S. J., Balogh A. 1994, J. Geophys. Res., 99, (A12) 23371-23381.

Wilcox, J. M., Boley, F. I., Desilva , A. W.: 1960, Phys. Fluids 3, 15.

Wu, D. J. 2003, Phys. Plasmas, 10, 1364.

Wu, D. J., Fang, C. 2003, Astrophys. J., 596, 656-662

Wu, D. J., Fang, C. 1999, Astrophys. J., 511, 958.

Wu, D. J., Fang, C. 2007, Astrophys. J. Lett., 659, L181.

Wu, D. J., Yang, L., 2007, Astrophys. J., 659, 1693.

Wu, D. J., Yang, L. 2006, Astron. Astrophys., 452, L7-L10.

Woo, R., Habbal, S. R., 2005, J. Lett., 629, L129– L132.

Wu, D. J., Chao, J. K. 2004, J. Geophys. Res., 109, A06211.

Wu D. J., Chen, L. 2013, Astrophysical J., 771, 3.

Wu, D. J., Wang, D. Y., Huang, G. L. 1997, 4, 611.

Wu, D.J., Huang, G.L., Wang, D.Y., Carl, G.F., 1996, Phys. Plasmas 3, 2879.

Wygant, J.R., Keiling, A., Cattell, C. A., Lysak, R. L., Temerin, M., Mozer, F. S., Kletzing, C. A., Scudder, J. D., Streltsov, V., Lotko, W., Russell, C. T. 2002, , J. Geophys. Res., 107, A8, 1201.

Wygant, J. R., Keiling, A., Cattell, C. A., Johnson, M., Lysak, R. L., Temerin, M., Mozer, F. S., Kletzing, C. A., Scudder, J. D., Peterson, W., Russell, C. T., Parks, G., Brittnacher, M., Germany, G., Spann, J., 2000, J. Geophys. Res. 105, 18675.

Xu, T., Tian, B., Li, L. -L., Lu, X., Zhang, C. 2008, Phys. Plasmas, 15, 102307.

Yukhimuk, A. K., Fedun, V. M., Sirenko, E. K., Voitenko, Y. M., Voytsekhovskaya, A. D., 2000, Kinematika Fiz. Nebesnykh Tel Suppl. 3, 477–480.

Zakharov, V.E., Synakh, V.S., 1975, The nature of self-focusing singularity, Sov. Phys. JETP. 41, 465-468.

Zhao, J. S., Wu, D. J., Lu, J. Y. 2013, Astrophysical J., 767,109.

Zhou, C., He, X. T., Chen, S. 1992, Phys. Rev. A, 46, 2277-2285.

Zhou, C., Hi, X. T. 1994, Phys. Rev. E, 49, 4417-4424

Zhao, J. S., Voitenko Y. M., Wu, D. J., Yu, M. Y. 2016, J. Geophys. Res. Space Physics, 121, 5-18.

Zimbardo, G., Greco, A., Valvo, L. S., Perri, S., Vörös, Z., Aburjania, G., Chargazia, K., Alexandrova, O., 2010, Space Sci. Rev. 156, 89.

Coherent structures and spectral shapes of kinetic Alfvén wave turbulence in solar wind at 1 AU

Hemam Dinesh Singh and Bheem Singh Jatav

Department of Physics, Sikkim University, Gangtok, Sikkim, 737102, India; *hemamdine@gmail.com*

Abstract This paper presents the generation of kinetic Alfvén wave (KAW) coherent structures of magnetic filaments applicable to solar wind at 1 AU, when the background plasma density is modified by parallel ponderomotive force and Joule heating. The inhomogeneity in the magnetic field, which was included as a perturbation in the transverse direction of the magnetic field, takes energy from the main pump KAWs and generates the filamentary structures. When the intensity is high enough, the filaments are broken down and the energy initially confined to low wavenumbers is redistributed to higher wavenumbers, leading to cascades of energy at small scales less than the ion acoustic gyroradius or comparable to electron gyroradius. The magnetic field spectral profile is generated from the numerical simulation results, and its dependence on different directions of the wavevector and initial conditions of the simulation representing the transverse magnetic field inhomogeneity is studied. The relevance of these results with other spacecraft observations and measurements is also pointed out.

Key words: plasmas — turbulence — waves — solar wind

1 INTRODUCTION

In a magnetized plasma, Alfvén waves are produced by the restoring force coming from the magnetic tension while the ion mass provides the inertia to maintain the wave. Kinetic Alfvén waves (KAWs) are low frequency (compared to ion cyclotron frequency), dispersive, shear Alfvén modes that exist when their perpendicular wavelength is comparable to either the ion gyroradius or the electron inertial length, while the parallel wavelengths are longer than the ion inertial length (here, the perpendicular (parallel) direction means transverse (along) to the ambient (background) magnetic field direction). Their plasma β is in the intermediate range ($m_e/m_i \ll \beta \ll 1$), where $\beta = 8\pi n_0 T/B_0^2$ (thermal to magnetic pressure ratio), n_0 is the unperturbed plasma number density, $T(= T_e \approx T_i)$ is the plasma temperature, B_0 is the external ambient direct current (DC) magnetic field and m_e/m_i is the electron to ion mass ratio. In this plasma β regime, the electron thermal speed exceeds the Alfvén speed, thereby allowing the electrons to move fast enough to respond to any adiabatic changes in density or field profile.

Many studies (Li et al. 2016; Tu & Marsch 1993; Bavassano et al. 1998; Neugebauer 2004) have shown that the Alfvénicity measured by the correlation of the field and velocity components decreases with solar distances. At a solar distance of 0.3 AU, an Alfvénicity of around 3 was found (Tu et al. 1990; Marsch & Tu 1990). At a solar distance of 1 AU, it becomes around less than 0.7 (Tu & Marsch 1995) showing that as the solar wind expands, the plasma becomes magnetically dominated. However, Wang et al. (2012) pointed out the existence of large-amplitude Alfvén waves near 1 AU, with an Alfvénicity of around 1. There are many independent observational evidences showing the existence of KAWs in the solar wind in the form of KAW turbulence at 1 AU and perhaps throughout of the heliosphere (Podesta 2013; Howes et al. 2006, 2008b,c, 2011b; Schekochihin et al. 2008, 2009; Boldyrev & Perez 2012).

KAWs develop field aligned electric fields which can lead to the acceleration and heating of the charged particles along the magnetic field direction (Hasegawa & Chen 1975; Wu 2003; Wu & Chao 2004), thus producing anisotropic and mass-dependent energization of heavy

Anisotropic turbulence of kinetic Alfvén waves and heating in solar corona

Hemam Dinesh Singh and Bheem Singh Jatav⋆

Department of Physics, Sikkim University, Gangtok, Sikkim, 737102, India; *hemamdine@gmail.com*

Abstract Understanding solar coronal heating has been one of the unresolved problems in solar physics in spite of the many theories that have been developed to explain it. Past observational studies suggested that kinetic Alfvén waves (KAWs) may be responsible for solar coronal heating by accelerating the charged particles in solar plasma. In this paper, we investigated the transient dynamics of KAWs with modified background density due to ponderomotive force and Joule heating. A numerical simulation based on pseudo-spectral method was applied to study the evolution of KAW magnetic coherent structures and generation of magnetic turbulence. Using different initial conditions in simulations, the dependence of KAW dynamics on the nature of inhomogeneous solar plasma was thoroughly investigated. The saturated magnetic power spectra follows Kolmogorov scaling of $k^{-5/3}$ in the inertial range, then followed by steep anisotropic scaling in the dissipation range. The KAW has anisotropy of $k_\parallel \propto k_\perp^{0.53}$, $k_\parallel \propto k_\perp^{0.50}$, $k_\parallel \propto k_\perp^{0.83}$ and $k_\parallel \propto k_\perp^{0.30}$ depending on the kind of initial conditions of inhomogeneity. The power spectra of magnetic field fluctuations showing the spectral anisotropy in wavenumber space indicate that the nonlinear interactions may be redistributing the energy anisotropically among higher modes of the wavenumber. Therefore, anisotropic turbulence can be considered as one of the candidates responsible for the particle energization and heating of the solar plasmas.

Key words: plasmas — turbulence — waves — Sun: corona

1 INTRODUCTION

One of the fundamental unsolved issues of astrophysics is the solar coronal heating problem, where the outer atmosphere of the Sun has a high temperature corona of around 2×10^6K as compared to the photosphere of around 6000K. In the past few decades, many spacecraft observations from the *Solar and Heliospheric Observatory* (*SOHO*), *Transition Region and Coronal Explorer* (*TRACE*), *Hinode* and *Solar Dynamics Observatory* (*SDO*) have revealed that the solar atmosphere is in nature far from dynamical and thermal equilibrium. It has inhomogeneity in magnetic field and density. Therefore, the nonuniform heating processes of magnetoplasma fine structures play a very significant role in the coronal heating. These coherent structures or filaments are often identified as the manifestation of field aligned density (or temperature) striations and their heating mechanisms are closely related to solar magnetic fields.

The solar corona is generally divided into coronal holes (open regions) and coronal loops (closed regions).

The cooler and less dense coronal holes are the sources of solar wind. The associated magnetic field lines are carried away from these regions to space by the solar winds through the escaping energetic particles. The first coronal heating mechanism involving the role of solar magnetic field lines was proposed by Alfvén (1942) using Alfvén waves (AWs). Since then many theories were put forward to explain the coronal heating and solar wind acceleration (Marsch 2006; Sirenko et al. 2002; Cranmer et al. 2007; Cranmer 2009). Among them, two prominent theories are: heating by waves (Narain & Ulmschneider 1996; Hood et al. 1997; Goossens 1994; Priest et al. 2000; Poedts et al. 1989; Ruderman 1999) and heating by flares or magnetic reconnection (Jain et al. 2005; Hood et al. 2009; Sturrock et al. 1999; Cassak & Shay 2012). However, there is still no universally accepted self-consistent model to explain the physical processes behind the coronal heating and solar wind acceleration. Recently, there are many observational and theoretical evidences showing that AWs are the main candidates for being able to transport sufficient energy in the solar atmosphere to reach the temperature of million Kelvins in the coronal regions (Parker 1979; De

24th Raman Memorial Conference

"Unravelling Physics of Advanced Materials"

23rd - 24th February, 2018

CERTIFICATE

This is to certify that,

Mr./ Ms./ Mrs. / Dr. ....Bheem........Singh......Jatav..................

affiliated to ....Sikkim......University............................... has presented

~~thesis~~/~~or~~al/poster/~~participated~~ in 24th Raman Memorial Conference held

on 23rd & 24th February, 2018 at the Department of Physics, Savitribai Phule

Pune University, Pune.

RMC - 2018
Organizing Comittee
Department of Physics,
Savitribai Phule Pune University,
Pune

Head,
Department of Physics,
Savitribai Phule Pune University,
Pune.

6th PSSI Plasma Scholars Colloquium

छ्वीं पी. एस. एस. आई. प्लाज़्मा विद्वान कॉलोक्वियम

Plasma Science and Technology

प्लाज़्मा विज्ञान और प्रौद्योगिकी

24 - 26 August 2018

२८ - २६ आगस्त २०१८

Organized by

PSSI & Department of Physics, Sikkim Manipal Institute of Technology,
Majitar, Rangpo, Sikkim

Certificate of Appreciation

प्रशंसा प्रमाण पत्र

This is to certify that Prof./Dr./Mr./Ms. Bheem Singh Jatav from Sikkim Univ.

has given Keynote Lecture / only participated / participated and presented the paper titled Numerical simulation of IAW to study Nonlinear structure and spectral index for Aurora. in the Colloquium.

He/She is awarded the .... in the Oral/Poster presentation.

Dr. Utpal Deka
Convener, 6th PSSI PSC-2018

Dr. Ashis Sharma
Director, SMIT

ESTD 1978
PSSI

SMIT
SIKKIM MANIPAL INSTITUTE OF TECHNOLOGY

# 12th International Conference on Plasma Science & Applications (ICPSA-2019)

11th–14th November, 2019
Lucknow, India

Certificate

This certificate is proudly presented to Bhem Singh Jatav, Sikkim University ....

for participating in the 12th International Conference on Plasma Science and Applications,

held during 11th–14th November, 2019 organized by Department of Physics, University of

Lucknow, India. He/She also presented an oral talk/poster at the conference.

Paul Lee
Dr. Paul Lee
Secretary AAAPT

Dr. Punit Kumar
Chair, ICPSA-2019
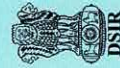
This is to certify that

Bheem Singh Jatav

has participated in

NARIT COMAC 2018

"MHD Simulations in Astrophysics and Space Plasma"

2 - 6 July 2018

Chiang Mai, Thailand

Saran Poshyachinda, Ph.D.
Executive Director of NARIT